RICE UNIVERSITY

MODULATING PROTEIN HOMEOSTASIS TO AMELIORATE LYSOSOMAL STORAGE DISORDERS

by

Fan Wang

A THESIS SUBMITTED
IN PARTIAL FULFILLMENT OF THE
REQUIREMENTS FOR THE DEGREE

Doctor of Philosophy

APPROVED, THESIS COMMITTEE

Laura Segatori, Chair
T.N. Law Assistant Professor,
Chemical and Biomolecular Engineering

George Bennett
E. Dell Butcher Professor,
Biochemistry and Cell Biology

Kathleen Matthews
Stewart Memorial Professor,
Biochemistry and Cell Biology

Kyriacos Zygourakis
A.J. Hartsook Professor,
Chemical and Biomolecular Engineering

HOUSTON, TEXAS
April 2012

ABSTRACT

Modulating Protein Homeostasis to Ameliorate Lysosomal Storage Disorders

by

Fan Wang

The goal of this project has been to develop therapeutic strategies for protein misfolding diseases caused by excessive degradation of misfolded proteins and loss of protein function. The focus for this work is lysosomal storage disorders (LSDs), a group of more than 50 known inherited metabolic diseases characterized by deficiency in hydrolytic enzymes and consequent buildup of lysosomal macromolecules. Gaucher's Disease (GD) is used as a representative of the family of LSDs in this study. GD is caused by mutations in the gene encoding lysosomal glucocerebrosidase (GC) and consequent accumulation of the GC substrate, glucocerebroside. The most prevalent mutations among GD patients are single amino acid substitutions that do not directly impair GC activity, but rather destabilize its native folding. GC normally folds in the ER and trafficks through the secretory pathway to the lysosomes. GC variants containing destabilizing mutations misfold and are retrotranslocated to the cytoplasm for ER-associated degradation (ERAD). However, evidence shows that if misfolding-prone, mutated GC variants are forced to fold into their 3D native structure, they retain catalytic activity. This study describes strategies to remodel the network of cellular pathways that maintain protein homeostasis and to create a folding environment favorable to the folding of unstable, degradation-prone lysosomal enzyme variants. We demonstrated that folding

and trafficking of mutated GC variants can be achieved by modulating the protein folding network in fibroblasts derived from patients with GD to i) upregulate the expression of ER luminal chaperones, ii) inhibit the ERAD pathway, and iii) enhance the pool of mutated GC in the ER amenable to folding rescue. We also demonstrated that the same cell engineering strategies that proved successful in rescuing the folding and activity of mutated GC enable rescue of mutated enzyme variants in fibroblasts derived from patients with Tay-Sachs disease, a LSD caused by deficiency of lysosomal hexosaminidase A activity. As a result, the current study provides insights for the development of therapeutic strategies for GD based on the modulation of general cellular pathways that maintain protein homeostasis that could in principle be applied to the treatment of multiple LSDs.

Acknowledgments

Many thanks from the deepest part of my heart to my advisor Dr. Laura Segatori for her guidance, patience, understanding, and encouragement through my Ph.D study. She taught me how to be an independent thinker. I could never have reached the heights or explored the depth without her advice.

I also sincerely thank my wonderful colleagues for their helpful discussions on the project and technical support on the experiments.

Finally, I am heartfully thankful to my dearest parents and my David for their love and support. During the past five years, we shared time of pain and frustration, but somehow we all knew that this wonderful day will come.

Contents

List of Figures

List of Tables

Nomenclature

ATF4, Activating transcription factor 4;

ATF6, Activating transcription factor 6;

BiP, Binding immunoglobulin protein;

BAK, Bcl-2 homologous antagonist/killer;

BAX, Bcl-2-associated X protein;

Bcl-2, B-cell lymphoma 2;

CHOP, C/EBP homologous protein;

CNX, Calnexin;

CRT, Calreticulin;

EDEM, ER degradation-enhancing α-mannosidase-like lectins;

EerI, Eeryastatin I;

EndoH, Endoglycosidase H;

ERAD, ER-associated degradation;

ERT, Enzyme Replacement Therapy;

GC, Glucocerebrosidase;

GD, Gaucher's Disease;

HexA, β-hexosaminidase A;

IRE1, Inositol requiring kinase 1;

Kif, Kifunensine;

LSD, Lysosomal Storage Disorders;

PERK, Double-stranded RNA-activated ER kinase;

Xbp-1, X-box binding protein-1;

UGGT, UDP-glucose:glycoprotein glucosyltransferase;

UPR, Unfolded Protein Response.

Chapter 1

Introduction

1.1. Protein folding

1.1.1. From polypeptide sequence to native three-dimensional structure

Proteins are biochemical molecules involved in almost every biological process in the cell. They consist of linear chains of amino acids joined together by peptide bonds. In order to display biological functions, newly synthesized polypeptides need to fold three-dimensionally to assume their native structure (Alberts et al., 2002).

Anfinsen's pioneer experiments on protein folding demonstrated that proteins can fold spontaneously into their native structure *in vitro*. This evidence suggests the native folding of a protein, which is the biologically functional conformation, is the most thermodynamically favored among all possible three-dimensional conformations that a polypeptide sequence can assume. In other words, three-dimensional folding of proteins is dictated solely by information contained in the amino acid sequence (Anfinsen, 1973;

Anfinsen et al., 1961). However, unassisted folding may occur in time scales too slow to be compatible with cellular physiology (Griffiths and Simons, 1986). Therefore, living organisms have evolved proteins that, by chaperoning newly synthesized proteins through their folding process, accelerate the folding of proteins *in vivo* (Figure 1.1) (Ellis and Hartl, 1999). Molecular chaperones include a variety of proteins that promote native folding of unfolded or misfolded proteins and prevent interactions between misfolded or partially folded protein intermediates, which would otherwise lead to deleterious consequences for the cell, including the formation of insoluble aggregates (Dobson, 2003; Fink, 1999).

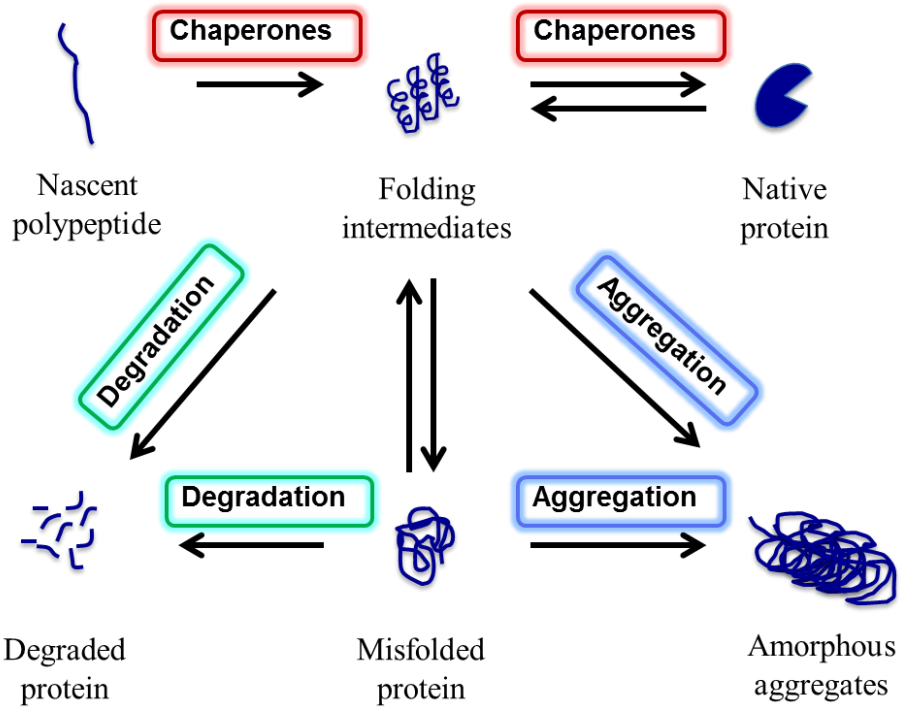

Figure 1.1. Protein folding *in vivo*. Each protein is present in a dynamic equilibrium between folded and unfolded conformations. Molecular chaperones promote the native folding of a protein and prevent interactions between misfolded or partially folded protein intermediates. Misfolded proteins are either rapidly degraded or aggregate into insoluble deposits, which are resistant to degradation.

A number of competing biological pathways maintain the conformational integrity of the proteome to ensure their biological functions. These pathways, which regulate protein synthesis, folding, trafficking, and degradation, comprise an integrated network that maintains protein homeostasis (known as proteostasis network) (Balch et al., 2008; Mu et al., 2008b). Impairment of folding is often due to the inability of the proteostasis network to cope with destabilizing effects of genetic mutations or environmental factors. Recent efforts have been devoted to devising strategies to modulate the proteostasis network to promote folding of unstable, degradation-prone proteins (Hartl et al., 2011). Modulation of the proteostasis network is expected to remodel the folding free energy landscape of unstable proteins, thus limiting the accumulation of misfolding intermediates and maximizing native folding (Figure 1.2) (Powers et al., 2009).

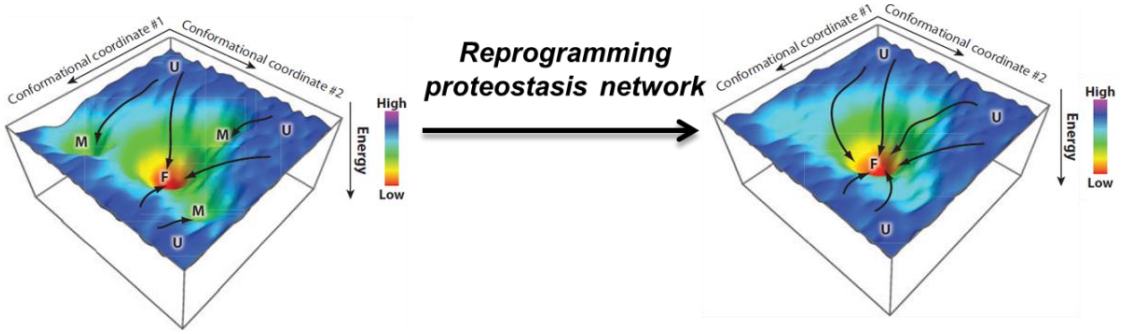

Figure 1.2. Modulating the proteostasis network to enhance the cellular folding capacity. The folding process is driven by a free-energy funnel. The unfolded state of a protein, at the top of the funnel, is associated with the highest free energy. Protein folding involves the progression of the unfolded protein through a number of folding intermediates characterized by lower free energy. Folding intermediates may also reach relatively stable off-pathway conformations. Reprogramming proteostasis network influences the folding free energy landscape and lowers the population of misfolded proteins. U: unfolded state; M: misfolded state; F: folded state. (Adapted from Powers *et al*. 2009)

1.1.2. Protein misfolding

A number of factors including genetic mutations (Hochstrasser, 1996) or environmental conditions (Dobson, 1999; Jaenicke, 1991) cause impairment of protein folding and lead to accumulation of misfolded intermediates. The fate of misfolded proteins is either degradation or aggregation into insoluble deposits (Figure 1.1) (Bence et al., 2001). Because the native structure of a protein is tightly linked to its biologic activity, failure of a protein to achieve its native fold or to remain correctly folded results in loss of protein activity, which, in turn, often gives rise to the development of a wide variety of human diseases depending on the identity of the misfolded protein (Dobson, 2003). Protein misfolding diseases encompass a large group of ailments ranging from neurodegenerative diseases such as Alzheimer's and Parkinson's disease, to metabolic diseases such as LSDs and type II diabetes, and include even many types of cancers. Protein misfolding diseases can be generally classified as: i) loss-of-function diseases, which are caused by rapid disposal of misfolded protein through the cell's degradation system, and ii) gain-of-toxic-function diseases, which are characterized by the aberrant accumulation of misfolded proteins and formation of insoluble aggregates (Dobson, 1999).

1.2. The protein quality control system

The protein Quality Control (QC) system is a complex network of pathways that promotes folding and trafficking of newly synthesized proteins (Bukau et al., 2006). The QC system is composed of i) molecular chaperones, which facilitate the folding of

proteins into their native conformations and prevent misfolding and aggregation (Lee and Tsai, 2005), and ii) the ubiquitin-proteasome system, which catalyzes the degradation of misfolded proteins (Ravid and Hochstrasser, 2008). This sophisticated network guarantees the biogenesis of properly folded, biologically active proteins and avoids the formation of non-native off-pathway events such as the accumulation of misfolded or aggregated proteins (Trombetta and Parodi, 2003).

Misfolded proteins typically expose patches of hydrophobic amino acid residues on their surfaces, which often cause the formation of aberrant intermolecular interactions and lead to the deposition of insoluble, possibly toxic aggregates (Kiefhaber et al., 1991). Molecular chaperones assist folding and assembly of nascent proteins or folding intermediates by shielding these hydrophobic patches (Lee and Tsai, 2005), thereby greatly reducing the risk of non-native interactions between folding intermediates within the crowded cellular milieu. As correctly folded proteins are released by the molecular chaperones, they can undergo post-translational modifications and reach their cellular localization (Lee and Tsai, 2005). Proteins that do not fold into their native conformations are rapidly eliminated by the ubiquitin-proteasome system (Bukau et al., 2006). The ubiquitin-proteasome system is a complex multi-enzymatic degradation machinery that catalyzes the degradation of misfolded proteins by preventing the accumulation of misfolded proteins. The ubiquitin-proteasome system contributes to maintaining a physiologic balance between folded and misfolded proteins (Ravid and Hochstrasser, 2008).

1.2.1. Folding of proteins traversing the secretory pathway

Approximately one-third of proteins in eukaryotic cells are destined to extracytoplasmic compartments, including the extracellular space, organelles such as lysosomes, and the cell membrane. This project focuses on folding and trafficking of lysosomal proteins; thus these processes will be analyzed in this section in details. Proteins destined to extracytoplasmic compartments are translocated into the Endoplasmic Reticulum (ER) immediately after translation and are processed through the secretory pathway. Folding of secretory proteins occurs in the ER. Only natively folded proteins can exit the ER and move through the Golgi apparatus to their final destinations (Trombetta and Parodi, 2003).

The ER consists of an interconnected network of tubules, vesicles and cisternae (Rapoport, 1992). Secretory proteins are synthesized by ribosomes that are docked onto the ER membrane, guided by the protein sequence that targets the ER (Daniel et al., 2008). Newly synthesized polypeptide chains enter the ER lumen co-translationally through Sec61, a translocation channel embedded in the ER membrane (Daniel et al., 2008). As they are translocated into the ER lumen, polypeptide chains immediately interact with ER resident proteins that assist their folding (Ellgaard et al., 1999). Proteins that achieve a folded state exit the ER and move to the Golgi apparatus, whereas misfolded proteins are retrotranslocated to the cytoplasm for ER-associated degradation (ERAD; (Werner et al., 1996)).

The Golgi apparatus is comprised of a series of five to eight membrane-covered sacs called Golgi cisternae (Griffiths and Simons, 1986). Vesicles that contain ER proteins fuse with the *cis*-Golgi network, progress through the stacks of Golgi cisternae,

and reach the *trans*-Golgi network (Arvan et al., 2002). Each Golgi cisterna contains a variety of enzymes that catalyze glycosylation of secretory proteins and promote their packaging into secretory vesicles. These vesicles are then discharged from the *trans*-Golgi network and move to their final destinations (Alberts et al., 2002; Traub and Kornfeld, 1997).

Lysosomes are acidic organelles rich in hydrolases that catalyze degradation of a variety of metabolic byproducts such as lipids, polysaccharides, and glycoproteins (Kornfeld and Mellman, 1989). The recognition and targeting of lysosomal proteins is mediated by specific receptor proteins, such as the mannose-6-phosphate receptor (M6PR) protein, on the membrane of sorting vesicles that shuttle between the *trans*-Golgi network and lysosomes (Matovcik et al., 1990). Lysosomal hydrolase precursor proteins are tagged with mannose-6-phosphate (M6P) molecules in the *cis*-Golgi apparatus. The M6PR recognizes the M6P tag and thereby mediates sorting and trafficking of lysosomal proteins (Griffiths et al., 1988).

Because lysosomes play a fundamental hydrolytic role in the cell, deficiency in activities of lysosomal hydrolases typically results in accumulation of lysosomal substrates, which often causes the development of devastating human diseases collectively referred to as lysosomal storage disorders (LSDs; Futerman and van Meer, 2004).

1.2.2. The ER folding quality control system

ER chaperones, which make up about 10% of the proteins of the ER lumen, play an important role in promoting protein folding and maturation, and targeting irreversibly

misfolded proteins to ER-associated degradation (ERAD) (Figure 1.3) (Hammond and Helenius, 1995; Nishikawa et al., 2005). As newly synthesized polypeptides are translocated into the ER, they immediately interact with glucose-regulated protein 78 (GRP78/BiP), which facilitates their folding while preventing their aggregation (Nishikawa et al., 2001). Substrates are labeled with oligosaccharide precursors (GlcNAc2-Man9-Glc3) and subsequently trimmed by ER glucosidases to allow recognition by the lectin chaperones (calnexin (CNX) and calreticulin (CRT); (Vembar and Brodsky, 2008)). Upon removal of the outermost glucose residue (GlcNAc2-Man9), natively folded proteins exit the ER and proceed through the secretory pathway, whereas misfolded intermediates are re-glucosylated by UDP-glucose:glycoprotein glucosyltransferase (UGGT). This cycle repeats itself until substrates either fold into their native conformation or are recognized as irreversibly misfolded. Misfolded proteins are extracted from the folding cycle by ER degradation-enhancing α-mannosidase-like lectins (EDEM, (Fagioli and Sitia, 2001; Hosokawa et al., 2003; Lederkremer and Glickman, 2005)). ER mannosidases, particularly mannosidase I, trim three to four mannose residues on the oligosaccharide group to mark misfolded substrates for ERAD (Fagioli and Sitia, 2001; Nakatsukasa and Brodsky, 2008; Wu et al., 2006). Misfolded proteins are then polyubiquitinated by ubiquitin ligases and retrotranslocated via the p97 complex from the ER to the cytoplasm for proteasomal degradation (Figure 1.3) (Fiebiger et al., 2004).

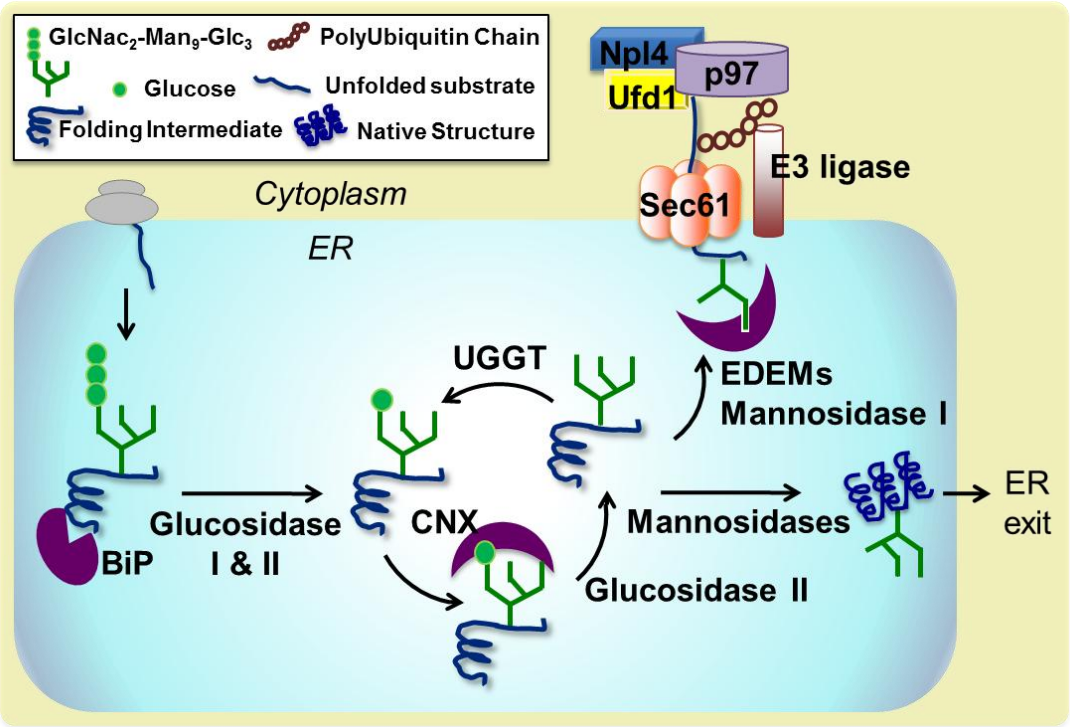

Figure 1.3. The ER quality control system. As newly synthesized polypeptides are translocated into the ER, they are immediately recognized by BiP, which promotes substrate folding and solubility. They are then marked with an oligosaccharide precursor (GlcNAc2-Man9-Glc3), which is sequentially trimmed to allow substrate interaction with the lectin chaperones calnexin (CNX) and calreticulin (CRT). Specifically, interaction with the lectin chaperones occurs upon cleavage of the two terminal glucoses by glucosidase I and II and is terminated by removal of the last outermost glucose residue (GlcNAc2-Man9) by glucosidase II. At this point, natively folded proteins exit the ER while partially folded intermediates are reglucosylated by UDP-glucose:glycoprotein glucosyltransferase (UGGT) and re-enter the lectin folding cycle. In order to prevent excessive accumulation of folding intermediates, unstable misfolding-prone substrates are processed by ER mannosidase I, which cleaves three to four mannose residues from the oligosaccharidic group and promotes substrate binding with the ER degradation-enhancing α-mannosidase-like lectins (EDEM). ERAD substrates are then retrotranslocated to the cytoplasm via the Sec61 retrotranslocon, and polyubiquitinated. Substrate retrotranslocation is mediated by the p97 complex, which includes ubiquitin fusion degradation 1 (Ufd1) and nuclear protein localization 4 (Npl4). p97 ATPase provides the driving force for substrate extraction and shuffling to the proteasome.

Aberrant accumulation of misfolded proteins triggers ER stress, which in turn leads to the induction of the unfolded protein response (UPR) (Hampton, 2000). The

UPR consists of a series of intracellular signal transduction pathways to restore a physiologic balance between folded and misfolded proteins in the ER (Schroder and Kaufman, 2005). The UPR sets two primary responses in the cell: i) inhibition of protein synthesis to reduce the load of newly synthesized proteins that enter the ER and ii) upregulation of ER chaperones. If, however, proteotoxic stress persists, the UPR culminates with induction of apoptosis (Ron and Walter, 2007).

1.3. Lysosomal Storage Disorders (LSDs)

1.3.1. Cellular pathogenesis of LSDs

Lysosomal storage disorders (LSDs) are a group of more than 50 known inherited metabolic diseases characterized by intra-lysosomal accumulation of undegraded metabolites (Futerman and van Meer, 2004). Substrate accumulation gives rise to progressive cellular impairment and organ dysfunction; hence, LSDs affect nearly every part of the body in people of all ages and races. Although leading to different clinical manifestations, the pathogenesis of most LSDs is caused by mutations in genes encoding for specific lysosomal enzyme and loss of the corresponding lysosomal hydrolytic function, which results in substrate accumulation (Futerman and van Meer, 2004).

1.3.2. Gaucher's Disease

Gaucher's disease (GD) is the most common among LSDs with an overall prevalence of 1 in 60,000 people worldwide (Agmon et al., 1993) and with the highest frequency (1 in 1,000) encountered in the Ashkenazi Jewish population (Beutler et al., 1993). GD is an autosomal recessive disorder mainly caused by loss of lysosomal glucocerebrosidase (GC) activity and consequent accumulation of GC substrate, glucosylceramide (Schueler et al., 2004). Affected organs include the spleen, liver, kidneys, lungs, bone marrow and in some patients, even the brain. Patients show varied degrees of hepatosplenomegaly, anemia, thrombocytopenia, skeletal lesion symptoms, and neurodegeneration (Zhao and Grabowski, 2002). GD has been classified in three common clinical subtypes (Grabowski, 1997). Type 1 (adult form) is the most common type of GD, especially in the Ashkenazi Jewish population. Type 2 (acute infantile) and type 3 (chronic) are rarer than type 1, but are associated with neuronopathic symptoms such as brain damage (Grabowski, 1997).

More than 200 mutations in the gene encoding GC (GBA; Hruska et al., 2008) have been identified. Nonsense and splice-site mutations or deletions and insertions have an inactivating effect on the enzyme. Most missense mutations do not directly impair GC catalytic activity but rather destabilize its folding (Grace et al., 1994; Schmitz et al., 2005). Unstable GC variants are retrotranslocated to the cytoplasm for ERAD, leading to partial or complete loss of GC activity in the lysosomes (Figure 1.4). However, unstable GC variants containing misfolding mutations could retain catalytic activity if forced to fold into their native 3D structures (Sawkar et al., 2002; Sawkar et al., 2006b; Yu et al., 2007).

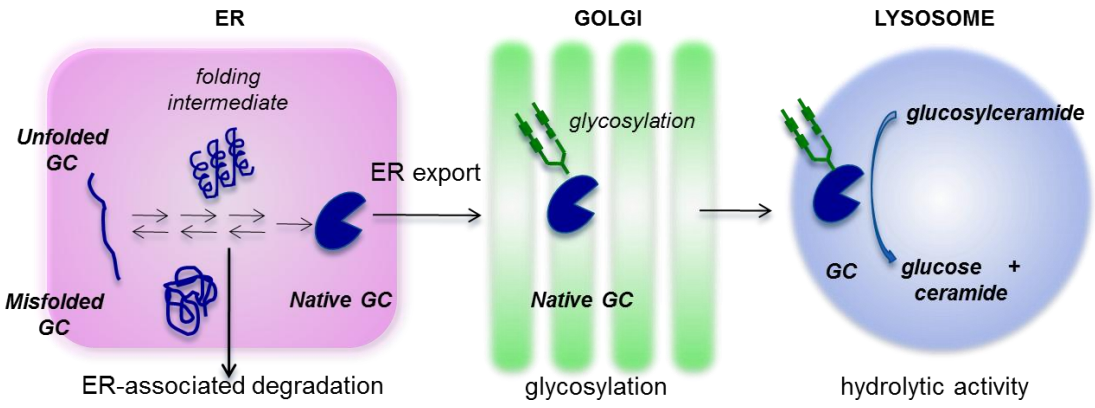

Figure 1.4. Glucocerebrosidase (GC) folding and trafficking through the secretory pathway. Newly synthesized GC progresses through a series of folding intermediates in the ER until it reaches native folding. GC traffics through the Golgi apparatus to the lysosome, where it hydrolyses glucosylceramide to glucose and ceramide. Destabilized GC variants are targeted for degradation through ERAD.

The Leu→Pro substitution at position 444 (L444P) is one of the most frequently encountered misfolding mutations (Figure 1.5) (Schmitz et al., 2005). GD patients who are homozygous for the L444P GC allele typically present severe neuronopathic symptoms (Grabowski, 1997). The L444P substitution severely destabilizes the native structure of GC and results in complete loss of its activity (Grabowski, 1997). L444 is located in the hydrophobic core of a domain structurally distinct from the enzyme catalytic domain. The L444P substitution most likely causes a local conformational change that disrupts the domain's hydrophobic core and leads to domain misfolding (Dvir et al., 2003; Grace et al., 1994). In this study, fibroblasts derived from GD patients homozygous for L444P were used to investigate strategies to modulate the proteostasis network and rescue the native folding of this severely destabilized variant.

Another common mutation is the Asn→Ser substitution at position 370 (N370S; Figure 1.5; Jonsson et al., 1987). N370 resides in the enzyme active site domain. The

N370S GC variant retains about 10% hydrolytic activity of the wild type enzyme (Grace et al., 1994). Although there is no clear link between genotype and phenotype, patients carrying the N370S mutation never present CNS symptoms, suggesting that the residual activity of the N370S GC is sufficient to avoid severe manifestation of the disease.

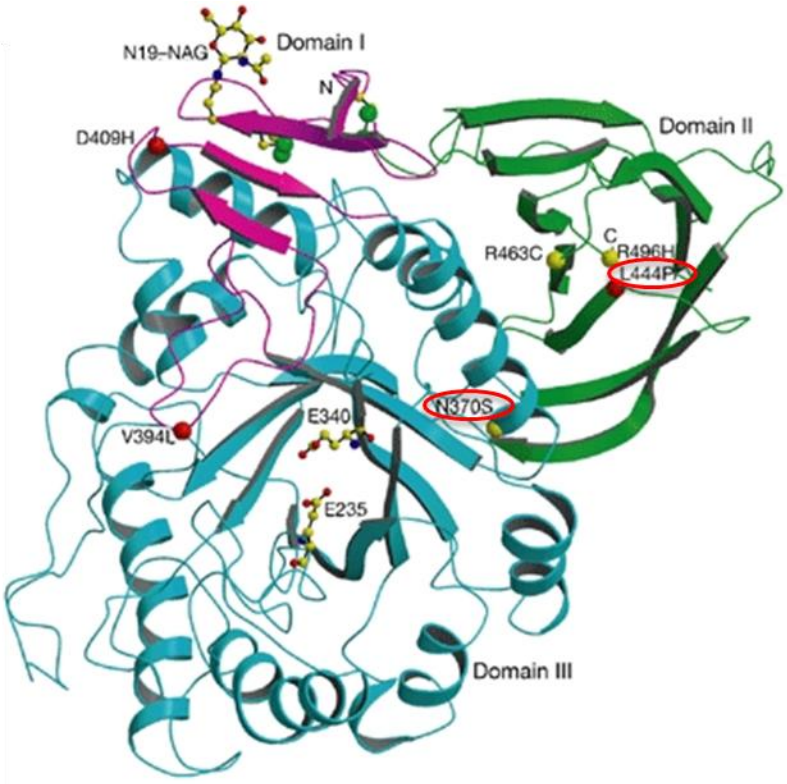

Figure 1.5. X-ray structure of glucocerebridosidase (GC). GC structure contains three domains, which are represented in magenta, green and blue. The two most prevalent GC mutations, L444P and N370S, are circled in red. (Adapted from Dvir *et al*. 2003)

1.3.3. Therapeutic options for Gaucher's disease

Currently available therapeutic options for GD are enzyme replacement therapy (ERT) and substrate reduction therapy (SRT) (Futerman et al., 2004). ERT (Cerezyme®)

consists of intravenous injection of the native enzyme (Beutler, 2004). Although safe and successful for the Type I form of the disease, it is inadequate for neuronopathic forms due to the inability of the injected protein to cross the blood-brain barrier and reach the CNS (Altarescu et al., 2001). In addition, because of the short half-life of the enzyme and consequent poor delivery to certain affected areas, such as bones and lungs, this treatment imposes significant burdens on the patients, including weekly injections and considerably high costs (Desnick and Schuchman, 2002; Wraith, 2006). An alternative treatment is SRT, which is based on the use of small molecule N-butyldeoxynojirimycin (NB-DNJ, Zavesca®) (Cox et al., 2000; Platt et al., 2001). NB-DNJ prevents the synthesis of glucosylceremide by inhibiting glucosyltransferase, an enzyme involved in the biosynthesis of glycosphingolipids in the Golgi (Futerman and Pagano, 1991; Jeckel et al., 1992; Trinchera et al., 1991). Glucosyltransferase inhibition allows restoring the cellular physiologic ratio of substrate concentration to GC hydrolytic activity, thereby reducing substrate buildup in the lysosome. However, because NB-DNJ treatment reduces synthesis of all the gluco-based glycolipids, considerable side effects arise (Buccoliero et al., 2002; Kolter et al., 2002). Thus, SRT is only used to treat non-neuronopathic GD patients for whom ERT is not an option (Cox et al., 2003).

A number of small molecule "chemical chaperones" have been recently reported to provide an alternative therapeutic option for the treatment of GD based on rescuing the native folding of mutated GC variants. Chemical chaperones are small molecules that are structurally similar to the enzyme inhibitors, bind to the misfolding-prone enzymes and stabilize their conformations, thus facilitating ER export and trafficking to the lysosomes (Fan, 2003; Ulloa-Aguirre et al., 2004). Natively folded mutated enzyme variants are

often stable once they reach the lysosome, as they were evolutionarily selected to be stable at acidic pH. Chemical chaperones are displaced by the enzyme substrate, which is typically present at high concentration in the lysosomes. Chemical chaperone-based treatments have been recently explored to rescue the folding of mutated enzyme variants in GD cells (Sawkar et al., 2006b). In particular, treatment of fibroblasts from GD patients with N-(n-nonyl)-deoxynojirimycin (NN-DNJ) enhances ER secretion and lysosomal activity of N370S GC (Sawkar et al., 2002). Chemical chaperone therapy (CCT) has the potential to combine the advantages of both ERT and SRT, namely oral bioavailability, potential to cross the blood brain barrier, and low cost. However, only GC variants containing mutations in the active site domain are amenable to chemical chaperoning. This feature is likely due to the intrinsic mechanism of chemical chaperones that stabilize the folded enzyme pool by mimicking the mechanism of binding of the enzyme inhibitor and thus interacting specifically with the enzyme active site. GD cells harboring the L444P GC mutation, which resides in a structural region separate from the enzyme active site domain, are rarely responsive to CCT (Khanna et al., 2010). As mentioned before, L444P is the most common mutation associated with the neuronopathic form of GD. Hence, the cure of neuronopathic GD, as well as a number of other neuronopathic LSDs, remains a completely unmet medical need.

1.3.4. Tay-Sachs disease

Tay-Sachs disease is caused by deficient activity of lysosomal enzyme hexosaminidase A (HexA) and cellular storage of gangliosides GM2 (N-AcGalβ1,4(NeuAcα2,3)Galβ1,4Glc-ceramide) (Jeyakumar et al., 2002; Tropak et al.,

2004). Mutations in the gene encoding HexA impair HexA folding and lead to extensive ERAD, which causes loss of HexA activity in the lysosome (Jeyakumar et al., 2002). The G269S substitution, one of the most prevalent HexA mutations, is a misfolding, non-inactivating mutation (Maegawa et al., 2007). Similar to GC variants containing misfolding mutations, native folding of G269S HexA mutant results in increase in enzymatic activity (Mu et al., 2008b; Tropak et al., 2004).

1.4. Ca^{2+} homeostasis

1.4.1. Intracellular Ca^{2+} homeostasis

The ER is the main dynamic Ca^{2+} storage compartment in the cell (Meldolesi and Pozzan, 1998). This organelle regulates Ca^{2+} flows in response to extracellular stimuli or intracellular signaling by releasing Ca^{2+} ions from the ER ($[Ca^{2+}]$=1 mM) and taking up Ca^{2+} ions from the cytosol ($[Ca^{2+}]$=100 nM) (Brostrom and Brostrom, 2003; Verkhratsky, 2005). Even though $[Ca^{2+}]_{ER}$ is estimated to be in the mM range, the concentration of free Ca^{2+} ions in the ER is much lower due to the presence of Ca^{2+}-binding proteins that bind Ca^{2+} ions with high capacity and low affinity (Meldolesi and Pozzan, 1998). Some of these proteins function as Ca^{2+} buffers and are capable of rapidly releasing large fluxes of Ca^{2+} to the cytosol upon ER channel openings. Other Ca^{2+}-dependent proteins are ER luminal chaperones such as BiP, Calnexin, and Calreticulin. Thus, fluctuations in $[Ca^{2+}]_{ER}$ affect the activities of ER chaperones and the maintenance of Ca^{2+} homeostasis is crucial to guarantee the folding of proteins in the ER (Michalak et al., 2002).

The maintenance of intracellular Ca^{2+} homeostasis is achieved by regulating Ca^{2+} channels in the ER membrane as well as those in the plasma membrane. Ca^{2+} is released from the ER through ryanodine receptors (RyR) or inositol 1,4,5-trisphosphate (IP3) receptors, and pumped into the ER by Ca^{2+}-ATPases (SERCA pumps; Figure 1.6) (Baumann and Walz, 2001). The entry of Ca^{2+} across the cell membrane involves voltage and ligand-gated Ca^{2+} channels, such as L-type voltage-gated Ca^{2+} channels (LTCC) (Lee et al., 2002; Putney et al., 2001).

1.4.2. Impairment of Ca^{2+} homeostasis in GD

The hallmark of GD is the accumulation of glucosylceramide, GC substrate, which may lead to impairment of neuronal functions. Particularly, neurons show enhanced levels of tubular ER elements and an increase in ER Ca^{2+} release (Korkotian et al., 1999). Analyses of Ca^{2+} release from rat brain microsomes cultured in the presence of glucosylceramide revealed that glucosylceramide induces Ca^{2+} release via RyR (Figure 1.6), through a mechanism that may involve the redox sensor of the RyR, but has no effect on Ca^{2+} release via IP3 receptors. A number of other glycosphingolipids and sphingolipids were not found to affect Ca^{2+} release (Lloyd-Evans et al., 2003). In addition, it was shown that enhancement of ER Ca^{2+} release by glucosylceramide via the RyR leads to neuronal cell death, suggesting that impaired Ca^{2+} homeostasis may play a significant role in the neuropathophysiology of GD (Pelled et al., 2005).

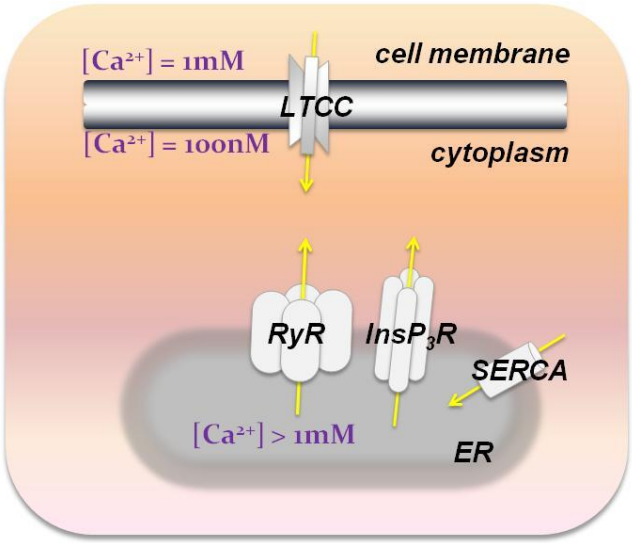

Figure 1.6. Impairment of Ca^{2+} homeostasis in GD cells. $[Ca^{2+}]_{ER}$ is regulated by ryanodine receptors (RyR), inositol 1,4,5-trisphosphate ($InsP_3R$) receptors, and Ca^{2+}-ATPases (SERCA pumps). L-type voltage-gated Ca^{2+} channels (LTCC) mediate Ca^{2+} flow through the plasma membrane. The accumulation of GC substrate, glucosylceramide, causes Ca^{2+} release via RyR.

1.4.3. Impairment of Ca^{2+} homeostasis is a common theme among LSDs

Evidence shows impairment of Ca^{2+} homeostasis in a number of LSDs. Excessive accumulation of ganglioside GM2 in a mouse model of Sandhoff disease significantly reduces the rate of ER Ca^{2+} uptake through SERCA pumps. This effect was prevented by feeding Sandhoff disease mice with N-butyl-deoxynojirimycin (NB-DNJ), an inhibitor of glycolipid synthesis that reduces GM2 storage (Pelled et al., 2003). Changes in SERCA activity could be mimicked by culturing neuronal cells derived from the mouse model of Sandhoff disease in the presence of a SERCA inhibitor, thapsigargin, or by adding GM2 to the culture medium (Pelled et al., 2003). Reduced ER Ca^{2+} uptake through SERCA pump caused by substrate accumulation was also observed in a mouse model of Niemann–Pick A disease (Ginzburg and Futerman, 2005).

Chapter 2

State of the art

2.1. Proteostasis regulators

Modulation of the proteostasis network was recently explored as a strategy to rescue the folding of unstable proteins. Small molecules that modulate general cellular pathways to influence protein folding and degradation were reported to rescue the folding of unstable, degradation-prone proteins (Lu et al., 2010; Mu et al., 2008b). These small molecules were thus defined as proteostasis regulators (Balch et al., 2008). Proteostasis regulators were shown to enhance the folding, trafficking and activity of multiple enzyme variants associated with the development of two clinically distinct LSDs, namely Gaucher's and Tay-Sachs disease (Mu et al., 2008b). A table summarizing the small molecules used in this study is reported in Appendix A.

2.1.1. Celastrol

The heat shock response is a conserved reaction of the cell in all organisms to elevated temperatures (heat shock or heat stress) or other stressful stimuli (Lindquist, 1986). Its activation leads to the upregulation of heat shock proteins that promote native folding and prevent denaturation and aggregation of misfolded proteins (Lindquist, 1986; Morimoto et al., 1997). The expression of heat shock proteins is regulated by the transcription heat shock factor 1 (Wu, 1995).

Celastrol is a small molecule that induces the heat shock response in human cells through the activation of the heat shock transcription factor 1 (Appendix A; Westerheide et al., 2004; Wu, 1995). Treatment of fibroblasts derived from GD patients with celastrol was shown to partially restore the folding of multiple GC variants (Mu et al., 2008b). The activity of L444P GC was dramatically enhanced to 23% of wild type cellular activity, which would be compatible with effective treatment (Schueler et al., 2004). Celastrol treatment was also reported to enhance GC activity in GD cells harboring N370S and G202R GC variants (Mu et al., 2008b). However, the narrow therapeutic window of celastrol (0.2-1 μM, due to the cytotoxicity observed using higher concentrations) is a major concern associated with the use of celastrol as a drug candidate. Nevertheless, celastrol was used to demonstrate proof-of-principle that it is possible to modulate general pathways that control proteostasis to rescue the native folding of unstable proteins and to motivate the discovery of less toxic equivalents.

2.1.2. MG-132

Inhibition of proteasomal degradation causes accumulation of misfolded proteins, which, in turn, leads to upregulation of chaperone expression in the cytoplasm and in the ER (Awasthi and Wagner, 2005; Bush et al., 1997; Liao et al., 2006). Treatment of GD patient-derived cells with a widely used proteasome inhibitor, MG-132, dramatically rescues folding and activity of L444P GC (Appendix A; Mu et al., 2008b; Schueler et al., 2004). In cells treated with MG-132, the L444P GC variant, which is normally barely detectable in the lysosome due to extensive ERAD, is trafficked to the lysosome to an extent similar to WT GC (Sawkar et al., 2005). However, MG-132 also present a narrow therapeutic window (0.2-0.8 μM) and results in cytotoxicity if administered at high concentrations (Mu et al., 2008b).

2.1.3. Proteostasis regulation in fibroblasts derived from patients with Tay-Sachs disease

Modulation of the proteostasis network to rescue native folding of unstable, degradation-prone proteins was also explored in fibroblasts derived from patients with Tay-Sachs disease, an LSD clinically distinct from GD but also caused by deficiency of a fundamental lysosomal enzyme. As previously described, Tay-Sachs disease is caused by mutations in the gene encoding hexosaminidase A (HexA, (Tropak et al., 2004)). Impaired folding of HexA in the ER leads to extensive ERAD and consequent loss of lysosomal HexA activity (Jeyakumar et al., 2002). The G269S mutation destabilizes HexA native structure causing loss of enzyme activity. MG-132 treatment enhances

HexA activity to a level expected to ameliorate clinical symptoms (Mu et al., 2008b; Tropak et al., 2004). Similar results were observed in cells treated with celastrol (Mu et al., 2008b). Interestingly, the highest increase of HexA activity in Tay-Sachs cells was obtained using the same range of concentration of celastrol and MG-132 reported in the Gaucher's disease study.

2.2. Modulation of Ca^{2+} homeostasis

The use of inhibitors of Ca^{2+} channels was also explored as a strategy to enhance the cellular folding capacity by modulating the proteostasis network.. In GD neurons, glucosylceramide accumulation impairs Ca^{2+} homeostasis by depleting $[Ca^{2+}]_{ER}$ via RyRs (Korkotian et al., 1999; Lloyd-Evans et al., 2003; Pelled et al., 2005). The folding and activity of mutated GC was enhanced in GD cells cultured in the presence of calcium channel blockers, and in particular L-type Ca^{2+} channels (LTCC) blockers such as diltiazem and verapamil (Mu et al., 2008a).

LTCC blockers bind to high voltage activated channels on the plasma membrane and thus lower cytosolic free $[Ca^{2+}]$ (Hockerman et al., 1997; Triggle, 2006). Phenylalkylamines, benzothiazepines, and 1,4-dihydropyridines are the three main classes of LTCC blockers and act by binding to three distinct LTCC receptor sites (Hockerman et al., 1997). Verapamil and diltiazem, prototypes of phenylalkylamines and benzothiazepines, respectively, are FDA-approved drugs for the treatment of hypertension and cardiac arrhythmias (Hockerman et al., 1997). Mu *et al.* reported that treatment with either diltiazem or verapamil inhibits LTCC and partially restores the

activity of N370S and L444P GC in fibroblasts derived from GD patient (Mu et al., 2008a). The authors also reported that treatment with diltiazem or verapamil rescue the folding of mutated enzyme variants associated with neuronopathic forms of other LSDs, namely α-mannosidosis and type IIIA mucopolysaccharidosis (Mu et al., 2008a).

Chapter 3

Objectives

The objective of this work is to develop cell and protein engineering strategies to restore the folding and activity of unstable, degradation-prone enzyme variants associated with the development of lysosomal storage disorders (LSDs). LSDs are a group of inherited diseases characterized by deficient activities of lysosomal enzymes. A number of enzyme variants derive from mutations that do not impair enzyme activity, but rather destabilize their native folding. Mutated proteins that fail to fold into their native conformation are retrotranslocated to the cytoplasm for ER-associated degradation (ERAD). However, if these mutated protein variants can be forced to fold into their 3D native structure, they retain their catalytic activity. The aim of this work is to modulate endogenous cellular pathways that underlie maintenance of protein folding (the proteostasis network) to enhance the innate folding capacity of the cell and promote native folding of unstable protein variants.

Gaucher's disease (GD), the most common LSD, is used as a model system in this study. Evidence showed that culturing fibroblasts derived from GD patients at reduced permissive temperature results in enhanced folding and activity of mutated GC variants (Sawkar et al., 2006a). These culturing conditions are expected to influence the cellular folding pathways thereby providing a folding environment favorable for mutated GC folding. For this reason, we hypothesized that the innate protein folding machinery under physiologic conditions is unable to cope with the destabilizing effect of the L444P substitution. To test this hypothesis, we propose to modulate the proteostasis network to enhance the innate cellular folding capacity of fibroblasts derived from patients with GD and test the folding, cellular localization and activity of mutated enzyme variants.

Loss of GC activity has been repeatedly studied in patient-derived fibroblasts (Jonsson et al., 1987). The cellular accumulation and enzymatic activity of GC variants in fibroblasts are used as an indication of the severity of GD manifestations and of the development of neuronopathic symptoms (Beutler et al., 1984; Michelakakis et al., 1995). Moreover, patient-derived fibroblasts are specifically used for diagnostic purposes because residual activity of mutated GC variants is related to the clinical severity of the disease (Bodamer and Hung; Meivar-Levy et al., 1994). Thus, fibroblasts derived from patients with GD were used in this study. Particularly, we focused on fibroblasts derived from patients carrying the L444P GC allele because it is normally associated with neuronopathic symptoms in homozygous patients.

This work is organized under the following specific aims:

Aim 1. Modulating Ca^{2+} homeostasis to enhance the folding and activity of mutated GC. The accumulation of GC substrate, glucosylceramide, causes Ca^{2+} efflux

from the ER through RyRs. Since $[Ca^{2+}]_{ER}$ affects the function of the ER chaperones, we suspected that excessive $[Ca^{2+}]_{ER}$ efflux impairs ER folding in GD cells. We hypothesized that folding and activity of mutated GC variants could be rescued by counteracting the effect of glucosylceramide accumulation on **[**$Ca^{2+}]_{ER}$ depletion. We used RyR blockers and LTCC blockers to restore intracellular Ca^{2+} homeostasis and study the effect of $[Ca^{2+}]_{ER}$ on the folding of the L444P GC mutant in patient-derived fibroblasts.

Aim 2. Inhibiting ERAD to prolong ER retention of mutated GC. We hypothesized that ERAD, which catalyzes the degradation of misfolded proteins, is the rate limiting steps in the folding of unstable enzyme variants. We propose to inhibit specific steps of the ERAD pathway to prevent the disposal of mutated enzyme and enhance the pool of folding intermediates amenable to folding rescue. We treated fibroblasts derived from patients with GD with small molecules that target the recognition or retrotranslocation of misfolded substrates for ERAD pathway and evaluate the folding and activity of enzyme variants.

Chapter 4

Results

4.1. Ca^{2+} homeostasis modulation enhances the amenability of L444P glucosylcerebrosidase to proteostasis regulation in fibroblasts derived from patients with Gaucher's disease

4.1.1. Introduction

Ca^{2+} homeostasis plays a fundamental role in the biogenesis of secretory proteins. The activities of a number of ER chaperones including BiP/GRP78, Calnexin (CNX), and Calreticulin (CRT) are influenced by fluctuations in $[Ca^{2+}]_{ER}$ (Michalak et al., 2002), which is highly regulated through Ca^{2+} release and uptake mechanisms. In GD cells, the accumulation of GC substrate, glucosylceramide, causes excessive $[Ca^{2+}]_{ER}$ release, specifically via RyRs (Korkotian et al., 1999; Lloyd-Evans et al., 2003; Pelled et al., 2005). We speculated that by affecting ER Ca^{2+} mobilization, glucosylceramide accumulation impairs ER folding, and thus may further hamper the folding of unstable

GC variants. Interestingly, impairment of Ca^{2+} homeostasis is a common theme in LSDs, as substrate accumulation causes lowered $[Ca^{2+}]_{ER}$ in Sandhoff disease (Pelled et al., 2003) and Niemann-Pick type A disease (Ginzburg and Futerman, 2005)

Based on the notions that i) $[Ca^{2+}]_{ER}$ affects ER chaperone expression and activity (Michalak et al., 2002), and ii) mutated GC folding is rescued by enhancement of the innate cellular folding capacity (Mu et al., 2008b), we hypothesized that the folding of LSD-associated enzymes could be restored by inhibiting $[Ca^{2+}]_{ER}$ depletion. We used fibroblasts derived from patients with GD carrying the L444P GC allele to investigate the effect of $[Ca^{2+}]_{ER}$ modulation on the folding, trafficking and activity of this unstable GC variant. We demonstrated that modulation of $[Ca^{2+}]_{ER}$ through inhibition of RyRs in L444P GC fibroblasts, although not directly promoting considerable rescue of L444P GC folding, creates a "wild-type like" ER environment, more amenable to proteostasis regulation, particularly through upregulation of the ER chaperone BiP. We also profiled global gene expression of cells treated with a RyRs blocker and a proteostasis modulator, MG-132, and report mechanistic studies validating the influence of selected ER chaperones, and particularly BiP, on L444P GC folding.

4.1.2. Results

Inhibition of $[Ca^{2+}]_{ER}$ depletion enhances MG-132 function as a proteostasis regulator in fibroblasts derived from GD patients carrying L444P GC

Fibroblasts derived from patients with GD carrying the L444P GC variant were treated with small molecule RyRs blockers, including ryanodine (Appendix A; Buck et al., 1992; Nagasaki and Fleischer, 1988), dantrolene (Appendix A; Ward et al., 1986),

ruthenium red (Buck et al., 1992), and 1,1'-diheptyl-4,4'-bipyridinium (DHBP) dibromide (Buck et al., 1992; Kang et al., 1994), and GC activity was evaluated with the intact cell GC activity assay as previously described (Sawkar et al., 2002). L444P GC activity was observed to increase up to 1.3-fold in cells treated with ryanodine (10-20 μM final medium concentration) for 48 hrs, and decrease with increasing time of incubation. Although this modest increase in GC activity is expected to ameliorate GD symptoms (Schueler et al., 2004), we attempted to further enhance ryanodine-mediated L444P GC folding by combining ryanodine with a proteostasis regulator, MG-132, which is known to rescue L444P GC folding through a mechanism distinct from $[Ca^{2+}]_{ER}$ modulation (Mu et al., 2008b). Co-administration of ryanodine (20 μM) and MG-132 (0.4 μM) for 72 hrs resulted in a 2.6-fold increase ($p<0.001$) in L444P GC activity compared to untreated cells, which is higher than the increase in activity observed using ryanodine (1.1-fold) or MG-132 (2.1-fold) under the same conditions (Figure 4.1.1A). We hypothesized that ryanodine at least partially restores Ca^{2+} homeostasis, reestablishing a "wild type-like" folding environment in the ER of L444P GC fibroblasts that is normally characterized by Ca^{2+} efflux induced by substrate accumulation and thus impaired folding. Restoring a more "wild-type like" ER environment is not sufficient to considerably enhance the folding of L444P GC, a severely destabilized enzyme variant normally immediately targeted to ERAD. However, by preventing $[Ca^{2+}]_{ER}$ depletion, ryanodine treatment renders L444P GC cells more amenable to proteostasis regulation via MG-132.

Among the RyRs blockers tested, dantrolene was also observed to enhance L444P GC activity increase induced by MG-132 treatment. Co-administration of dantrolene (1 μM) and MG-132 (0.4 μM) resulted in 2.1-, 2.3-, and 2.5-fold increase in L444P GC

activity after 48, 72 and 96 hours of incubation, respectively (Figure 4.1.1B). Ruthenium red and DHBP were observed to marginally influence L444P GC activity, and were not used in further studies due to their cytotoxic effect (data not shown).

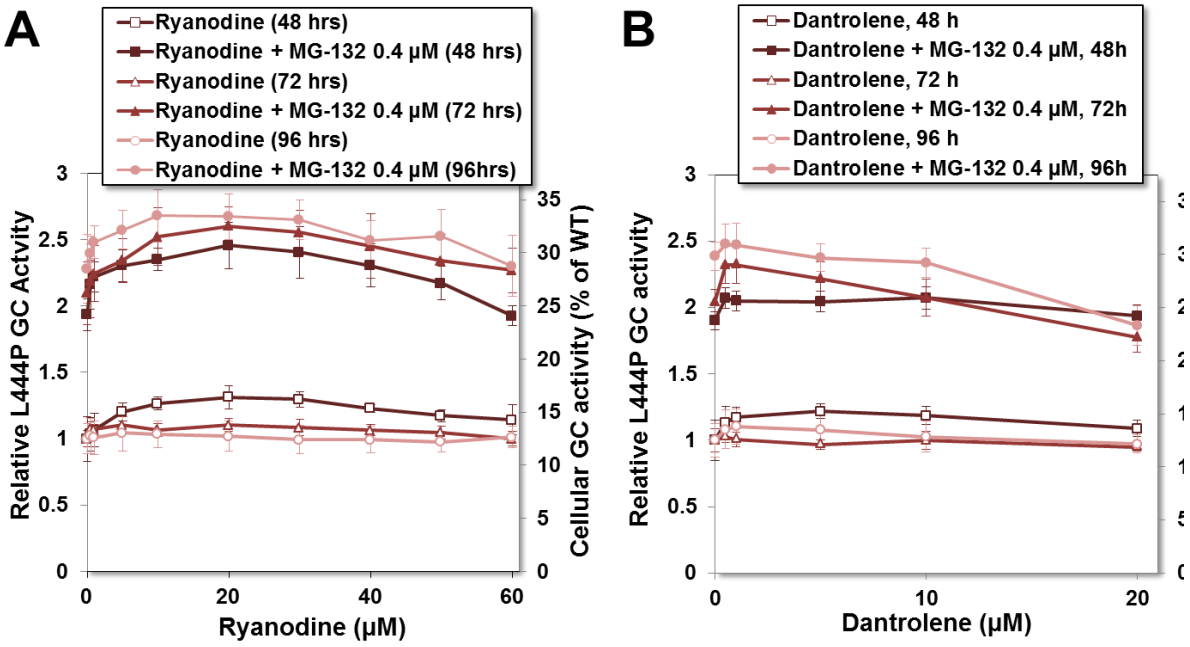

Figure 4.1.1. Treatment with RyRs blockers and MG-132 enhances GC activity in L444P GC patient-derived fibroblasts. Cells were cultured with **A)** ryanodine and MG-132, and **B)** dantrolene and MG-132. GC enzymatic assays were performed after 48, 72 and 96 hrs. Reported L444P GC activities were normalized to the activity of untreated cells (left y axis) and corresponded to the fraction of WT GC activity (right y axis). The data is reported as mean ± SD.

Because glucosylceramide accumulation causes $[Ca^{2+}]_{ER}$ depletion, we hypothesized that inhibition of glucosylceramide synthesis would provide an alternative mechanism to RyRs inhibition to prevent abnormal $[Ca^{2+}]_{ER}$ efflux. Inhibition of glucosylceramide synthesis was investigated using N-butyl-deoxynojirimycin (NB-DNJ; Appendix A) (Platt et al., 2001) and MG-132. A barely detectable increase in L444P GC activity was observed in patient-derived fibroblasts cultured with NB-DNJ for up to 192

hrs and assayed every 24hrs. However, co-administration of NB-DNJ (5 nM) and MG-132 (0.4 μM) resulted in 2.8-fold increase in L444P GC activity ($p<0.01$), which is higher than the 2.3-fold increase obtained with MG-132 alone (Figure 4.1.2), demonstrating that inhibition of glucosylceramide synthesis in GD cells recapitulates the effect of RyRs blockers on L444P GC folding.

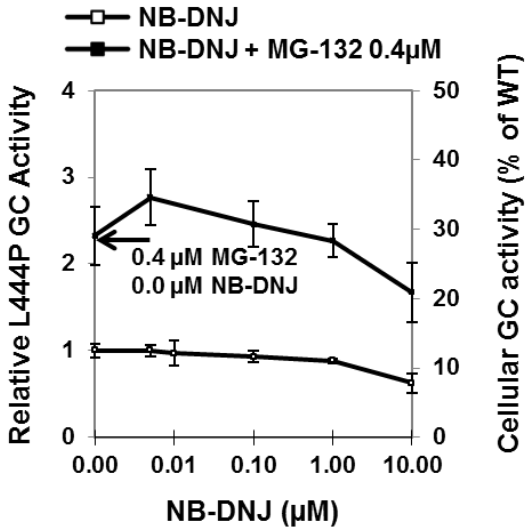

Figure 4.1.2. Inhibition of glucosylceramide synthesis enhances the activity of L444P GC in patient-derived fibroblasts. Cells were treated with NB-DNJ and MG-132 for 192 hrs. Relative GC activities ($p<0.01$) were calculated as described in Figure 4.1.1. Experiments were repeated three times; data points were reported as mean ± SD.

To confirm that the detected increase in GC activity is caused by partial restoration of L444P GC folding and trafficking, the protein's glycosylation state was evaluated with endoglycosidase H (EndoH). EndoH hydrolyzes immature N-glycan complexes; thus, Western blot analyses of EndoH treated proteins using a GC specific antibody reveal a low MW band corresponding to partially glycosylated, ER-retained GC (EndoH-sensitive) and a high MW band corresponding to fully glycosylated lysosomal GC (EndoH-resistant) (Maley et al., 1989). The total protein content of cells cultured

with ryanodine (20 μM), dantrolene (1 μM), MG-132 (0.4 μM), or a combination thereof, was subjected to EndoH treatment and GC was detected by Western blot (Figure 4.1.3A). The quantification of EndoH-sensitive or resistant bands is reported in Figure 4.1.3B. In untreated cells 90% of L444P GC was EndoH-sensitive, and total GC amount and glycosylation state did not change with cell growth (Figure 4.1.3A-B). Dantrolene or ryanodine treatment resulted in a 1.6- and 1.9-fold increase in total L444P GC, respectively, and a decrease of EndoH-sensitive fraction to 60% of total GC (Figure 4.1.3B). MG-132 treatment caused an increase of total and EndoH-resistant L444P GC, as previously reported (Mu et al., 2008b). In cells treated with MG-132 and ryanodine or MG-132 and dantrolene (corresponding to 2.5- and 2.1-fold activity increase, respectively), the total GC content increased 2.4- and 2.1-fold, respectively, and nearly 50% of L444P GC was present in the EndoH-resistant form (Figure 4.1.3B).

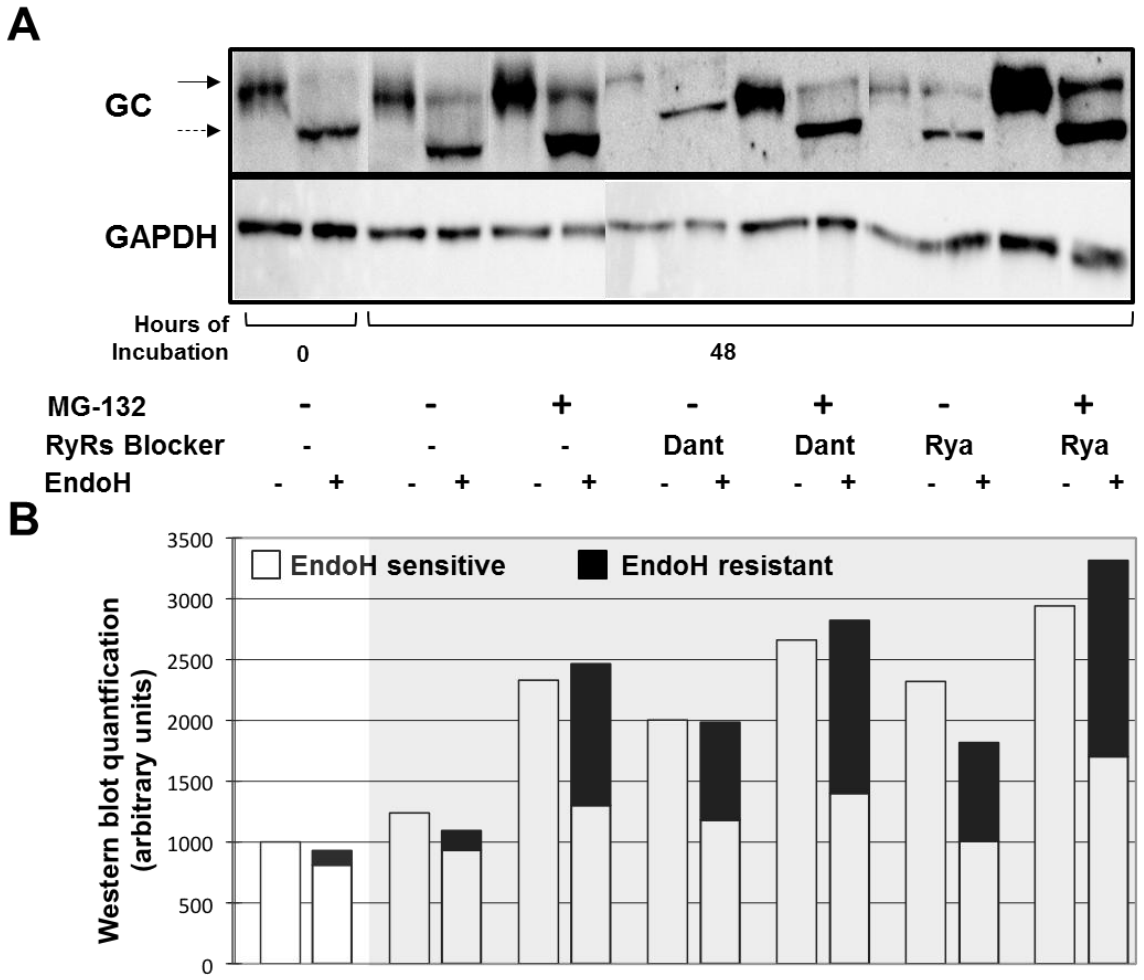

Figure 4.1.3. L444P GC glycosylation state of patient-derived fibroblasts treated with RyRs blockers and MG-132. A) L444P GC glycosylation state in cells treated with ryanodine (20 μM), dantrolene (1 μM), MG-132 (0.4 μM), or a combination thereof for 48 hrs. EndoH treated and untreated samples were analyzed by Western blot. **B**) Quantification of bands in EndoH-treated samples. EndoH-sensitive bands (ER retained GC) is reported in the white portion of the bars, and that of EndoH-resistant bands (lysosomal GC) is reported in the black top portions. Band analyses and quantifications were conducted using NIH Java Image analysis software. Dant: Dantrolene; Rya: Ryanodine.

BiP expression is upregulated in fibroblasts derived from GD patients carrying L444P GC treated with ryanodine and MG-132

Cell treatment with MG-132 and ryanodine partially restore L444P GC activity to 33% of wild type GC, which is expected to be compatible with effective treatment

(Schueler et al., 2004). Thus, RyRs blockers and MG-132 were used to identify transcriptional changes in the proteostasis network potentially associated with the rescue of L444P GC folding.

Quantitative RT-PCR of the mRNA for representative ER chaperones was used to investigate the influence of RyRs blockers and MG-132 on the ER folding machinery (Kleizen and Braakman, 2004). L444P GC cells were incubated with MG-132 (0.4 μM), dantrolene (1 μM), ryanodine (20 μM), or a combination thereof (Figure 4.1.4), and relative mRNA expression levels for BiP, Calnexin (CNX), Calreticulin (CRT), and GRP94 were evaluated. BiP expression was increased by ryanodine treatment (2.4-fold), and ryanodine and MG-132 co-treatment (6.0-fold). Similar results were obtained with dantrolene (2.7-fold), and dantrolene and MG-132 (2.9-fold) (Figure 4.1.4A). The difference in ryanodine- and dantrolene-mediated BiP upregulation might result from their binding to distinct sites of RyRs (Fill and Copello, 2002). Analogous results were observed for CNX expression upon treatment with ryanodine (3.1-fold), and ryanodine and MG-132 (5.3-fold), or treatment with dantrolene (1.8-fold), and dantrolene and MG-132 (3.2-fold) (Figure 4.1.4B). Enhancement of CRT and GRP94 mRNA expression was altered less than 2.5-fold (Figure 4.1.4C and D).

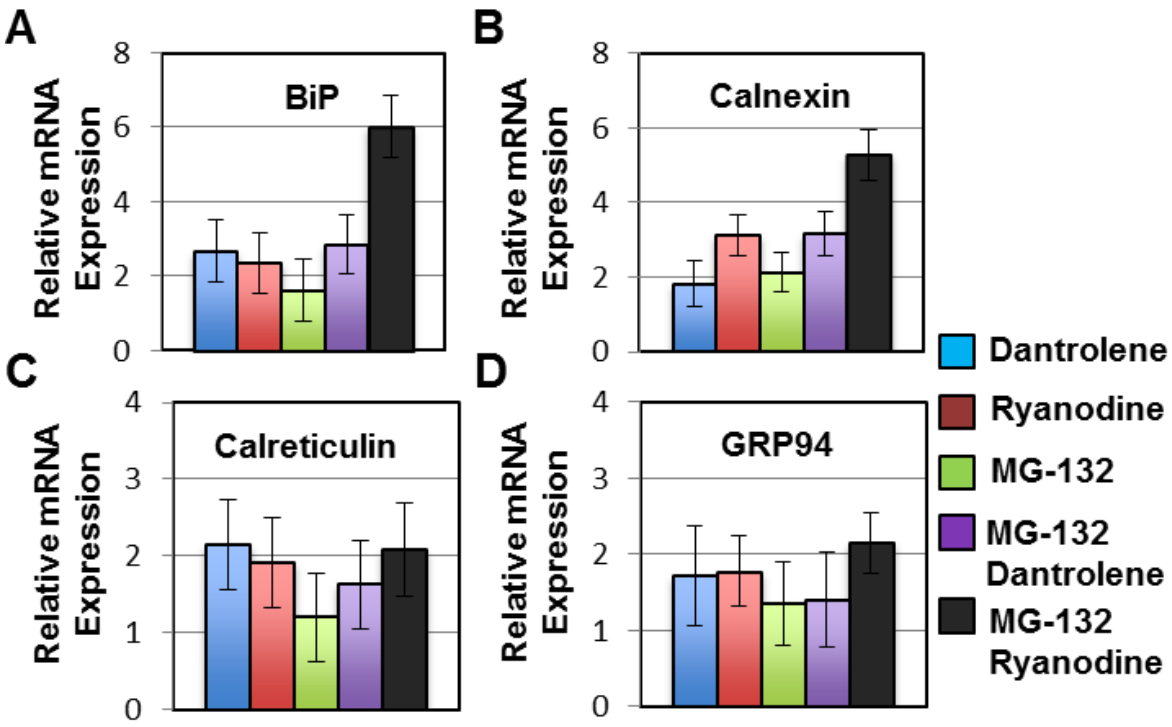

Figure 4.1.4. Transcriptional expression of representative ER chaperones in L444P GC patient-derived fibroblasts treated with RyRs blockers and MG-132. Relative mRNA expression of **A**) BiP ($p<0.01$), **B**) CNX ($p<0.01$), **C**) CRT ($p<0.05$), and **D**) GRP94 ($p<0.05$) evaluated by quantitative RT-PCR in L444P GC fibroblasts treated with ryanodine (20 μM), dantrolene (1 μM) and MG-132 (0.4 μM) for 24 hrs. mRNA expression levels of treated cells were corrected for the expression of the housekeeping gene GAPDH, and normalized to those of untreated cells. The data is reported as mean ± SD.

ER chaperone protein concentrations in cells treated with ryanodine and MG-132 were evaluated by Western blot (Figure 4.1.5A) and bands were quantified with ImageJ software (Figure 4.1.5B). BiP protein accumulation was enhanced by co-treatment with ryanodine and MG-132 (2-fold), compared to untreated cells or cells treated with either molecule, but we failed to observe significant changes in CNX, CRT, and GRP94 protein levels. These results are consistent with RT-PCR analyses; with the exception of CNX expression, for which the transcriptional increase is not reflected at the translational level,

suggesting that CNX upregulation induced by cell treatment with MG-132 and ryanodine does not translate into enhanced accumulation of CNX protein.

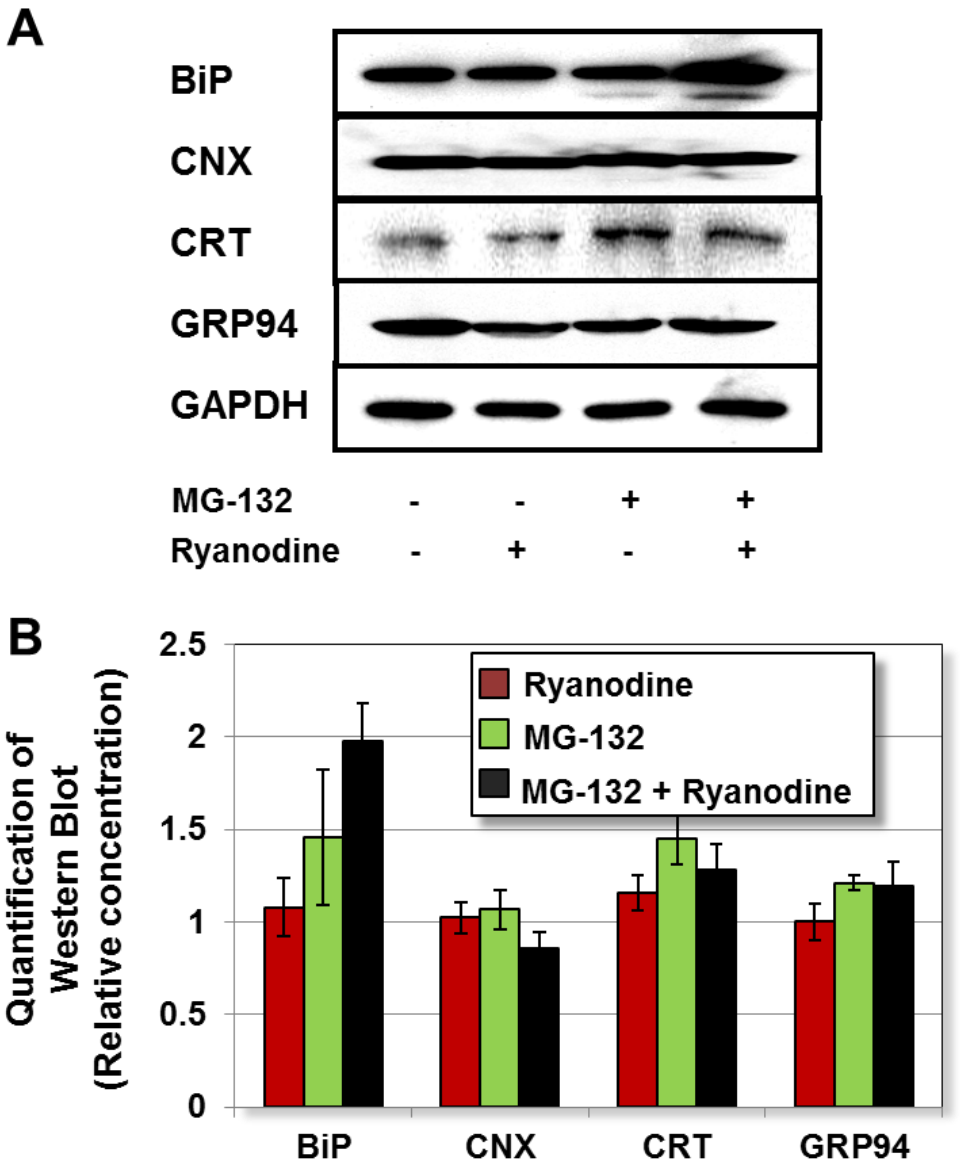

Figure 4.1.5. Translational expression of representative ER chaperones in L444P GC patient-derived fibroblasts. A) Western blot analyses and **B**) quantification of representative ER chaperones in cells treated with ryanodine (20 μM), and MG-132 (0.4 μM) for 48 hrs. GAPDH expression is used as loading control. Experiments were repeated three times and the data is reported as mean ± SD.

Proteostasis regulation and modulation of Ca^{2+} homeostasis alters global gene expression in fibroblasts derived from GD patients carrying L444P GC

Global gene expression was evaluated as described in Materials and Methods in cells treated with MG-132 (0.4 μM), ryanodine (20 μM), and both MG-132 and ryanodine, for 24 hrs. We particularly focused on the expression of genes encoding for ER chaperones, UPR-associated proteins, LSD, lipid metabolism, and ERAD (Figure 4.1.6; expression levels are reported as fold-change relative to untreated cells in Appendix B; $p<0.01$).

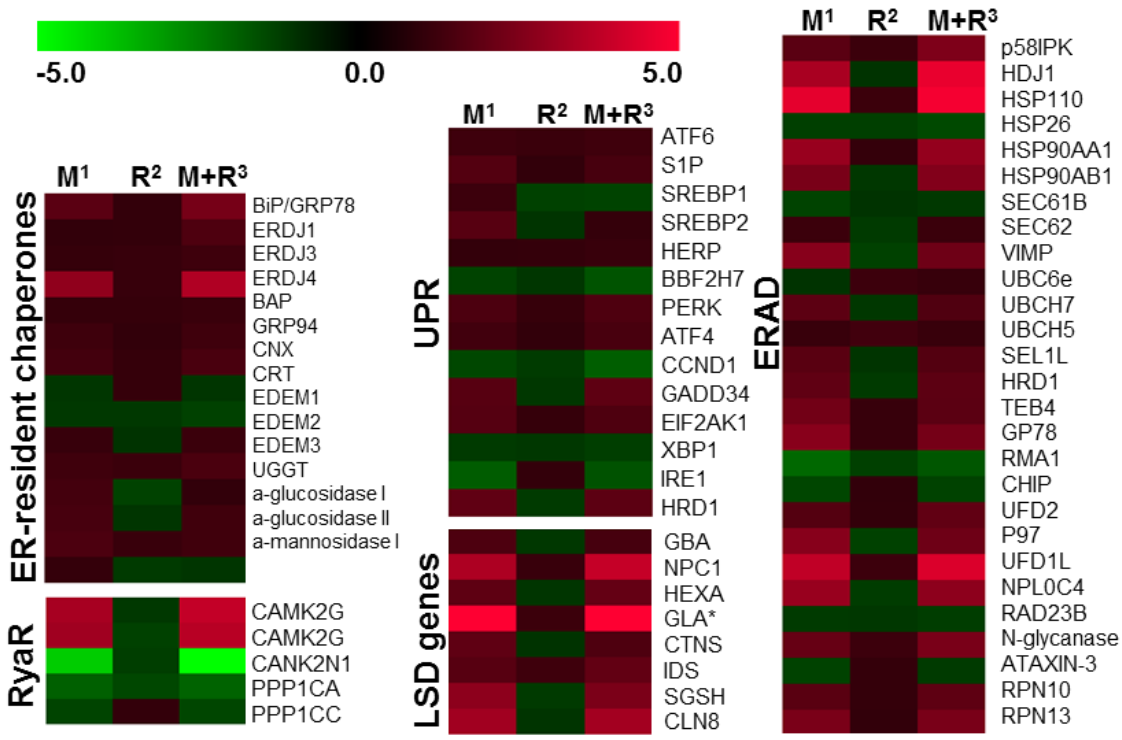

[1] M, MG-132; [2] R, Ryanodine; [3] M+R, MG-132+ ryanodine.
* Gene expression values exceed the heat map limits (M: 5.97; M+R: 7.35)

Figure 4.1.6. Profiling of gene expression in L444P GC patient-derived fibroblasts treated with MG-132 and ryanodine. Transcriptional modulation of genes encoding for ER-resident chaperones, and associated with UPR, LSD, lipid metabolism, and ERAD in L444P GC fibroblasts untreated and treated with MG-132 (0.4 μM) and ryanodine (20 μM). The expression of representative genes is reported as a heat map ($p<0.01$); colors in the heat map represent deviation from the average control phenotype: green, lower activity; red, higher activity.

Among ER chaperones, BiP was upregulated by MG-132 (1.8-fold increase), not considerably affected by ryanodine, but further upregulated by co-treatment with both MG-132 and ryanodine (2.3-fold). This data suggests a synergistic effect of RyRs inhibition and proteostasis regulation on BiP expression and that BiP expression level may correlate with the rescue of L444P GC activity. Other ER chaperones and BiP co-chaperones, including GRP94, Erdj1, Erdj3, and BAP were found to be modestly upregulated by MG-132 and ryanodine. Interestingly, even though their expression is virtually unaltered by treatment with ryanodine, in most cases co-administration of MG-132 and ryanodine resulted in upregulation of their expression to an extent higher than treatment with MG-132 alone. Analysis of the ER chaperones involved in the CNX/CRT cycle revealed that again treatment with ryanodine alone barely changes gene expression, but may attenuate or enhance the change in expression caused by MG-132. Particularly, ryanodine enhances the upregulatory effect of MG-132 on CNX and EDEM3, while it attenuates the upregulatory effect on α-glucosidase I and II, which suggests that ryanodine functions by enhancing the ER folding capacity and attenuating ERAD in cells treated with MG-132 (Appendix B).

The expression of genes involved in the unfolded protein response (UPR) was also analyzed. UPR is a complex tripartite pathway activated by excessive load of unfolded and misfolded proteins in the ER (Ron and Walter, 2007). Three ER transmembrane proteins are responsible for the transduction of UPR signals: double-stranded RNA-activated protein kinase-like ER kinase (PERK), inositol requiring kinase 1 (IRE1), and activating transcription factor 6 (ATF6, Ron and Walter, 2007). The three UPR signal transduction pathways are all induced upon culturing cells with MG-132, but

do not seem to be significantly affected by ryanodine. As part of the first UPR branch, activation of double-stranded RNA-activated ER kinase (PERK; Perkins et al., 1999) induces phosphorylation of the translation initiation factor-2α (eIF2α), which lowers translational initiation to reduce the load of protein that enters the ER. PERK and eIF2α were upregulated by MG-132 (1.5- and 1.4-fold respectively, Appendix B), but not significantly affected by treatment with ryanodine. Phosphorylated eIF2α also induces the translation of ATF4, a key regulator of the cellular response to amino acid deprivation (1.3-fold increase, MG-132; 1.5-fold increase, MG-132 and ryanodine; Kleizen and Braakman, 2004). When ER proteostasis is restored, PERK is quickly de-phosphorylated by GADD34, which expression was also found to be upregulated (1.7-fold, MG-132; 1.9-fold, MG-132 and ryanodine). These results, taken together, suggest that the PERK arm of the UPR is both upregulated and inhibited, suggesting that cell treatment with MG-132 and ryanodine simultaneously initiate cycles of moderate UPR activation and inhibition. We suggest that MG-132 and ryanodine cause brief pulses of UPR, optimal to induce controlled enhancement of the cellular folding capacity and to promote native folding of unstable, misfolding-prone GC variants without disruptive effects on the proteostasis network.

The second UPR branch is responsible for enhancement of the ER protein processing capacity. It consists in a relatively long adaptation process, which includes upregulation of ER chaperones expression, enhancement of ERAD, and enlargement of the ER, collectively initiated by the proteins ATF6 and XBP-1 (Schroder and Kaufman, 2005). IRE1 is an ER transmembrane protein structurally similar to PERK that contains an ER luminal signal sensing domain and a cytoplasmic protein kinase domain (Lee et

al., 2003). Binding of unfolded proteins to the IRE1 luminal domain triggers trans-autophosphorylation of its kinase domains, which is responsible for splicing of XBP1 mRNA, an activator of ER chaperones and ERAD genes expression (Lee et al., 2003). The unspliced form of XBP1 mRNA encodes for XBP1 precursor, a more labile protein that represses UPR target genes. As the cell recovers and IRE1 is inactivated, XBP1 precursor inhibits the pathway activated by the spliced XBP1 form. Interestingly, IRE1 is downregulated 2.0-fold in cells treated with MG-132, while ryanodine attenuates this downregulation to 1.6-fold decrease in expression (Appendix B). In cells treated with MG-132 the expression of unspliced XBP1 is downregulated (1.2-fold). Several XBP-1-dependent UPR target genes, as reported by Lee *et al.*, are listed in Appendix B, and include the DnaJ/Hsp40-like genes, p58IPK, ERdj4, and HEDJ, as well as EDEM, protein disulfide isomerase-P5, and ribosome-associated membrane protein 4 (RAMP4) (Lee et al., 2003). Depending on the specific co-chaperone interaction, BiP can promote either folding or ERAD of misfolded proteins. Erdj4 and p58IPK are both involved in BiP-mediated degradation via ERAD and are both upregulated (Erdj4: 2.8-fold by MG-132, and 4.6-fold by MG-132 and ryanodine; p58IPK: 1.8-fold by MG-132, and 2.5-fold by MG-132 and ryanodine). Other XBP-1-dependent UPR target genes are mildly upregulated by MG-132 and ryanodine. ATF6, along with XBP1, transduces the response of this branch of the UPR. ATF6 is a type II transmembrane glycoprotein with a stress-sensing segment that faces the ER lumen and a basic leucine zipper motif oriented to the cytoplasm (Schroder and Kaufman, 2005). Under ER stress, ATF6 is translocated from the ER to the Golgi where it is activated by site 1 protease (S1P) and site 2 protease (S2P) cleavage, which promote its translocation to the nucleus, where it induces the expression

of UPR genes (Figure 4.1.6. and Appendix B) (Schroder and Kaufman, 2005). Both ATF6 and its excising gene S1P are upregulated by MG-132 treatment (1.2- and 1.7-fold, respectively), suggesting that the ATF6-dependent branch of the UPR is induced. Several UPR target genes, such as SREBPs that promotes lipid biogenesis, are also activated by S1P and S2P by proteolytic cleavage.

The third branch of the UPR is activated when ER proteostasis cannot be re-established and culminates with induction of apoptosis (Scorrano et al., 2003). Cell death induced by ER stress is activated by translocation of the death effectors BAX and BAK from the ER to the mitochondria (Scorrano et al., 2003). IRE1-mediated activation of Jun N-terminal kinase (JNK) might contribute to cell death by inactivating the anti-apoptotic regulator BCL-2 (Urano et al., 2000). PERK-mediated upregulation of the transcription factor CHOP is also suggested to repress BCL-2 expression (Oyadomari and Mori, 2004). Gene expression profiling reported in Appendix B shows that BAX is downregulated by MG-132, thus preventing apoptosis, while BAK is upregulated (1.7-fold increase in expression), suggesting that MG-132 acts by inducing specific apoptotic-promoting machinery. Interestingly, although BCL-2 is downregulated 6.2-fold by MG-132, ryanodine attenuates MG-132 downregulation (5-fold), suggesting that restoring Ca^{2+} homeostasis through RyRs inhibition has an anti-apoptotic effect in GD cells.

LSD-associated genes were found to be generally upregulated by MG-132 and to exhibit a higher increase in expression upon treatment with both MG-132 and ryanodine. Specifically, genes associated with the development of Gaucher's, Niemann-Pick, Tay-Sachs, and Fabry diseases were upregulated by MG-132 (1.5-, 3.4-, 1.9- and 6.0-fold, respectively) and MG-132 and ryanodine (1.4-, 3.9-, 2.0- and 7.3-fold, respectively). The

increase in L444P GC expression by MG-132 and ryanodine co-treatment was confirmed at the protein level by Western blot analyses (Figure 4.1.7). UPR activation is known to enhance lipid metabolism to increase the size of the ER and dilute the load of misfolded proteins (Schroder and Kaufman, 2005). Because LSD-associated proteins are enzymes normally involved in lipid degradation, we suggest that LSD genes' upregulation in L444P GC cells treated with MG-132 and ryanodine is a response of the cell to MG-132-induced UPR activation. L444P GC and other LSD-associated enzyme variants are normally targeted to ERAD. Thus, increasing the concentration of newly synthesized enzyme through small molecule treatment could be a particularly appealing therapeutic strategy as it inevitably increases the pool of ER intermediates amenable to folding rescue.

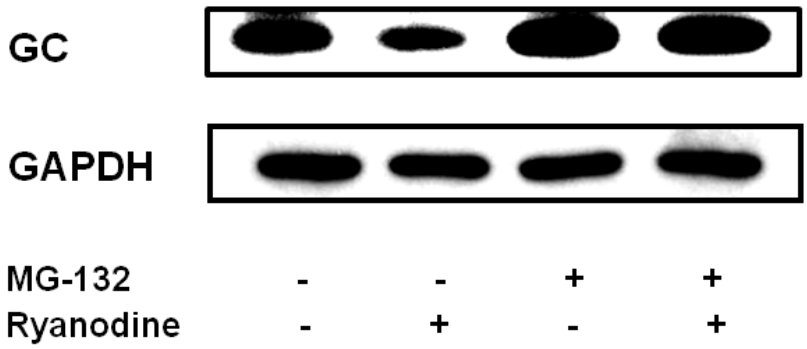

Figure 4.1.7. Total GC accumulation in L444P GC patient-derived fibroblasts treated with ryanodine and MG-132. Western blot analyses of total GC in cells treated with ryanodine (20 μM), and MG-132 (0.4 μM) for 48 hrs. GAPDH expression is used as loading control.

The ER membrane SREBP1 and SREBP2 regulate lipid metabolism (Schroder and Kaufman, 2005). They form a complex with SREBP cleavage-activating protein (SCAP). Changes in cellular lipid and cholesterol levels induce a conformational change

in SCAP, which in turn escorts SREBPs to the Golgi, where S1P and S2P sequentially activate their cytosolic domain by proteolytic cleavage. SREBP1 and 2 are upregulated by treatment with MG-132 (1.2- and 1.7-fold, respectively). However, co-treatment with ryanodine and MG-132 attenuates MG-132 upregulatory effect. In addition, the expression of a number of genes involved in sphingolipid biosynthesis that are upregulated by UPR (Schroder and Kaufman, 2005) is increased in cells treated with MG-132. For instance, serine palmitoyltransferase (SPTLC, LCB1) is composed of two subunits, and both of their expression is increased 1.5-fold by treatment with MG-132. Sphingomyelin synthase 1 (SGMS1) and sphingosine-1-phosphate phosphatase 1 (SGPP1) expression is also upregulated 1.2- and 2.5-fold, respectively, by MG-132 (Epstein et al., 2012).

This effect of MG-132 on L444P GC expression also explains the increase in L444P GC folding previously observed in GD cells treated with MG-132 and a chemical chaperone (N-(n-nonyl)-deoxynojirimycin, NN-DNJ) (Mu et al., 2008b). L444P GC was initially shown not to be amenable to chemical chaperoning (Sawkar et al., 2002), for which the mechanism, as mentioned before, is based on active site binding-mediated stabilization of the native enzyme structure, and most likely does not affect the independently folding domain containing the L444P substitution (Brumshtein et al., 2007). A dramatic increase in L444P GC activity was demonstrated by subjecting MG-132-treated L444P GC patient-derived cells to brief, temporally spaced pulses of low concentration NN-DNJ treatment. Such dosing schedule was devised to promote MG-132-mediated enhancement of the folded L444P GC pool that can be chaperoned through the secretory pathway by NN-DNJ (Mu et al., 2008b). MG-132-induced L444P GC

upregulation provides a complementary explanation to the synergistic effect of MG-132 and NN-DNJ on L444P GC folding. Although additional experiments are required to investigate this speculation, we suggest that GC upregulation could be exploited to enhance rescue of mutated GC folding by combining it with enhancement of cellular folding via proteostasis modulation.

UPR activates ERAD to enhance the degradation of misfolded proteins (Travers et al., 2000). Activation of ERAD, in turn, attenuates ER stress-induced UPR by lowering the accumulation of ERAD substrates, thus restoring proteostasis. Chaperones in the ER lumen sense the accumulation of misfolded proteins. As described above, ER chaperones, and particularly BiP, are upregulated by cell treatment with MG-132 and ryanodine. Recognition of misfolded proteins in the ER is typically coupled with their targeting to the cytoplasm through the retrotranslocation channel. Genes involved in non glycosylated substrates targeting are generally upregulated by MG-132 (Appendix B). SEL1L and Hrd1, which form an ER membrane retrotranslocation complex, undergo an 1.8- and 1.9-fold increase in expression, respectively. CNX/CRT-mediated retrotranslocation of glycosylated proteins involves EDEM3-catalyzed substrate extraction and retrotranslocation by p97. p97 is upregulated 1.3- and 2.7-fold by MG-132 treatment and MG-132 and ryanodine co-treatment, respectively. Sec61A1 and p58IPK, two components of the translocon complex are upregulated by both MG-132 treatment and MG-132 and ryanodine co-treatment (Sec61A1: 1.5- and 1.3-fold by MG-132 treatment and MG-132 and ryanodine co-treatment, respectively; p58IPK: 1.8- and 2.5-fold by MG-132 treatment and MG-132 and ryanodine co-treatment, respectively). As misfolded substrates are extracted from the ER to the cytoplasm, they are ubiquinated.

Retrotranslocation and ubiquitination of substrates are effectively coupled by the activity of E3 ubiquitin ligases. Among ubiquitination-associated proteins, UBE1, an ubiquitin-activating enzyme, is upregulated 1.4-fold by MG-132. E2 ubiquitin-conjugating enzyme UBC7, and E3 ubiquitin ligases SEL1L, HRD1, TEB4, GP78 all exhibit increases in mRNA expression (1.8-, 1.8-, 1.9-, 2.3- and 2.7-fold respectively; Appendix B), indicating a general upregulatory effect on the ubiquitination pathway. Finally, substrates are tethered to the proteasome and de-ubiquitinated prior to proteasomal degradation. The cytoplasmic complex P97-UFD1-NPL4 is involved in proteasomal targeting and degradation, and its three components are all significantly upregulated by MG-132 (2.7-, 3.8- and 3.0-fold, respectively), but not particularly affected by ryanodine treatment.

MG-132 and ryanodine treatment also influence the expression of proteins that directly affect the activity of RyRs. RyRs are inactivated by Ca^{2+}/calmodulin-dependent protein kinase II (CAMK2) phosphorylation (Wang and Best, 1992), an effect reversed by phosphatase PPP1C and by CAMK2 inhibitor (CAMK2N1). CAMK2 δ and γ subunits were upregulated by MG-132 (1.5- and 3.3-fold), and by MG-132 and ryanodine (1.6 and 3.8-fold), while CAMK2 inhibitor and PPP1C were greatly downregulated (CAMK2N1: 4.0-fold decrease, MG-132; 5.9-fold decrease, MG-132 and ryanodine. PPP1C α subunit: 1.9-fold decrease, MG-132).

Plasmid-induced BiP overexpression and chromosomal BiP upregulation enhance MG-132 function as a proteostasis regulator in fibroblasts derived from GD patients carrying L444P GC

In order to test whether ryanodine and MG-132-induced ER chaperone upregulation directly influences L444P GC folding, we attempted overexpressing the genes of interest in GD cells. Patient-derived fibroblasts were transfected with tetracycline-inducible plasmids encoding BiP, CNX, CRT, or GRP94 and induced for 24, 48, and 72 hrs as described in Methods. L444P GC activities are reported in Figure 4.1.8. As expected, GC activity was undetectable in untreated cells (cells transfected with empty vector, pcDNA4/TO). BiP overexpression resulted in modest restoration of L444P GC folding (1.4-fold upon induction with 0.2 μg/ml tetracycline for 72 hrs; Figure 4.1.8C). In order to recapitulate the effect of RyRs blockers and MG-132 co-treatment on BiP upregulation, cells transfected for BiP overexpression were cultured in the presence of MG-132. The combined effect of BiP overexpression (tetracycline 0.2 μg/ml) and MG-132 (0.4 μM) for 48 hrs resulted in 6.0-fold increase in L444P GC activity with respect to the activity of untreated cells, compared to a 3.3-fold increase in cells treated only with MG-132 (Figure 4.1.8B). Remarkably, this increase in L444P GC activity corresponds to 75% of wild type GC activity. Overexpression of CNX, CRT and GRP94 did not result in considerable increase in L444P GC activity, with the exception of a modest increase observed upon overexpression of CRT (Figure 4.1.8H).

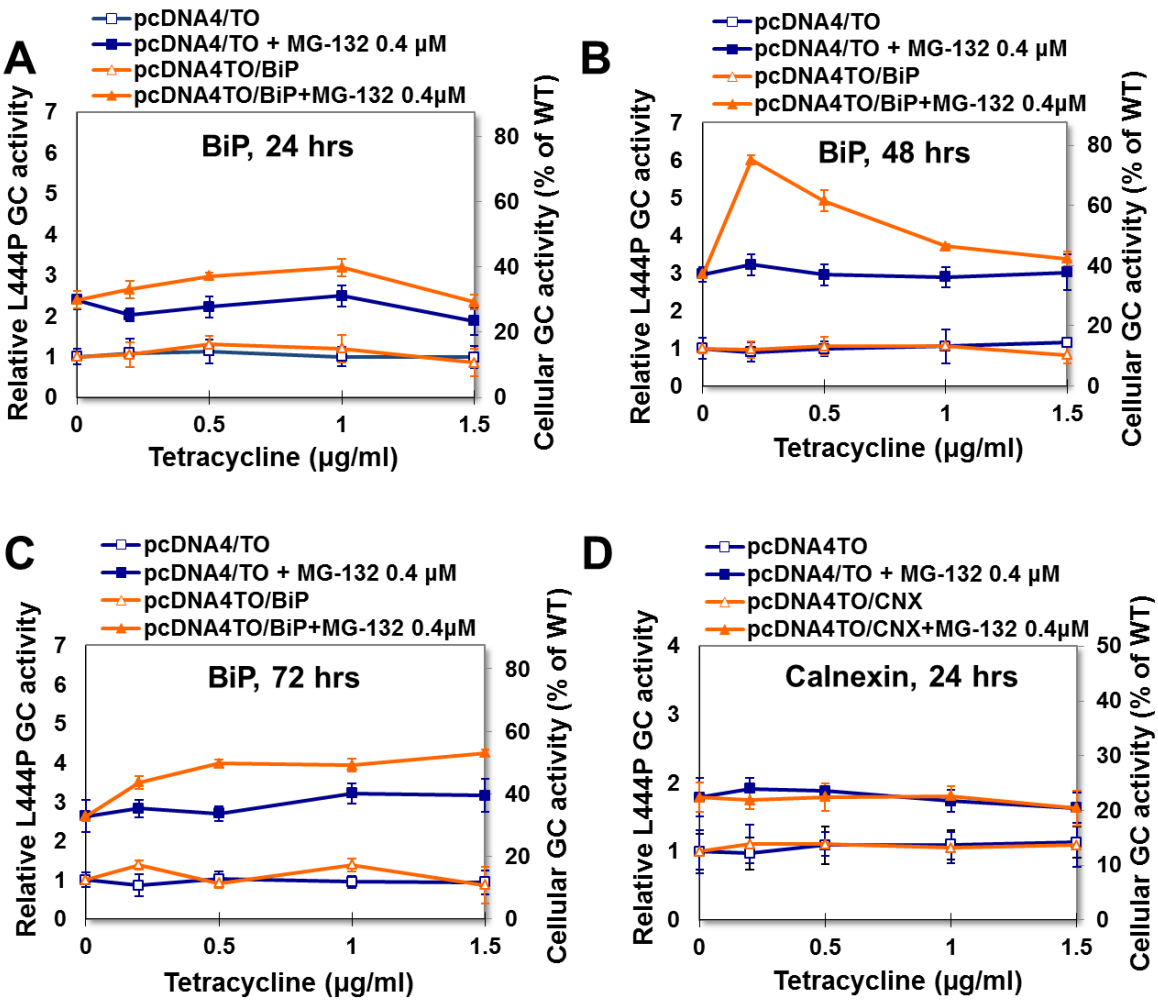
A
pcDNA4/TO
pcDNA4/TO + MG-132 0.4 μM
pcDNA4TO/BiP
pcDNA4TO/BiP+MG-132 0.4μM
BiP, 24 hrs
Relative L444P GC activity
Cellular GC activity (% of WT)
Tetracycline (μg/ml)
B
pcDNA4/TO
pcDNA4/TO + MG-132 0.4 μM
pcDNA4TO/BiP
pcDNA4TO/BiP+MG-132 0.4μM
BiP, 48 hrs
Relative L444P GC activity
Cellular GC activity (% of WT)
Tetracycline (μg/ml)
C
pcDNA4/TO
pcDNA4/TO + MG-132 0.4 μM
pcDNA4TO/BiP
pcDNA4TO/BiP+MG-132 0.4μM
BiP, 72 hrs
Relative L444P GC activity
Cellular GC activity (% of WT)
Tetracycline (μg/ml)
D
pcDNA4TO
pcDNA4/TO + MG-132 0.4 μM
pcDNA4TO/CNX
pcDNA4TO/CNX+MG-132 0.4μM
Calnexin, 24 hrs
Relative L444P GC activity
Cellular GC activity (% of WT)
Tetracycline (μg/ml)

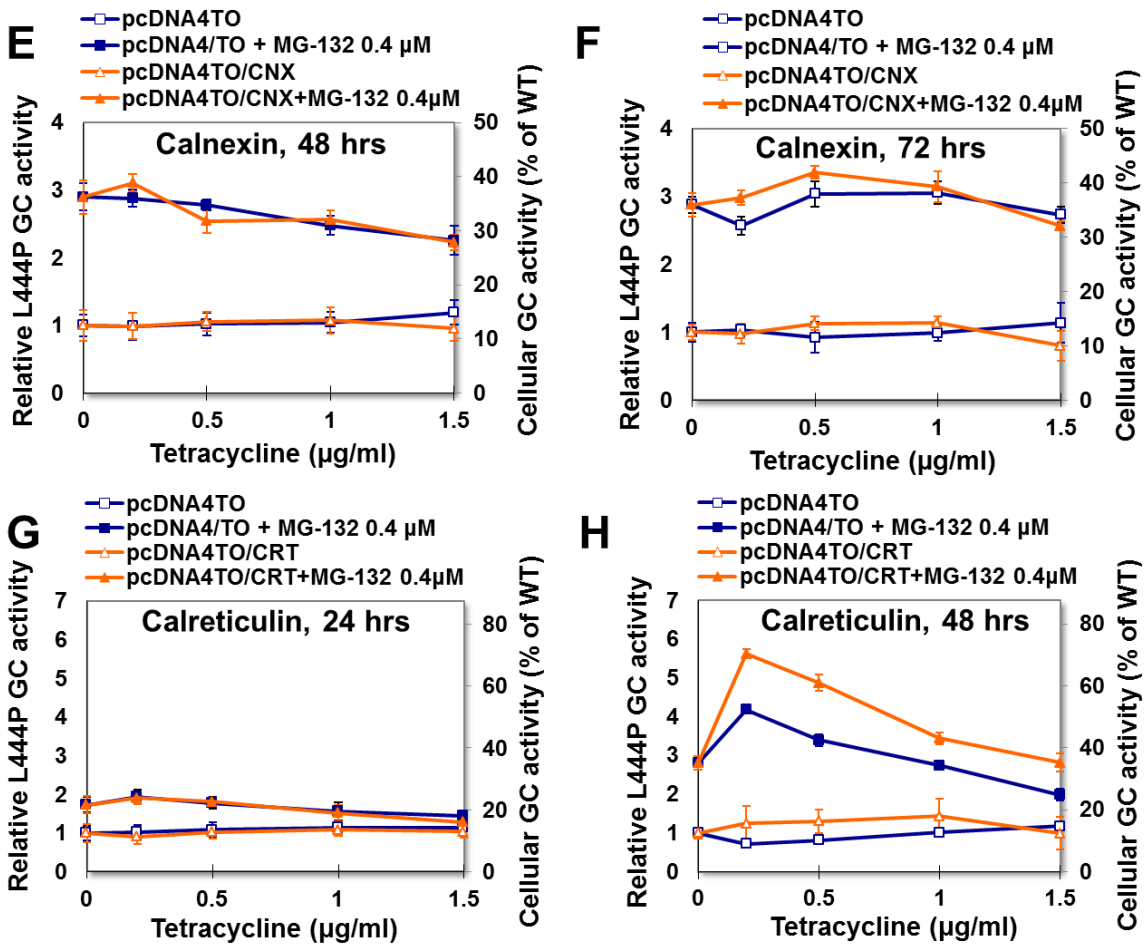
E
pcDNA4TO
pcDNA4/TO + MG-132 0.4 μM
pcDNA4TO/CNX
pcDNA4TO/CNX+MG-132 0.4μM
Calnexin, 48 hrs
Relative L444P GC activity
Cellular GC activity (% of WT)
Tetracycline (μg/ml)
F
pcDNA4TO
pcDNA4/TO + MG-132 0.4 μM
pcDNA4TO/CNX
pcDNA4TO/CNX+MG-132 0.4μM
Calnexin, 72 hrs
Relative L444P GC activity
Cellular GC activity (% of WT)
Tetracycline (μg/ml)
G
pcDNA4TO
pcDNA4/TO + MG-132 0.4 μM
pcDNA4TO/CRT
pcDNA4TO/CRT+MG-132 0.4μM
Calreticulin, 24 hrs
Relative L444P GC activity
Cellular GC activity (% of WT)
Tetracycline (μg/ml)
H
pcDNA4TO
pcDNA4/TO + MG-132 0.4 μM
pcDNA4TO/CRT
pcDNA4TO/CRT+MG-132 0.4μM
Calreticulin, 48 hrs
Relative L444P GC activity
Cellular GC activity (% of WT)
Tetracycline (μg/ml)

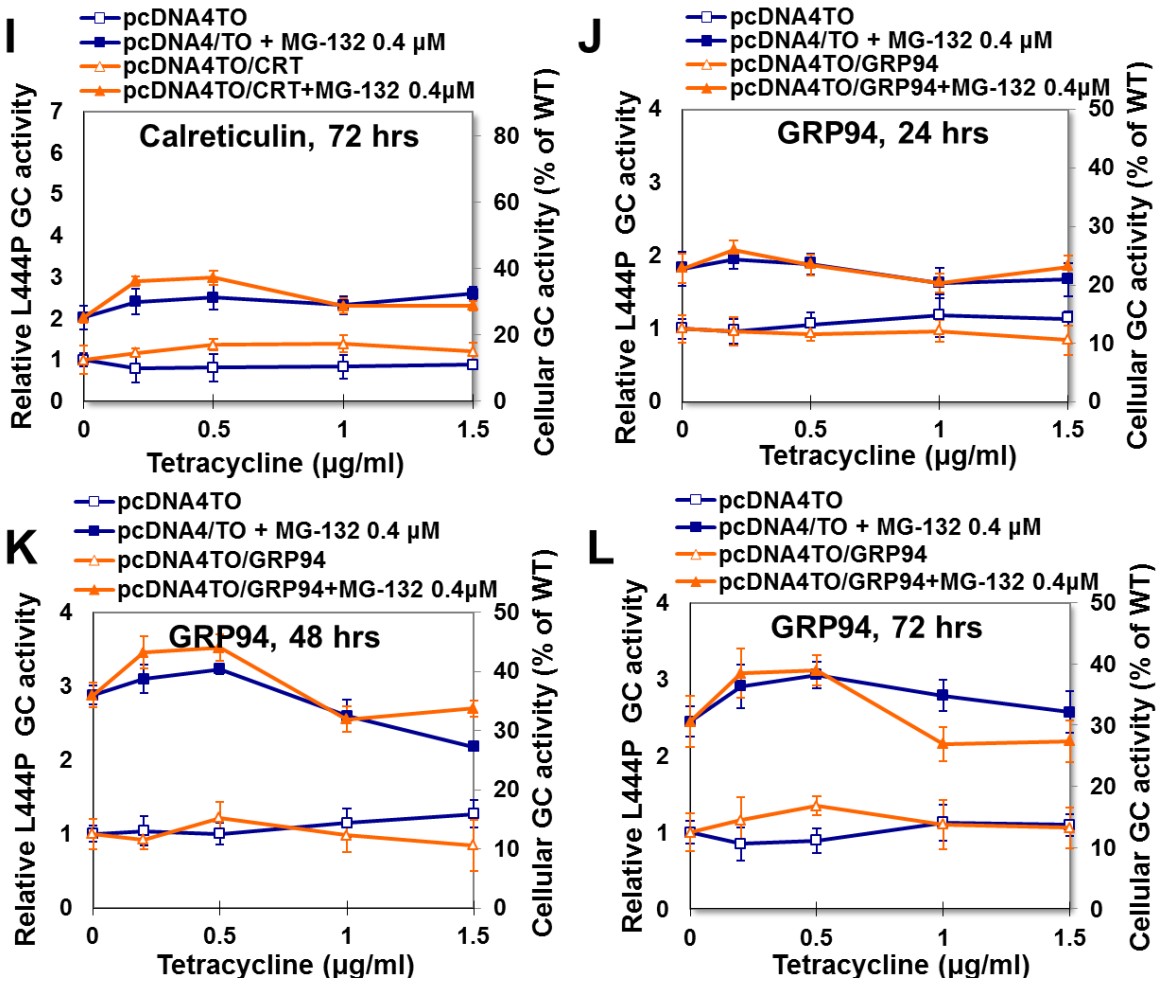

Figure 4.1.8. GC activities of L444P GC patient-derived fibroblasts overexpressing BiP, CNX, CRT, or GRP94 and treated with MG-132. Chaperone expression was induced by media changes with tetracycline-supplemented media 24 hrs post-transfection and every 24 hrs thereafter. GC enzymatic assays were performed after inducing the expression of (**A-C**) BiP, (**D-F**) CNX, (**G-I**) CRT, and (**J-L**) GRP94 for 24, 48, and 72 hrs. Relative GC activities were obtained normalizing the activity of cells transfected with empty pcDNA4/TO (□), cells transfected with empty pcDNA4/TO and treated with 0.4 µM MG-132 (■), cells transfected with chaperone-expressing pcDNA4/TO (△), and cells transfected with chaperone-expressing pcDNA4/TO and treated with 0.4 µM MG-132 (▲), by the activity of untreated cells transfected with empty pcDNA4/TO. The data is reported as mean ± SD.

Cellular accumulation of Myc-tagged recombinantly expressed chaperones was confirmed by ELISA analyses. Tetracycline induction (0.2 µg/ml) caused a 3 to 5-fold

increase in recombinant protein concentration (Figure 4.1.9). Because GC activity assays were conducted by investigating a range of induction conditions, this variability in protein accumulation did not hamper our ability to study the effect of different chaperones on L444P GC activity.

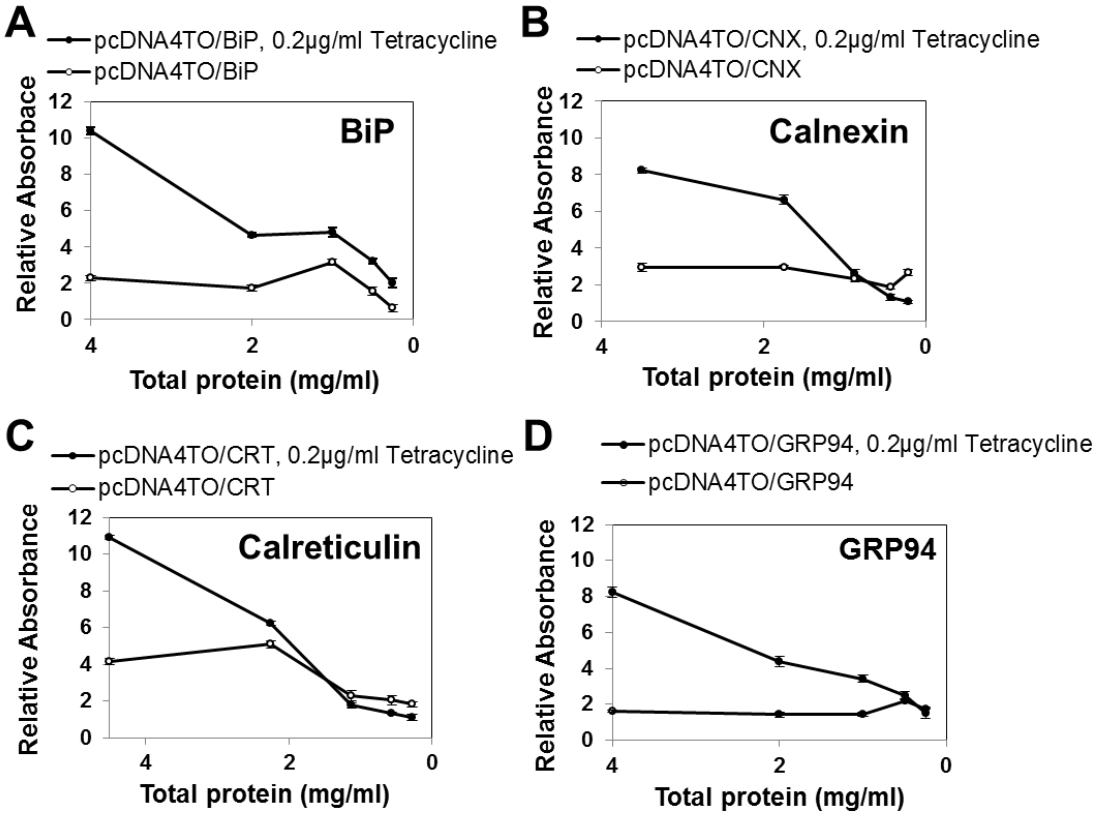

Figure 4.1.9. Plasmid-induced chaperone expression in L444P GC patient-derived fibroblasts. ELISA analyses of induced and non-induced transfected cells expressing **A**) BiP, **B**) CNX, **C**) CRT and **D**) GRP94. Chaperone expression was induced with 0.2 µg/ml tetracycline for 48 hrs before whole cell lysates were collected, and incubated in anti-Myc antibody coated plates. Recombinant chaperones were detected with chaperone specific antibodies.

To further test the hypothesis that BiP expression directly influences the rescue of L444P GC folding, we attempted upregulating chromosomal BiP expression. The Ca^{2+} ionophore A23187 is known to induce the BiP promoter (BiP670) at concentrations that

do not induce depletion of cytoplasmic [Ca^{2+}] (Appendix A; Chao and Lin-Chao, 1992; Drummond et al., 1987). GC activity was evaluated in L444P GC patient-derived fibroblasts cultured with A23187 and/or MG-132 (Figure 4.1.10). Co-treatment with A23187 and MG-132 resulted in a 2.7-fold increase in L444P GC activity, which is higher than what was observed in cells treated with A23187 (1.3-fold) and MG-132 (2.0-fold), confirming that upregulation of BiP expression enhances MG-132 mediated rescue of L444P GC folding.

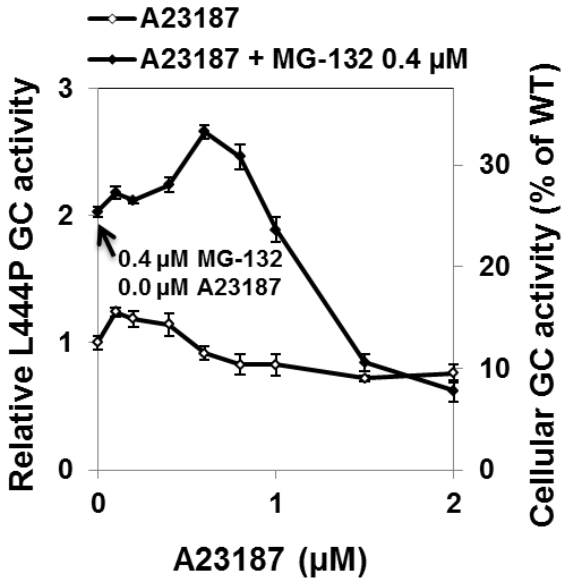

Figure 4.1.10. L444P GC activity of patient-derived fibroblasts treated with A23187 and MG-132. Relative L444P GC activities of cells treated with A23187 and MG-132 for 48 hrs ($p<0.01$). GC activities were obtained as described in Figure 4.1.1 and reported as mean ± SD.

Ryanodine ameliorates cytotoxicity induced by proteostasis regulation in fibroblasts derived from GD patients carrying L444P GC

Korkotian *et al* reported that treatment with ryanodine (50 μM) limits the neurotoxic effect of glucosylceramide accumulation and significantly reduces neuronal

death (Korkotian et al., 1999). We asked a) if ryanodine treatment also rescues cytotoxicity caused by glucosylceramide accumulation in L444P GC fibroblasts, b) if MG-132 treatment by inducing ER stress and UPR causes cytotoxicity and apoptosis, and, in that case, c) whether ryanodine treatment limits MG-132-induced cytotoxicity in L444P GC fibroblasts. Cells treated with these small molecules were tested with the CytoGLO^{TM} Annexin V-FITC Apoptosis Detection Kit and analyzed by flow cytometry. This assay allows detecting membrane rearrangement (Annexin V binding) and fragmentation (propidium iodide (PI) binding), which normally occur during early and late apoptosis, respectively. Fluorescence intensities of both Annexin V-FITC and PI in cells treated with small molecules were evaluated and compared to the values obtained from untreated cells. A total number of 10,000 cells were counted, and the number of cells that bind to Annexin V-FITC or PI in cells treated with small molecules was compared to the number of cells that bind to Annexin V-FITC or PI in untreated cells. As shown in Table 4.1, Annexin V binding increased 28% in wild type fibroblasts treated with MG-132, which was reduced to 15% by treatment with ryanodine and MG-132. Thapsigargin (1 μM) and tunicamycin (1 μM) were used as controls as they are known to induce cytotoxicity by activating the UPR (Chen et al., 2007; Duksin and Bornstein, 1977) and resulted in 14% and 13% increase in Annexin V binding, respectively, compared to untreated cells (Table 4.1). When the same experiment was conducted using GD fibroblasts carrying L444P GC, Annexin V binding increased 18% and 19%, respectively, suggesting that L444P GC cells are more susceptible to the cytotoxic effect induced by thapsigargin and tunicamycin treatment than wild-type fibroblasts. In L444P GC fibroblasts Annexin V binding increased 43% upon MG-132 (0.4 μM) treatment

(considerably higher than in wild-type fibroblasts). MG-132 treatment was also observed to cause a 12% increase in cell death (PI binding). However, Annexin V binding decreased 8% upon ryanodine (20 μM) treatment, recapitulating the results previously reported by culturing hippocampal neurons (Korkotian et al., 1999). Treatment with ryanodine and MG-132 caused Annexin V binding to decrease to 37%, and cell death to decrease to 9.3% (Table 4.1), suggesting that ryanodine alleviates MG-132 induced toxicity, and in agreement with the hypothesis that RyRs inhibition recreates a "wild type-like" ER folding environment in L444P GC fibroblasts.

Table 4.1. Cell toxicity assay (ryanodine treatment) ($p<0.01$)

Cell type	Cell treatment	Annexin V		PI	
		Population[1]	Binding[2]	Population[1]	Binding[2]
L444P GD	Thapsigargin	1.1 ±0.1	18 ±0.6	5.0 ±0.3	10 ±0.1
	Tunicamycin	-0.1 ±0.1	19 ±0.2	7.5 ±0.1	8.2 ±0.1
	MG-132	-3.4 ±0.1	43 ±0.3	12 ±0.4	7.0 ±0.1
	Ryanodine	-0.3 ±0.1	-7.9 ±0.7	4.7 ±0.6	-1.6 ±0.2
	MG-132+ryanodine	-2.2 ±0.1	37 ±0.5	9.3 ±0.5	1.8 ±0.1
WT	Thapsigargin	-9.1 ±0.1	14 ±0.2	5.7 ±1.6	21 ±0.4
	Tunicamycin	-11 ±0.1	13 ±0.4	7.1 ±0.7	41 ±0.2
	MG-132	-3.9 ±0.1	28 ±0.7	2.9 ±0.3	23 ±0.1
	Ryanodine	1.9 ±0.2	-12 ±1.5	0.9 ±0.6	-13 ±0.7
	MG-132+ryanodine	-3.2 ±0.1	15 ±1.8	1.7 ±0.1	43 ±0.7

[1] Change (%) in number of cells bound to Annexin V/PI compared to untreated cells.
[2] Change (%) in Annexin V/PI binding affinity compared to untreated cells.

Because one of the key mechanisms of MG-132-mediated rescue of mutated GC folding is UPR induction, we asked whether cell treatment with thapsigargin and tunicamycin could rescue L444P GC folding. GD cells treated with low concentrations of thapsigargin and tunicamycin (0.01-1 nM) for up to 48 hrs gave rise to a 4- and 2-fold increase in L444P GC activity, an effect that is quickly lost at higher concentrations and

longer incubation times (Figure 4.1.11), confirming that mild UPR activation promotes mutated GC folding as observed using MG-132.

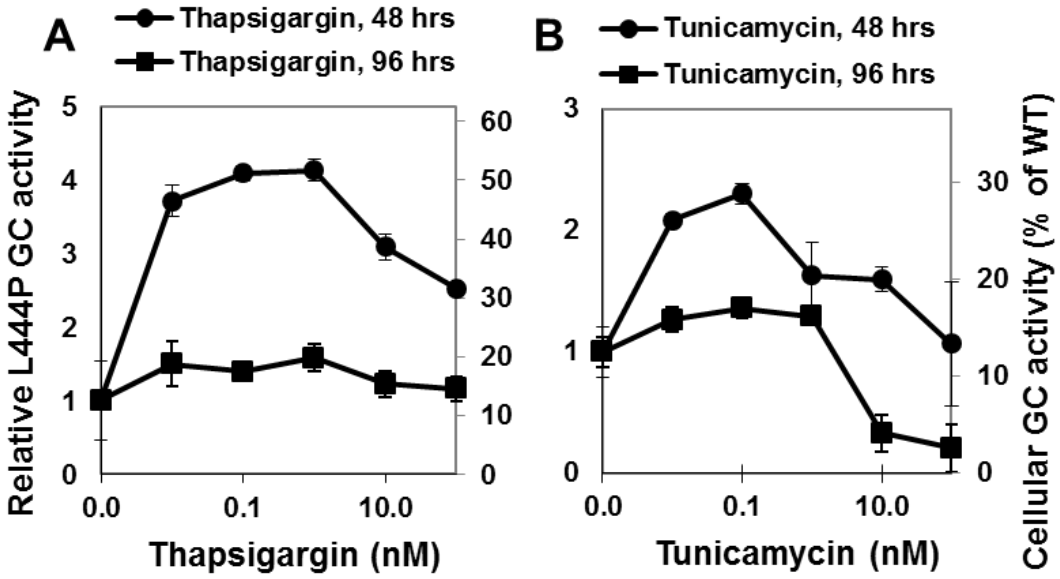

Figure 4.1.11. L444P GC activity of patient-derived fibroblasts treated with thapsigargin and tunicamycin. Relative L444P GC activities of cells treated with **A**) thapsigargin ($p<0.01$), and **B**) tunicamycin ($p<0.01$, 48 hrs; $p<0.001$, 96 hrs). GC activities were obtained as described in Figure 4.1.1 and reported as mean ± SD.

4.1.3. Discussion

We demonstrated that inhibiting glucosylceramide-induced $[Ca^{2+}]_{ER}$ depletion via RyRs enhances MG-132 ability to restore L444P GC proteostasis. Simply preventing $[Ca^{2+}]_{ER}$ efflux through inhibition of RyRs or inhibition of glucosylceramide synthesis only modestly increased L444P GC activity. In agreement with this finding, overexpression of L444P GC in wild-type fibroblasts does not to result in L444P GC native folding (Ron and Horowitz, 2005), suggesting that the innate (wild type) folding capacity cannot cope with the destabilizing effect of the L444P substitution. However,

creating a more "wild-type like" folding environment in the ER of GD cells harboring L444P GC via RyRs or glucosylceramide synthesis inhibition enhances MG-132-mediated L444P GC proteostasis.

Ong *et al.* recently reported a study showing rescue of mutated GC folding by $[Ca^{2+}]_{ER}$ modulation (Ong et al., 2010). siRNA knockdown of RyRs and treatment of GD fibroblasts with RyRs inhibitors was reported to modestly increase the pool of L444P GC that escapes ERAD and restore L444P GC activity. The enzyme activity in this study was measured with a lysed cell GC activity assay. Dantrolene at 25 μM was particularly effective (1.3-fold increase in L444P GC activity), in agreement with what is reported here using dantrolene and ryanodine (Figure 4.1.1). However, dantrolene (10 μM) treatment was reported to lower L444P GC activity, despite increasing the pool of EndoH-resistant glycosylated L444P GC that trafficks to the lysosome, implying that in cells treated with dantrolene L444P GC is natively folded, but is not enzymatically active. This result was attributed to L444P GC hypersensitivity inhibition (Ong et al., 2010), supported by i) the lowered L444P GC activity rescue observed in cells treated with MG-132 (0.25 μM) and dantrolene (10 μM) compared to increase in activity observed in cells treated with MG-132 alone, and by ii) dantrolene's (10-300 μM) inhibitory effect on wild type GC *in vitro*. We hypothesize that the lowered L444P GC activity observed in cells treated with MG-132 and dantrolene is due to the high dantrolene concentration and long incubation times used, which in our hands were observed to give rise to cell toxicity. Furthermore, we suggest that chemical chaperones can have an inhibitory effect on the folding of L444P GC due to their mechanism of action based on binding to the enzyme active site and stabilization of the native enzyme

structure (Pelled et al., 2005). This inhibitory effect is likely due to the fact that the L444P substitution is located in an independently folding domain (distinct from the active-site domain, (Brumshtein et al., 2007)) that is not stabilized by the interaction of chemical chaperones with the L444P GC active site. However, this inhibitory effect (Sawkar et al., 2002) is not likely to apply to proteostasis regulators, including MG-132, or small molecules, such as RyRs inhibitors, that do not directly bind to GC intermediates.

We demonstrated that BiP is upregulated in cells treated with MG-132, and, particularly, in cells treated with MG-132 and ryanodine (Figure 4.1.4A), and that BiP plasmid and chromosomal overexpression enhances MG-132-mediated L444P GC activity increase (Figure 4.1.8 and 4.1.10). BiP upregulation was previously reported to delay conformational maturation and ER export of misfolded substrates through enhanced formation of complexes with substrate intermediates (Gorbatyuk et al., 2010; Muresan and Arvan, 1998; Xu and Robinson, 2009). The concentration-dependence of BiP-mediated increase in ER retention was repeatedly observed only for BiP *bona fide* substrates (Dorner and Kaufman, 1994; Dorner et al., 1992). These studies support the notion that increasing BiP expression enhances BiP binding to L444P GC that, in turn, promotes folding and enhances residence time in the ER. The fact that BiP overexpression does not accelerate substrate folding and ER export is also in agreement with our finding that BiP overexpression or ryanodine treatment alone does not considerably enhance L444P GC activity (Figure 4.1.8A and 4.1.1A).

BiP is an ER lumenal protein whose specific function as promoter of ER folding or ERAD critically depends on a number of interaction partners (Vembar et al., 2010).

The question of how BiP plasticity can be channeled for the enhancement of L444P GC folding still remains open. However, based on the notions that i) enhanced BiP binding retards substrate conformational maturation, but does not promote substrate ERAD and ii) this effect is only observed for BiP physiologic substrates, and thus would not compromise the folding of other proteins, we speculate that BiP function as an ER folding-inducing chaperone rather than ERAD-inducing chaperone. This feature can be exploited to effectively rescue the folding of L444P GC. BiP also plays a fundamental role in activating the UPR. Accumulation of misfolded proteins results in BiP release and activation of the three UPR transducers, IRE1, PERK, and ATF6 (Ron and Walter, 2007). We suggest that BiP upregulation mediated by RyRs inhibitors, as well as plasmid or chromosome induced BiP overexpression, results in increased ER capacity to cope with the accumulation of misfolded proteins without activation of the UPR. This notion is supported by evidence that ryanodine treatment does not induce UPR, as shown by global gene expression analysis (Figure 4.1.6 and Appendix B), and that it ameliorates the cytotoxic effect of MG-132, as shown above (Table 4.1).

Constitutive overexpression of CNX, among ER chaperones, was previously reported to modestly enhance L444P GC proteostasis by increasing the formation of complexes between L444P GC and CNX (Ong et al., 2010). Increased binding of CNX to endogenous or overexpressed GC mutants, was also previously demonstrated (Ron and Horowitz, 2005), and the instability of different GC variants, their ER retention, and CNX binding were correlated to their ERAD targeting. As shown herein, L444P GC activity increase correlates strongly with the chaperone expression levels, which were modulated uniquely through the use of a tetracycline-inducible plasmid. The study

reported herein reveals that CNX mRNA levels were upregulated by small molecule treatment to a lower extent than what was observed for BiP mRNA (Figure 4.1.4), and overexpression of CNX did not significantly increase L444P GC activity (Figure 4.1.8B). Our findings, together with previously reported evidence (Ron and Horowitz, 2005), suggest that CNX does not play a key role in the rescue of L444P GC folding.

Cellular [Ca^{2+}] measurements reported recently (Ong et al., 2010) revealed an increase in $[Ca^{2+}]_{ER}$ and decrease in cytoplasmic [Ca^{2+}] in cells treated with RyRs inhibitors. This data supports our conclusion that RyRs blockers restore a more "wild-type like" ER environment in L444P GC cells through modulation of Ca^{2+} homeostasis. However, we suggest that careful consideration of small molecule concentrations be used in these studies to avoid misinterpreting the effect of cell treatment with [Ca^{2+}] modulators on the folding of L444P GC activity. For instance, contrary to what has been previously reported (Mu et al., 2008a; Ong et al., 2010), we show that thapsigargin greatly enhances the folding of L444P GC if used at concentrations (0.01-1 nM) that moderately induce UPR, but are too low to have a significant effect on $[Ca^{2+}]_{ER}$ depletion (100 nM, (Yoshida et al., 2006)) (Figure 4.1.11). Cell treatment with considerably higher thapsigargin concentrations (>100 nM) causes $[Ca^{2+}]_{ER}$ depletion, sustained UPR activation, and induction of apoptosis (Futami et al., 2005; Jin, 2006), and is not compatible with L444P GC folding rescue as previously reported (Mu et al., 2008a; Ong et al., 2010).

In summary, results from this study suggest that modulation of Ca^{2+} homeostasis, and, particularly, inhibition of excessive $[Ca^{2+}]_{ER}$, synergize with proteostasis regulation to rescue the folding and trafficking of L444P GC in fibroblasts derived form GD

patients. Partial restoration of L444P GC folding is attributed to the function of the main ER chaperone, BiP, and modest upregulation of the UPR. BiP mRNA and protein levels were found to be increased (6- and 2-fold, respectively) in cells treated with a RyRs blocker (ryanodine) and a proteostasis regulator (MG-132). BiP overexpression and chromosomal induction were shown to enhance MG-132 mediated L444P GC activity. Global gene expression analysis revealed that UPR genes were upregulated by MG-132 treatment, as expected (Mu et al., 2008b). However, UPR inhibition genes, normally activated as protein homeostasis is restored, were also found to be induced (Figure 4.1.6). MG-132 seems to partially restore L444P GC folding by inducing short pulses of UPR, or possibly moderate UPR activation, which is likely to promote folding of this destabilized GC variant without disruptive effects on native protein homeostasis. Gene expression analysis also revealed that ryanodine mediated RyRs inhibition does not directly induce heat-shock stress and UPR, but slightly enhances or attenuates MG-132-induced modulation of key genes of the proteostasis network, thereby boosting the folding-promoting activity of MG-132 (Figure 4.1.6). In addition, RyRs inhibition partially rescues GD cells from MG-132-induced cytotoxicity and apoptosis induction (Table 4.1). These results i) strengthen our hypothesis that RyRs inhibition counteracts the deleterious effect of substrate accumulation on Ca^{2+} homeostasis and promotes a more "wild-type like" folding environment in L444P GC fibroblasts, and ii) underscore the value of RyRs blockers as research tools to investigate proteostasis modulation in GD cells.

4.2. Lacidipine remodels protein folding and Ca2+ homeostasis in Gaucher's disease fibroblasts: A mechanism to rescue mutant glucocerebrosidase activity

4.2.1. Introduction

Ca^{2+} homeostasis influences the biogenesis of secretory proteins and the activity of a number of ER chaperones (Michalak et al., 2002). The data reported in the previous chapter suggested that restoring Ca^{2+} homeostasis in GD fibroblasts enhances the ER folding capacity and facilitates native folding of highly unstable, degradation-prone L444P GC folding (Wang et al., 2011a). Treatment with ryanodine receptor (RyRs) blockers was shown to counteract the effect of glucosylceramide accumulation on $[Ca^{2+}]_{ER}$ efflux, re-establish Ca^{2+} homeostasis, and create an environment more conducive to native folding of L444P GC. However, it resulted in only limited rescue of L444P GC folding (Chapter 4.1).

L-Type Ca^{2+} channel (LTCC, Figure 4.2.1) blockers bind to high-voltage activated channels on the plasma membrane and lower cytosolic free $[Ca^{2+}]$ (Hockerman et al., 1997; Triggle, 2006). Phenylalkylamines, benzothiazepines, and 1,4-dihydropyridines are the three main classes of LTCC blockers and include molecules that bind to three distinct LTCC receptor sites (Hockerman et al., 1997). Verapamil and diltiazem, prototypes of phenylalkylamines and benzothiazepines, respectively, are FDA-approved drugs for the treatment of hypertension and cardiac arrhythmias (Hockerman et al., 1997). They were previously reported to partially rescue the folding of GC variants, but their mechanism remains elusive (Mu et al., 2008a; Sun et al., 2009). We asked

whether this reported rescue of mutated GC folding is a general property of LTCC blockers and whether their ability to modulate intracellular [Ca^{2+}] correlates with the resulting increase in mutated GC activity. We investigated LTCC blockers with 1,4-dihydropyridine structure including the prototype nifedipine and a series of second and third generation derivatives (Epstein, 1999; Pepine, 1989). We found that cell treatment with lacidipine, a third generation 1,4-dihydropyridine that antagonizes Ca^{2+} mobilization through LTCC and RyRs (Gunther et al., 2008; Wishart et al., 2008) results in enhanced folding, trafficking and activity of mutated GC variants. Particularly, we show here that lacidipine functions as a proteostasis regulator in patient-derived GD fibroblasts and rescues L444P GC folding with considerably higher efficiency than any other Ca^{2+} channel blocker reported in this study or previously (Mu et al., 2008a; Ong et al., 2010; Wang et al., 2011a). By investigating lacidipine-induced modulation of intracellular [Ca^{2+}] and of cellular folding pathways, we demonstrated that lacidipine functions by lowering cytoplasmic [Ca^{2+}], by remodeling the expression of ER chaperones and the unfolded protein response (UPR), and by reducing cellular toxicity and apoptosis induction. Thus, lacidipine activates mechanistically different cellular events that have been previously reported in association with distinct small molecule proteostasis regulators (Wang et al., 2011a).

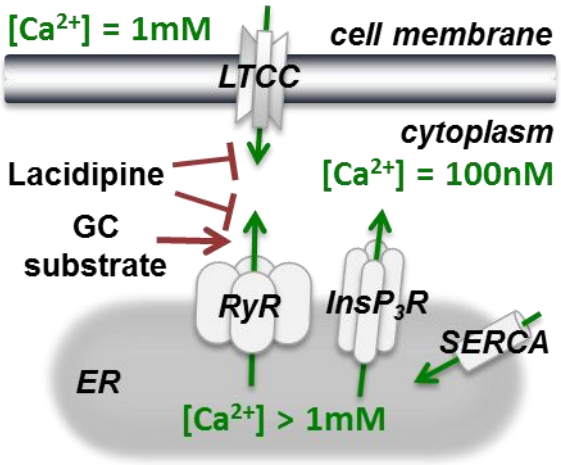

Figure 4.2.1. Lacidipine modulates intracellular Ca^{2+} homeostasis. $[Ca^{2+}]_{ER}$ is regulated by ryanodine receptors (RyRs), IP_3 receptors, and SERCA pumps. L-type voltage-gated Ca^{2+} channels (LTCC) mediate Ca^{2+} flow through the plasma membrane. Lacidipine inhibits extracellular Ca^{2+} influx through LTCC and ER Ca^{2+} efflux through RyRs.

4.2.2. Results

Treatment with small molecule LTCC and RyRs blockers enhances folding, trafficking and activity of mutated GC in fibroblasts derived from patients with Gaucher's disease

We investigated a series of LTCC blockers with a 1,4-dihydropyridine structure, particularly lacidipine, lercanidipine, nicardipine, nifedipine, and nitrendipine (Appendix A; Triggle, 2003). Patient-derived fibroblasts harboring L444P GC were treated with a range of Ca^{2+} blocker concentrations for 5 days, and GC activities were evaluated every 24 hours with the intact cell GC enzymatic activity assay (Mu et al., 2008b). Verapamil and Diltiazem, prototypes of the other two classes of LTCC blocker (phenylalkylamines and benzothiazepines, respectively; Appendix A) were included for comparison in these experiments as they were previously reported to partially rescue mutated GC folding (Mu

et al., 2008a). Culturing conditions resulting in maximal rescue of L444P GC activity are reported in Figure 4.2.2. L444P GC activity was observed to increase up to 2.0-fold in cells treated with lacidipine (20 μM, final medium concentration, $p<0.001$) for 72 hrs compared to untreated cells, which corresponds to about 25% of the WT cellular activity, and is expected to ameliorate GD symptoms (Schueler et al., 2004). A milder increase in L444P GC activity (1.2-fold, $p<0.01$) was detected in the same cells treated with lercanidipine and nicardipine (20 μM) for 72 hrs, compared to untreated cells (Figure 4.2.2). Nifedipine and nitrendipine treatment failed to rescue the activity of L444P GC (data not shown). Lacidipine was observed to enhance the activity of L444P GC to a considerably higher degree than diltiazem and verapamil tested under the same conditions. Maximal L444P GC activity increase was observed upon treatment with diltiazem (10 μM, 1.4-fold) and verapamil (5 μM, 1.1-fold) for 120 hrs (Figure 4.2.2).

Similar to diltiazem and verapamil, lacidipine blocks LTCC on the plasma membrane as well and RyRs on the ER membrane (Gunther et al., 2008). Nicardipine and lercanipine are known to block LTCC and were reported to interfere with the release of Ca^{2+} from the ER (Wishart et al., 2008), while nifedipine and nitrendipine are thought to only interact with LTCC (Gunther et al., 2008). These reported binding interactions, together with results from the GC activity assays described above (Figure 4.2.2), suggest a correlation between the mechanism of Ca^{2+} mobilization and the extent of L444P GC folding rescue. Specifically, treatment with Ca^{2+} blockers that antagonize both LTCC and RyRs result in a higher increase in L444P GC activity.

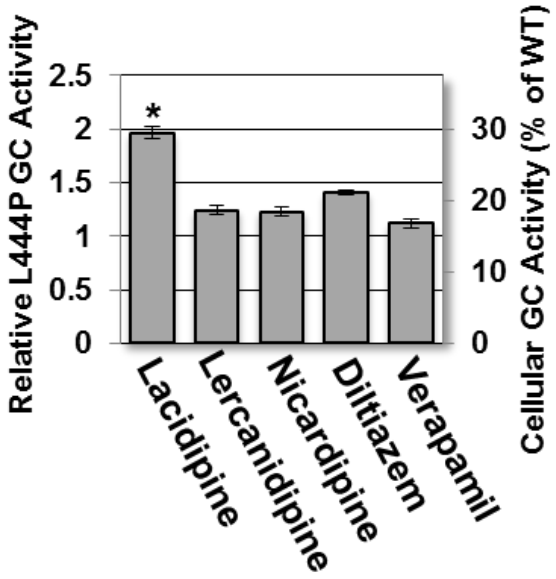

Figure 4.2.2. Treatment of GD patient-derived fibroblasts with LTCC blockers enhances L444P GC activity. Relative L444P GC activities in cells treated with lacidipine (20 μM), lercanidipine (20 μM) and nicardipine (20 μM) for 72 hrs, and diltiazem (10 μM) and verapamil (5 μM) for 120 hrs. Relative GC activities were evaluated by normalizing GC activities measured in treated cells to the activity of untreated cells (left y axis), ($p<0.01$ if not specified; $*p<0.001$). The corresponding fraction of WT GC activity is reported (right y axis). Experiments were repeated three times and data points are reported as mean ± SD.

We asked whether treatment with proteostasis regulators, such as MG-132 and celastrol, applied in combination with LTCC blockers enhance the rescue of L444P GC folding, as previously demonstrated for RyRs blockers (Chapter 4.1). Proteostasis regulation was achieved via cell treatment with either MG-132 (0.6 μM) or celastrol (0.6 μM), which are known to rescue L444P GC folding through a mechanism distinct from Ca^{2+} homeostasis modulation (Mu et al., 2008b). Patient-derived fibroblasts were cultured in medium supplemented with an LTCC blocker and a proteostasis regulator for up to 5 days, and GC activity was measured every 24 hours (Figure 4.2.3A-E). Co-administration of lacidipine (20 μM) and MG-132 for 72 hrs resulted in a dramatic increase in L444P GC activity compared to untreated cells (5.1-fold, $p<0.001$; Figure

4.2.3A), which corresponds to 64% of wild type GC activity and is significantly higher than what was observed treating the cells only with lacidipine (2.0-fold, Figure 4.2.2) or MG-132 (2.7-fold, Figure 4.2.3A). Addition of lacidipine was observed to also enhance celastrol mediated increase in L444P GC activity (2.6-fold, Figure 4.2.3A). Interestingly, lercanidipine (20 μM) and nicardipine (5 μM) enhanced MG-132 mediated L444P GC activity rescue (4.3-fold and 3.2-fold, respectively; $p<0.001$), but failed to improve celastrol activity (Figure 4.2.3B-C). Diltiazem and verapamil were observed to synergize with proteostasis regulators with lower efficiency than 1,4-dihydropyridines. Particularly, treatment with diltiazem (10 μM) and verapamil (5 μM) moderately enhanced celastrol mediated L444P GC folding rescue (2.1- and 1.9-fold, respectively), and failed to alter MG-132 mediated rescue (Figure 4.2.3D-F).

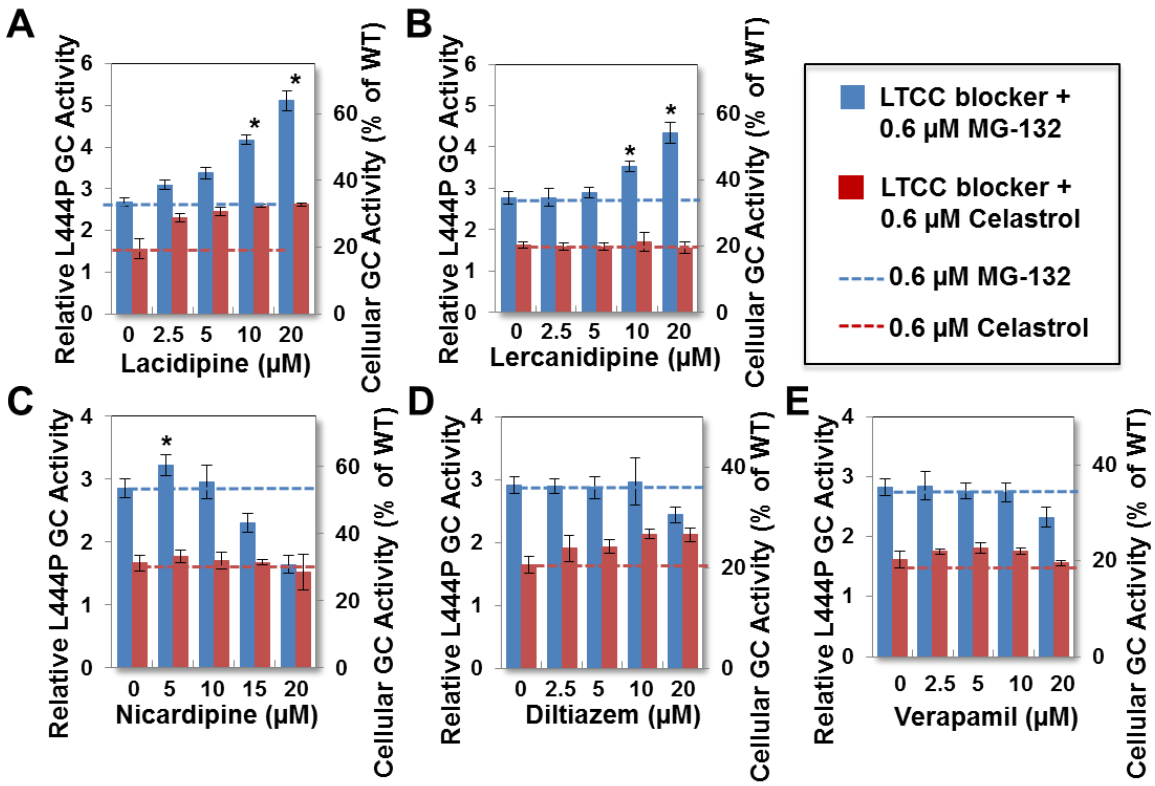

Figure 4.2.3. LTCC blockers synergize with proteostasis regulators to enhance L444P GC activity patient-derived fibroblasts. Relative L444P GC activities in L444P GC cells treated with a proteostasis regulator (MG-132, 0.6 μM; celastrol, 0.6 μM) and an LTCC blocker: **A**) lacidipine, **B**) lercanidipine, and **C**) nicardipine for 72 hrs, **D**) diltiazem, and **E**) verapamil for 120 hrs. GC activities were obtained as described in 4.2.2 and are reported as mean ± SD.

N370S GC is the most prevalent GC variant among patients with GD (Meivar-Levy et al., 1994). Cellular folding rescue and enhancement of N370S GC activity was previously reported (Mu et al., 2008a; Mu et al., 2008b; Offman et al., 2010; Sawkar et al., 2002; Wang et al., 2011a; Yu et al., 2007). As opposed to L444P GC, N370S GC folding was previously shown to be amenable to rescue with GC specific chemical chaperones, suggesting that the location and nature of these two mutations have different destabilizing effects on the enzyme's native folding and cellular trafficking (Sawkar et al., 2005; Sawkar et al., 2002). In addition, GD patients carrying the N370S GC variant

never present the neuronopathic GD symptoms typically associated with L444P GC (Michelakakis et al., 1995). To verify whether lacidipine mediated rescue of mutated GC folding is restricted to the L444P GC variant, GD patient-derived fibroblasts carrying N370S GC were cultured in the presence of lacidipine and proteostasis regulators, and GC activities were measured. Diltiazem was used for comparison, as it was previously shown to elicit an increase in N370S GC folding (Mu et al., 2008a). Similar to what was reported above for L444P GC fibroblasts, lacidipine (20 μM) treatment for 72 hrs resulted in an increase in N370S GC activity (1.8-fold, $p<0.001$; Figure 4.2.4A), which was enhanced by the addition of MG-132 and celastrol (3.4- and 2.0-fold, respectively, Figure 4.2.4B). Diltiazem (10 μM, 1.4-fold; Figure 4.2.4A) mediated increase in N370S GC activity was enhanced by the addition of MG-132 and celastrol (3.1- and 1.7-fold, respectively, Figure 4.2.4C). These results suggest that lacidipine rescues the folding and activity of different mutated GC variants and thus functions as a proteostasis regulator in fibroblasts derived from patients with GD.

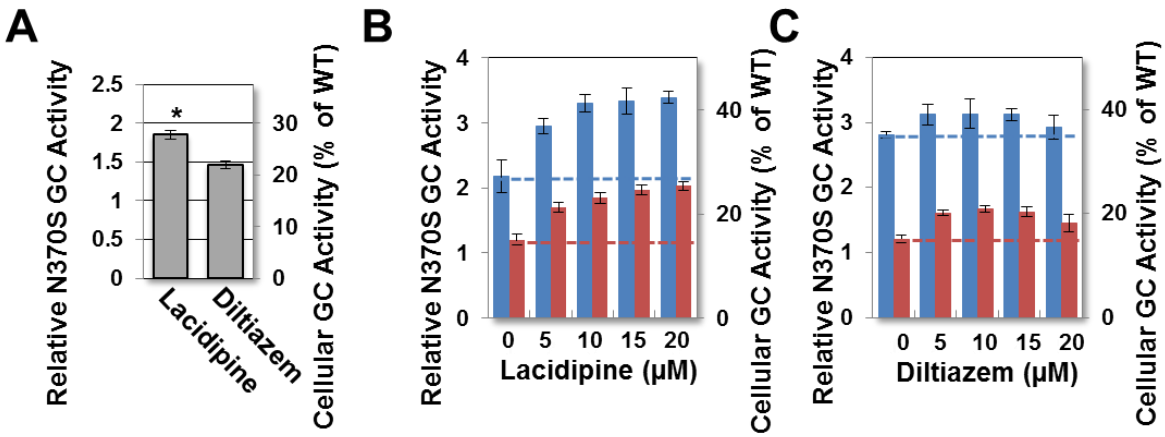

Figure 4.2.4. The activity of N370S GC is enhanced in cells treated with LTCC blockers. A) Relative N370S GC activities in cells treated with lacidipine (20 μM) and diltiazem (10 μM) for 72 hrs. Relative N370S GC activities in cells treated a proteostasis regulator (MG-132, 0.6 μM; celastrol, 0.6 μM) and an LTCC blocker: **B**) lacidipine, and **C**) diltiazem. Relative GC activities were obtained as described in Figure 4.2.2 and are reported as mean ± SD.

In order to confirm that the increase in activity detected in cells treated with lacidipine results from rescue of mutated GC folding and trafficking to the lysosome, we tested the glycosylation state and cellular localization of L444P GC.

GC glycosylation state was investigated by endoglycosidase H (EndoH) treatment (Maley et al., 1989), which, as describe in Chapter 4.1, allows distinguishing between partially glycosylated GC retained in the ER (low molecular weight) and fully glycosylated, lysosomal GC (high molecular weight) in Western blot analyses. The total protein content of cells cultured in media supplemented with lacidipine (20 μM), MG-132 (0.6 μM), celastrol (0.6 μM), or a combination thereof for 48 hrs was subjected to EndoH treatment, and GC was detected by western blot. A representative western blot is shown in Figure 4.2.5A, and quantification of EndoH-resistant and EndoH-sensitive GC bands is shown in Figure 4.2.5B. In untreated cells, nearly all L444P GC was detected as

EndoH-sensitive, as expected (Mu et al., 2008b). However, a band corresponding to EndoH-resistant L444P GC was detected in cells treated with lacidipine and its intensity was comparable to that detected in cells cultured with MG-132 or celastrol (the results obtained from the experiments conducted with MG-132 and celastrol have been published previously (Mu et al., 2008b), and are reported here for comparison). Interestingly, lacidipine treatment resulted in an about 1.5-fold increase of total L444P GC, and a decrease of the EndoH-sensitive fraction to 80% of total GC. Co-treatment with lacidipine and MG-132 was observed to cause a 2.5- and 1.7-fold increase in the EndoH-resistant pool of L444P GC, compared to cells treated only with lacidipine and MG-132, respectively (Figure 4.2.5A-B). This increase in mature, fully glycosylated GC correlates with results obtained from GC enzymatic assays.

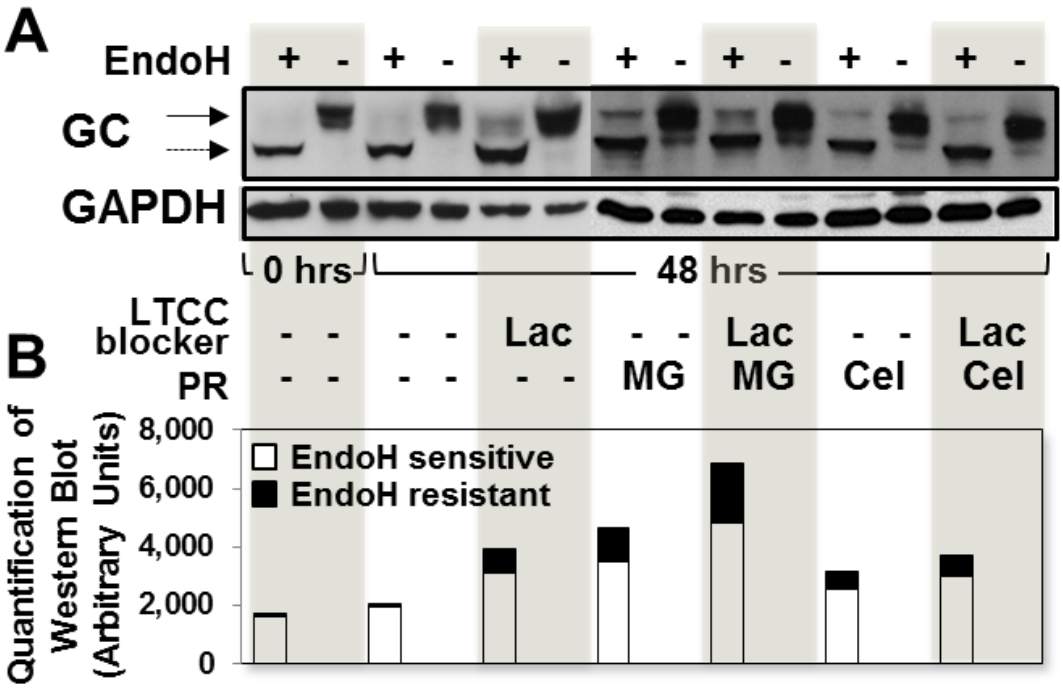

Figure 4.2.5. Treatment of GD patient-derived fibroblasts with lacidipine promotes L444P GC glycosylation. A) Western blot analyses of EndoH treated and untreated total protein content of L444P GC fibroblasts cultured with lacidipine (20 μM), MG-132 (0.6 μM), and celastrol (0.6 μM) for 48 hrs and detected using GC-specific antibody. The solid and dashed arrows indicate, respectively, EndoH resistant and EndoH sensitive bands. PR, proteostasis regulator. Lac, lacidipine; Dil, diltiazem; MG, MG-132; Cel, celastrol. **B**) Quantification of GC bands detected by western blot. Lower MW, EndoH-sensitive bands corresponding to GC retained in the ER were quantified and are reported in the white portion of the bars, and quantification of higher MW, EndoH-resistant bands corresponding to lysosomal GC are reported in the black top portions. Band analyses and quantifications were conducted using NIH Java Image analysis software.

L444P GC cellular localization was evaluated using immunofluorescence microscopy of fibroblasts derived from patients with GD carrying the L444P GC variant treated with lacidipine (20 μM) and/or MG-132 (0.6 μM) for 48 hrs and using antibodies specific for GC, for an ER marker (Calnexin, CNX), and for a lysosomal marker (LAMP-1). Co-localization of GC and CNX (Figure 4.2.6A) and GC and LAMP-1 (Figure 4.2.6B) is reported in green. L444P GC was barely detectable in untreated cells, presumably due to extensive ERAD (Figure 4.2.6A-B), as previously reported

(Michelakakis et al., 1995). Analysis of merged images revealed the presence of a large pool of enzyme in the ER (Figure 4.2.6A) and in the lysosome (Figure 4.2.6B) in lacidipine-treated cells, suggesting that lacidipine treatment increases the pool of folded L444P GC that escapes ERAD and trafficks to the lysosomes. Moreover, co-treatment with lacidipine and MG-132 further increased the pool of ER and lysosomal GC (Figure 4.2.6A-B), demonstrating that these two molecules synergize to rescue L444P GC folding and trafficking, and confirming the results obtained from enzymatic assays (Figure 4.2.3A).

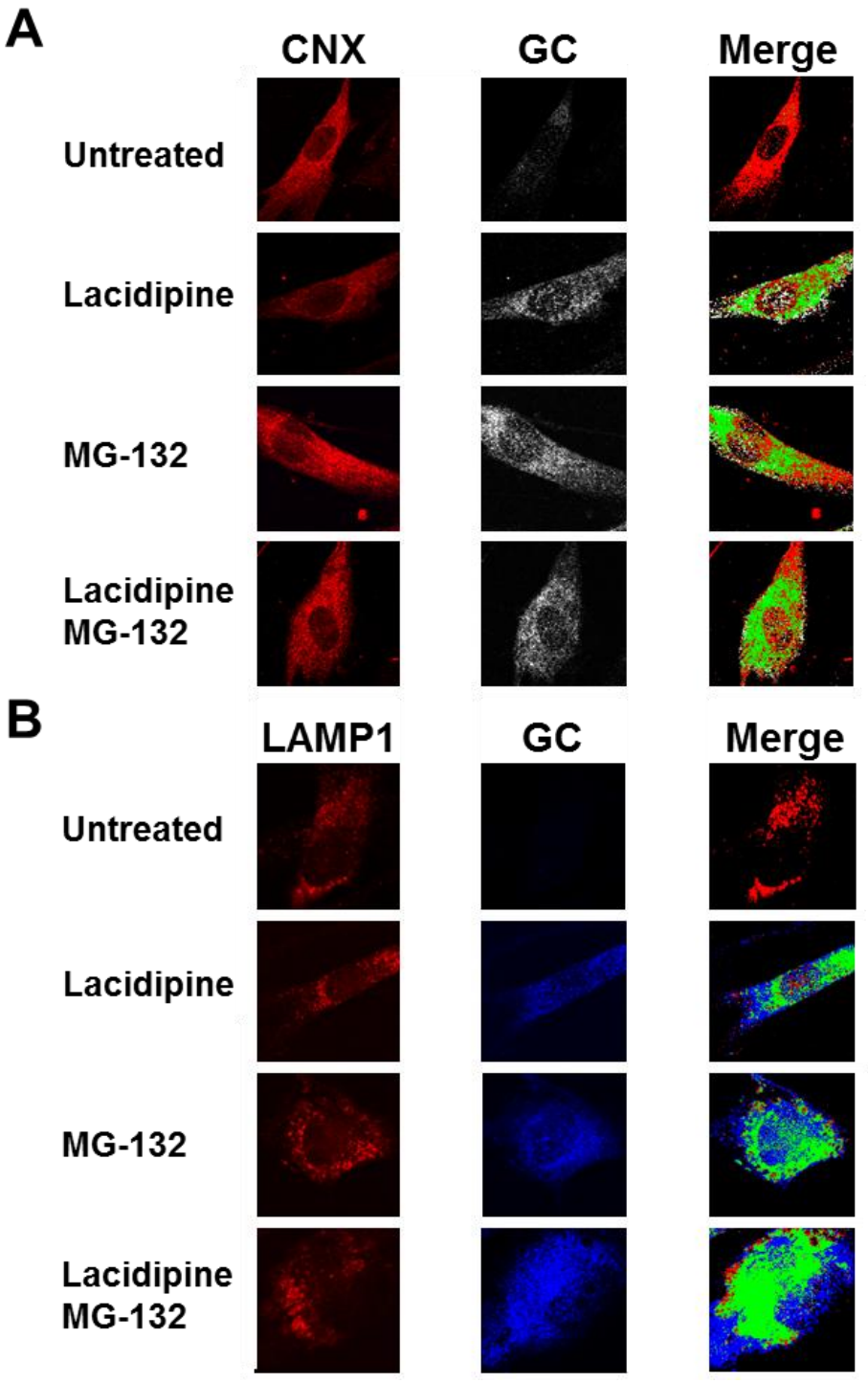

Figure 4.2.6. Cellular localization of L444P GC in patient-derived fibroblasts treated with lacidipine. Immunofluorescence microscopy of (**A**) GC and CNX (an ER marker), and (**B**) GC and LAMP1 (a lysosomal marker) in L444P GC fibroblasts. Cells were treated with lacidipine (20 μM) and MG-132 (0.6 μM) for 48 hrs. Colocalization of CNX (red, column 1) and GC (grey, column 2) is shown in green (column 3). Colocalization of LAMP1 (red, column 1) and GC (blue, column 2) is also shown in green (column 3).

We previously showed that RyRs inhibition creates an ER environment more amenable to L444P GC proteostasis in patient-derived fibroblasts (Chapter 4.1). The results reported here suggest that combining inhibition of RyRs and LTCC enables direct rescue of L444P GC proteostasis. Lacidipine treatment, however, seems to rescue L444P GC folding and activity more efficiently than the other LTCC blockers tested. This result suggests that lacidipine is a more potent modulator of intracellular [Ca^{2+}] than other Ca^{2+} blockers used here and previously (Mu et al., 2008a; Ong et al., 2010; Wang et al., 2011a) or that cell treatment with lacidipine rescues mutant GC folding by activating other cellular mechanisms that influence the mutated GC folding free energy diagram. The following studies were conducted to investigate these possibilities. Diltiazem was used as comparison in these studies because, although it also inhibits LTCC and RyRs and was reported to enhance the folding of mutated GC variants (Mu et al., 2008a), it is shown here to rescue L444P GC folding to a significantly lower extent than lacidipine. In addition, the mechanism involved in rescue of folding for GC variants by diltiazem treatment still remains elusive.

Lacidipine depletes cytosolic free [Ca^{2+}] in fibroblasts derived from patients with Gaucher's disease

Glucosylceramide buildup causes $[Ca^{2+}]_{ER}$ efflux and elevation of cytosolic [Ca^{2+}] in GD cells (Korkotian et al., 1999). Lacidipine and diltiazem, by binding to LTCC and RyRs, are expected to lower cytosolic [Ca^{2+}] and increase $[Ca^{2+}]_{ER}$, respectively. We asked whether the larger increase in GC activity observed upon cell treatment with lacidipine compared to diltiazem correlates with their different effects on intracellular

Ca^{2+} mobilization. Cytosolic free [Ca^{2+}] was evaluated by monitoring changes in Fura-2 fluorescence (Ong et al., 2010) in fibroblasts carrying L444P GC, N370S GC, or wild type GC treated with lacidipine or diltiazem (Figure 4.2.7). Lacidipine treatment was observed to deplete cytosolic [Ca^{2+}] with higher efficiency than diltiazem treatment in all cell types. In addition, depletion of cytosolic [Ca^{2+}] is markedly more enhanced in L444P GC than in N370S GC cells, suggesting a correlation between LTCC blocker mediated Ca^{2+} homeostasis modulation and rescue of mutated GC variants' folding.

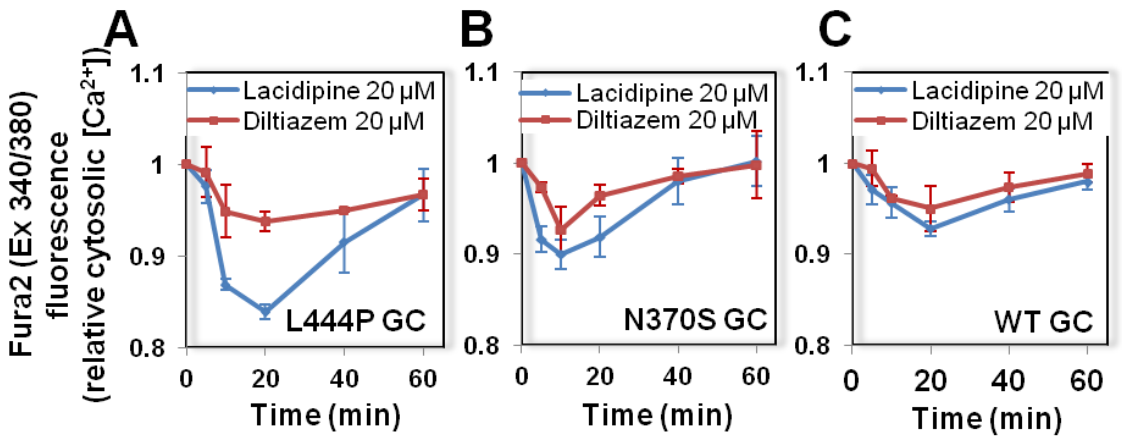

Figure 4.2.7. LTCC blockers reduce cytosolic [Ca^{2+}] levels in patient-derived fibroblasts. **A**) L444P GD, **B**) N370S GD, and **C**) WT fibroblasts were cultured with lacidipine (20 µM) and diltiazem (20 µM) for 5, 10, 20, 40 and 60 min respectively. Cytosolic [Ca^{2+}] was evaluated by measuring excitation 340/380 ratio of fura-2 acetoxymethyl ester and normalized to that at time zero. The data is reported as mean ± SD.

Lacidipine treatment upregulates BiP expression in fibroblasts derived from patients with Gaucher's disease carrying the L444P GC variant

We previously reported that the ER luminal chaperone BiP plays a key role in L444P GC folding. Upregulation of BiP expression, in combination with moderate UPR induction through MG-132 treatment, was shown to dramatically enhance the folding of

L444P GC (Chapter 4.1). We asked whether cell treatment with lacidipine influences the expression of ER chaperones and conducted quantitative RT-PCR analyses to measure the expression of the representative chaperones BiP, Calnexin (CNX), and Calreticulin (CRT) in L444P GC fibroblasts treated with lacidipine (20 μM), diltiazem (10 μM), MG-132 (0.6 μM), celastrol (0.6 μM), or a combination thereof (Figure 4.2.8A-C). BiP expression (Figure 4.2.8A) was upregulated by lacidipine treatment (5.6-fold, $p<0.01$) and by lacidipine and MG-132 co-treatment (13.1-fold, $p<0.01$). Diltiazem treatment resulted in a milder increase in BiP expression (1.8-fold), even when used in combination with MG-132 (3.1-fold). Even though celastrol treatment was observed to cause a modest increase in BiP expression (1.9-fold), supplementing celastrol-containing medium with a LTCC blocker did not influence BiP transcription.

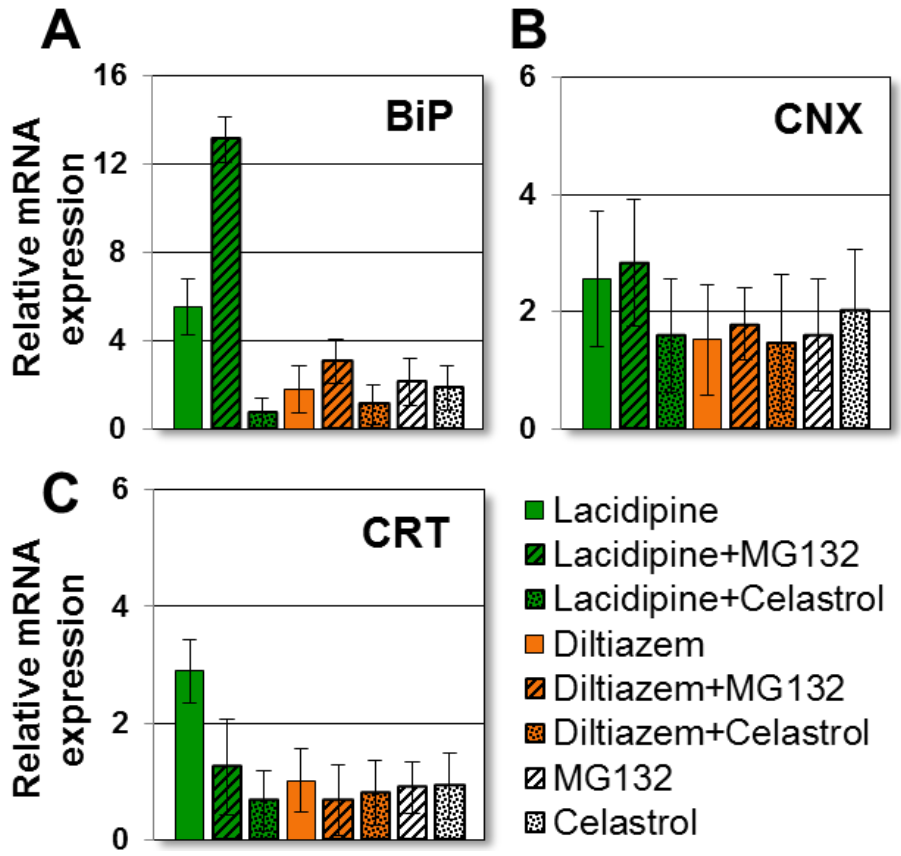

Figure 4.2.8. Upregulation of BiP transcription in patient-derived fibroblasts treated with lacidipine. Relative mRNA expression levels of **A**) BiP ($p<0.01$), **B**) CNX ($p<0.05$), and **C**) CRT in L444P GC fibroblasts treated with lacidipine (20 μM), diltiazem (10 μM), MG-132 (0.6 μM), and celastrol (0.6 μM) for 24 hrs were obtained by quantitative RT-PCR, corrected by the expression of the housekeeping gene GAPDH, and normalized to those of untreated cells. The data is reported as mean ± SD ($p<0.05$).

ER chaperone expression in cells treated with lacidipine (20 μM), diltiazem (10 μM), and MG-132 (0.6 μM) was confirmed by Western blot using chaperone specific antibodies (Figure 4.2.9). BiP protein accumulation was enhanced by treatment with lacidipine alone or in combination with MG-132 compared to untreated cells, but only slightly enhanced by diltiazem and MG-132 treatment. CNX and CRT protein levels did not seem to be drastically altered. These results are consistent with RT-PCR analyses,

and confirm the key role of BiP expression in promoting native folding of L444P GC (Wang et al., 2011a).

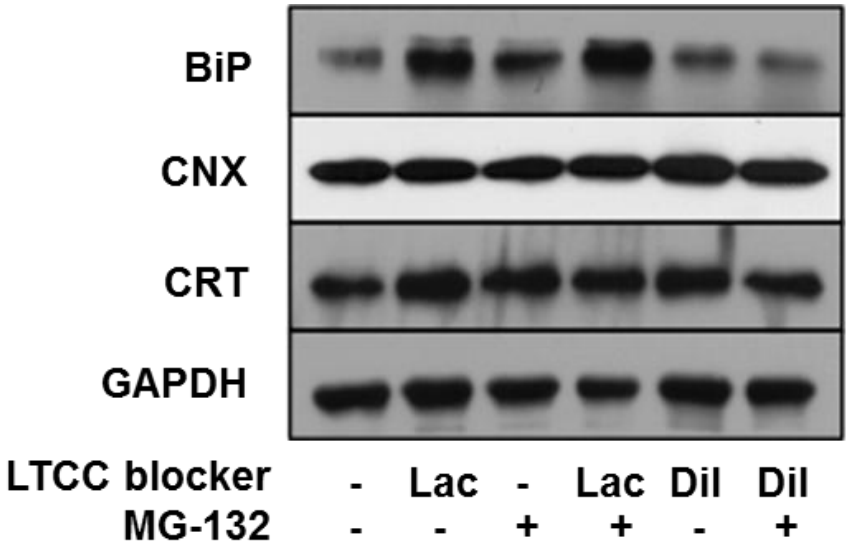

Figure 4.2.9. Protein accumulation levels of ER chaperones in cells treated with lacidipine. Western blot analyses of BiP, CNX, CRT, and GAPDH (used as loading control) accumulation in cells treated with lacidipine (20 μM) and MG-132 (0.6 μM) for 48 hrs. Lac, lacidipine; Dil, diltiazem.

As opposed to what was previously observed in investigating RyRs blockers, which despite dramatically enhancing MG-132 mediated L444P GC folding rescue do not directly modulate the expression of ER chaperones (Chapter 4.1), this data indicates that lacidipine's mechanism of action is based on extensive remodeling of ER chaperone pathways. However, we found that although cell treatment with lacidipine significantly enhances BiP expression, it does not alter its cellular localization. Particularly, immunofluorescence studies conducted to test BiP localization in the ER and in the Golgi revealed that BiP is still primarily localized in the ER (Figure 4.2.10).

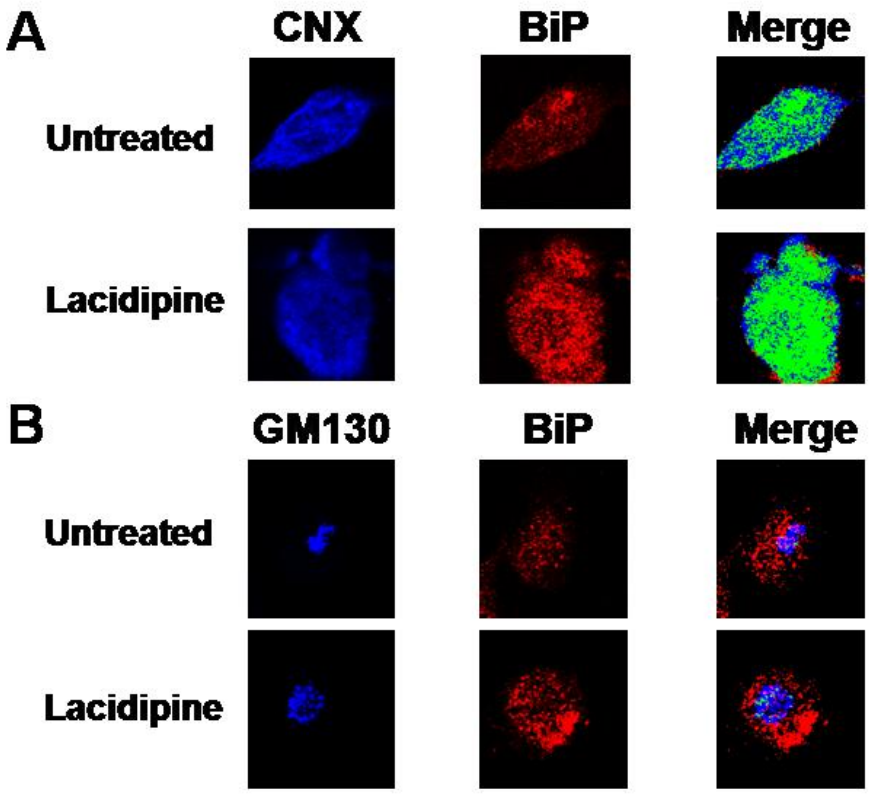

Figure 4.2.10. BiP cellular localization upon lacidipine treatment. Immunofluorescence microscopy of **A**) CNX (an ER marker) and BiP, and **B**) GM130 (a Golgi marker) and BiP in L444P GC fibroblasts. Cells were treated with lacidipine (20 μM) for 48 hrs. Colocalization of CNX (blue, column 1) and BiP (red, column 2) is shown in green (column 3). Colocalization of GM130 (blue, column 1) and BiP (red, column 2) is also shown in green (column 3).

Lacidipine treatment causes modest activation of all three arms of the UPR, but does not induce cytotoxicity in fibroblasts derived from patients with Gaucher's disease carrying the L444P GC variant

We next investigated the activation of the unfolded protein response (UPR), which, as described previously (Chapter 4.1) plays a significant role in the native folding of severely destabilized GC variants and is often induced by cell tratement with proteostasis regulators (Wang et al., 2011a). As described above, the UPR is a tripartite

signal transduction cascade activated in response to the accumulation of misfolded proteins in the ER. Briefly, UPR induction is mediated by the activation of three integral ER membrane proteins, namely inositol requiring kinase 1 (IRE1), activating transcription factor 6 (ATF6), and double-stranded RNA-activated ER kinase (PERK) (Schroder and Kaufman, 2005), which lead to the upregulation of UPR related genes, including chaperones and ERAD proteins. The expression of ATF6, PERK, and IRE1 was investigated in this study to evaluate UPR induction in fibroblasts derived from GD patients treated with lacidipine and diltiazem. Lacidipine was found to activate two of the three arms of the UPR, and with higher efficiency than diltiazem. The increase in expression of genes of the UPR pathway in cells treated with lacidipine was considerably enhanced by the addition of MG-132. These results correlate with measurements of L444P GC activity reported above, in which maximal increase was obtained upon co-treatment with lacidipine and MG-132 (Figure 4.2.3A).

Activation of IRE1 causes X-box binding protein-1 (Xbp-1) mRNA cleavage (Ron and Walter, 2007). The product of Xbp-1 spliced mRNA acts as an activator of UPR target genes, whereas the product of the unspliced Xbp-1 precursor acts as a repressor (Ron and Walter, 2007). RT-PCR experiments followed by gel electrophoresis were conducted to evaluate the accumulation of the spliced and unspliced forms of Xbp-1 in L444P GC fibroblasts treated with LTCC blockers (lacidipine (20 μM) or diltiazem (10 μM)) and a proteostasis regulator (MG-132 (0.6 μM) or celastrol (0.6 μM)) for 24 hrs (Figure 4.2.11A). Treatment with MG-132 enhanced Xbp-1 splicing in L444P GC fibroblasts, as previously reported (Mu et al., 2008b). Spliced Xbp-1 was barely detectable in cells treated with lacidipine. However, a 4.8-fold increase in spliced Xbp-1

accumulation was observed upon co-treatment with lacidipine and MG-132 compared to treatment with MG-132 only (Figure 4.2.11A-B), recapitulating the synergistic effect of lacidipine and MG-132 observed in enzymatic assays (Figure 4.2.3A). A 4.3-fold increase in spliced Xbp-1 was detected in L444P GC fibroblasts treated with diltiazem and MG-132 compared to that measured in fibroblasts treated with MG-132 only. Even though cell treatment with celastrol causes increase in Xbp-1 splicing and in L444P GC folding rescue (Mu et al., 2008b), addition of celastrol to the media of lacidipine- or diltiazam-treated cells did not increase Xbp-1 splicing. Taken together, these results suggest a synergistic effect of LTCC blockers lacidipine and diltiazem and the proteostasis regulator MG-132 on the activation of the IRE1 arm of the UPR in L444P GC patient-derived fibroblasts. Among the culturing conditions investigated, the highest degree of Xbp-1 splicing was observed in cells displaying the maximum increase of L444P GC activity (lacidipine and MG-132 treatment, Figure 4.2.1), suggesting a key role of IRE1 activation in rescuing L444P GC folding.

The second arm of the UPR is mediated by ATF6 activation (Ron and Walter, 2007). Quantitative RT-PCR was used to evaluate ATF6 expression in cells treated as described above. Lacidipine treatment resulted in ATF6 upregulation (2.1-fold), which was further enhanced by the addition of MG-132 (3.5-fold), suggesting that the ATF6 arm of the UPR is also activated by treatment with lacidipine, particularly when used in combination with MG-132 (Figure 4.2.11C). Diltiazem treatment barely affected ATF6 expression, and the addition of neither MG-132 nor celastrol to diltiazem-supplemented media caused significant changes.

The third branch of the UPR is induced by PERK oligomerization and phosphorylation of the eukaryotic translation initiation factor-2 (eIF2α). eIF2α induces the expression of the transcription factor ATF4 and a subset of ATF4 target genes, including CHOP (Ron and Walter, 2007). Lacidipine treatment caused CHOP upregulation (3.7-fold), which was considerably enhanced by the addition of MG-132 (5.0-fold), indicating that the PERK arm of the UPR is activated in response to lacidipine treatment (Figure 4.2.11D). Treatment with diltiazam alone or in combination with a proteostasis regulator did not cause significant changes in CHOP expression (Figure 4.2.11D).

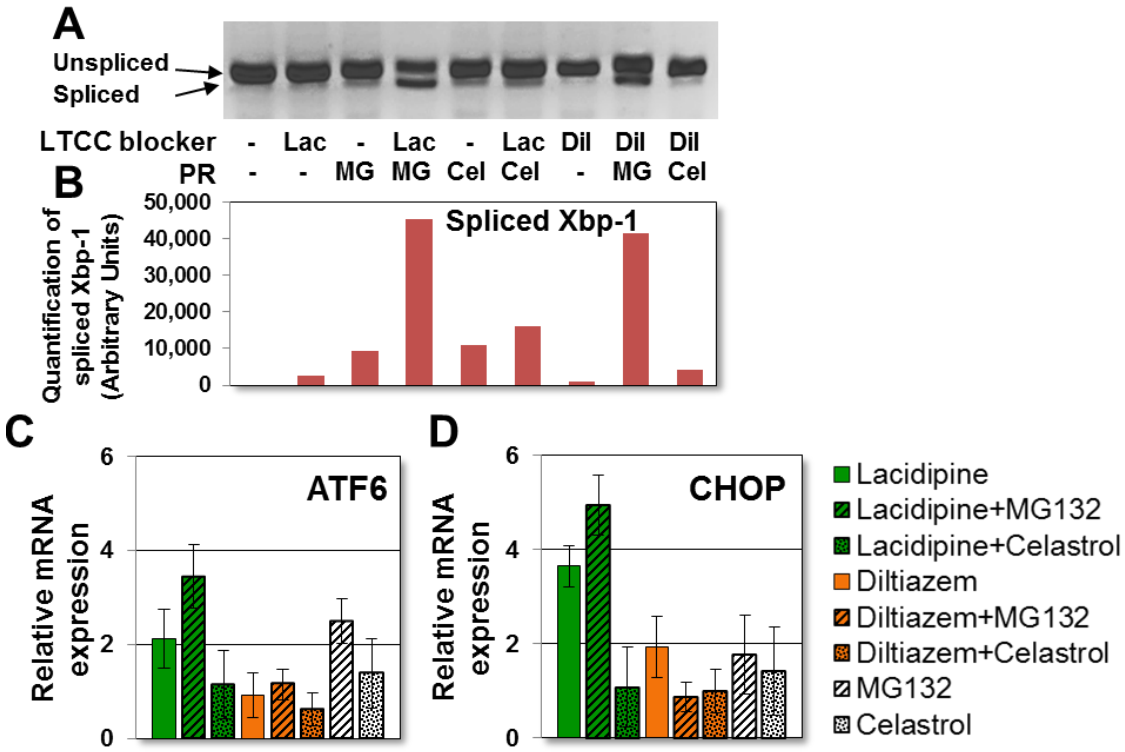

Figure 4.2.11. Upregulation of UPR genes in patient-derived fibroblasts treated with lacidipine. Cells were treated with lacidipine (20 μM), diltiazem (10 μM), MG-132 (0.6 μM), and celastrol (0.6 μM) for 24 hrs. **A**) Xbp-1 expression and splicing was determined by RT-PCR and separation on agarose gel and quantification of spliced Xbp-1 band intensities **B**) conducted using the NIH Java Image analysis software. PR, proteostasis regulator; Lac, lacidipine; Dil, diltiazem; MG, MG-132; Cel, celastrol. Relative mRNA expression levels of **C**) ATF6 and **D**) CHOP were obtained by quantitative RT-PCR and calculated as described in Figure 4.2.8. The data is reported as mean ± SD ($p<0.01$).

Prolonged induction of the UPR and inability of the ER folding capacity to cope with the load of misfolded proteins leads to apoptosis. A number of genes are involved in the regulation of apoptosis induction, including the pro-apoptotic genes encoding for Bcl-2 homologous antagonist (BAK) and Bcl-2-associated X protein (BAX) (Scorrano et al., 2003), and the anti-apoptotic gene encoding the apoptosis regulator Bcl-2 (Rodriguez et al., 2010). The expression of BAK, BAX, and Bcl-2 was investigated in cells treated with LTCC blockers and proteostasis regulators as described before. MG-132 and celastrol

treatments caused upregulaton of the pro-apoptotic proteins BAK and BAX. Specifically, MG-132 induced upregulation of BAK (2.1-fold, Figure 4.2.12A) and celastrol induced upregulation of BAX (3.1-fold, Figure 4.2.12B). Lacidipine did not significantly alter either BAX or BAK expression, while diltiazem caused upregulation of both BAK (1.9-fold) and BAX (2.1-fold). Co- treatment with lacidipine and MG-132 was compared to treatment with MG-132. When cells were co-treated with lacidipine and MG-132, BAK expression was barely altered, but BAX expression was observed to decrease, compared to cells treated with MG-132 only. This result is interesting because lacidipine and MG-132 were shown to have a synergistic effect on the rescue of L444P GC activity (Figure 4.2.1C) and on UPR activation (Figure 4.2.11A-D). Since enhanced UPR activation typically leads to enhanced apoptosis induction, both BAX and BAK expression would be expected to increase in cells treated under these conditions. Particularly, BAX expression was lowered 2.9-fold in cells treated with lacidipine and MG-132, suggesting that the mechanism of lacidipine-mediated L444P GC folding rescue involves inhibition of apoptosis via BAX downregulation. Interestingly, when diltiazem was used in combination with a proteostasis regulator, MG-132 mediated BAK upregulation was enhanced (2.9-fold), but celastrol-mediated BAX upregulation was lowered, which may explain why treatment with celastrol, but not with MG-132, results in enhancement of L444P GC activity increase mediated by diltiazem.

The expression of the anti-apoptotic Bcl-2 encoding gene was also evaluated (Figure 4.2.12C). Bcl-2 contributes to maintaining ER Ca^{2+} homeostasis by reducing $[Ca^{2+}]_{ER}$ efflux (Eckenrode et al., 2010; Rong et al., 2009), and was found to be upregulated in L444P GC fibroblasts cultured with either lacidipine or diltiazem (1.9-

fold), underscoring the therapeutic potential of Ca^{2+} homeostasis modulation in L444P GC fibroblasts. MG-132 treatment lowered Bcl-2 expression (0.8-fold), whereas celastrol treatment did not seem to affect it. The addition of a proteostasis regulator to lacidipine-treated cells resulted in lowered Bcl-2 expression, returning it to the level detected in untreated cells, whereas the addition of a proteostasis regulator to diltiazem-treated cells resulted in substantial downregulation of Bcl-2 (MG-132 and diltiazem: 2.3-fold; celastrol and diltiazem: 2.0-fold). Similar to what was reported above regarding the expression of pro-apoptotic genes, modulation of Bcl-2 expression correlates with the ability of LTCC blockers to rescue L444P GC folding when used alone or in combination with an UPR-inducing proteostasis modulator.

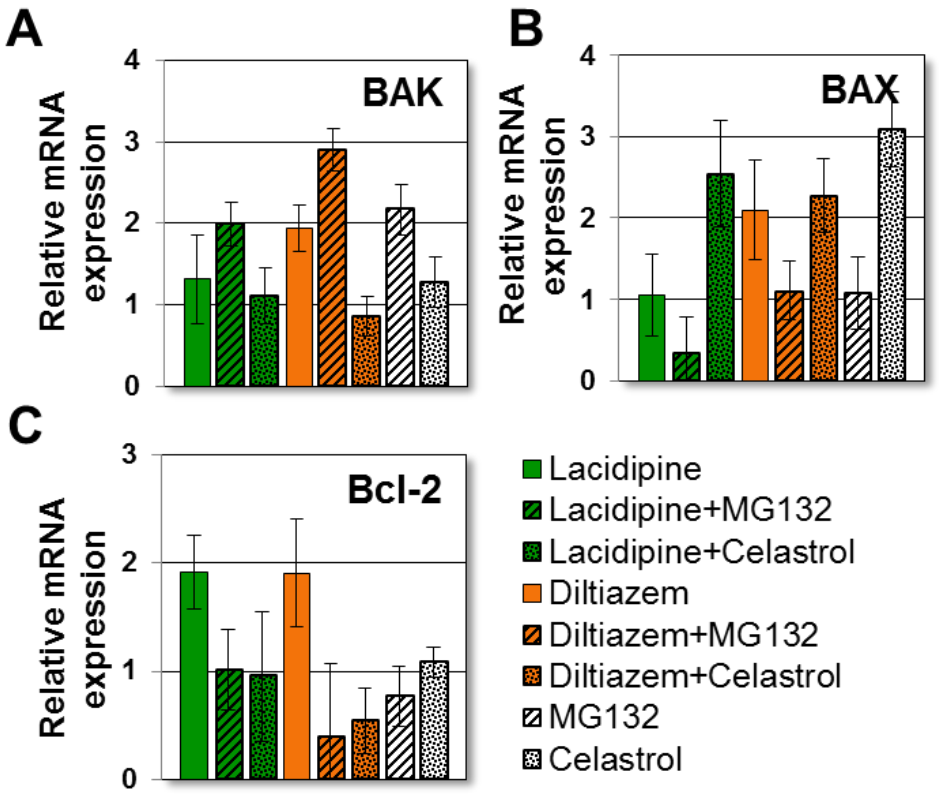

Figure 4.2.12. Upregulation of the anti-apoptotic gene Bcl-2 in patient-derived fibroblasts treated with lacidipine. Cells were treated with lacidipine (20 μM), diltiazem (10 μM), MG-132 (0.6 μM), and celastrol (0.6 μM) for 24 hrs. Relative mRNA expression levels of **A**) BAK, **B**) BAX, and **C**) Bcl-2 were obtained by quantitative RT-PCR and calculated as described in Figure 4.2.8. The data is reported as mean ± SD ($p<0.01$).

We next tested whether lacidipine-mediated changes in the expression of pro- and anti-apoptotic genes translate into differences in cytotoxicity and cell death, a common marker of cells treated for L444P GC folding rescue through UPR activators, such as MG-132, tunicamycin, and thapsigargin (Chapter 4.1). L444P GC patient-derived fibroblasts treated with Ca^{2+} blockers and proteostasis regulators as described above were tested using the CytoGLO™ Annexin V-FITC Apoptosis Detection Kit to monitor membrane rearrangement (Annexin V binding) and fragmentation (propidium iodide (PI) binding), which occur during early and late apoptosis, respectively (Table 4.2). Treatment

of L444P GC fibroblasts with lacidipine (20 μM) did not cause cytotoxicity, and the apoptosis induction was not significantly altered compared to untreated cells. MG-132 (0.6 μM) and celastrol (0.6 μM) resulted in 47% and 10% increase in Annexin V binding, and 7.4% and 4.7% increase in dead cell population, respectively. The addition of lacidipine to MG-132 or celastrol treated cells led to a decrease in Annexin V binding to 41% and 8.3% and to a decrease in dead cell population to 4.5% and 4.1%, respectively. These results indicate that lacidipine treatment under conditions observed to rescue mutated GC folding and induce UPR not only does not cause cytotoxicity, but also partially counteracts the cytotoxic effect of UPR inducing proteostasis regulators.

Interestingly, lacidipine mechanism of L444P GC folding rescue differs significantly from that of RyRs blockers shown in Chapter 4.1. While cell treatment with RyRs blockers does not activate the UPR but rescues GD fibroblasts from UPR-induced toxicity, lacidipine treatment concurrently activates the UPR and ameliorates UPR-induced toxicity in GD fibroblasts.

Table 4.2. Cell toxicity assay (lacidipine treatment) ($p<0.01$)

Cell treatment	Annexin V		PI	
	Population[1]	Binding[2]	Population[1]	Binding[2]
Lacidipine	1.8±0.4	-2.9±1.8	-3.3±0.9	2.5±1.3
MG-132	7.2±0.1	47±1.0	7.4±0.4	28±0.9
Lacidipine+MG-132	3.6±0.2	41±1.1	4.5±0.3	15±1.8
Celastrol	1.8±0.9	10±0.3	4.7±0.2	19±1.2
Lacidipine+Celastrol	1.0±0.5	8.3±1.2	4.1±1.0	13±0.2

[1] Change (%) in number of cells bound to Annexin V/PI compared to untreated cells.
[2] Change (%) in Annexin V/PI binding affinity compared to untreated cells.

Lacidipine treatment upregulates GC chromosomal expression in fibroblasts derived from patients with Gaucher's disease carrying the L444P GC variant

As indicated previously (Figure 4.2.5A-B), the total amount of L444P GC seems to be enhanced by lacidipine treatment. Upregulation of the gene encoding GC (GBA) as well as of other genes encoding for lysosomal enzymes involved in lipid metabolism was previously reported in cells treated for the rescue of L444P GC folding through UPR induction (Chapter 4.1). Particularly, we found that a number of genes associated with the development of lysosomal storage disorders, such as Niemann-Pick, Tay-Sachs, and Fabry diseases, were upregulated upon MG-132-induced UPR (see chapter 4.1). This finding resonates with the general increase in lipid metabolism that normally occurs during UPR (Schroder and Kaufman, 2005) and was suggested as a potentially therapeutic "side-effect" of mutated GC proteostasis regulation via UPR activation (Chapter 4.1).

Quantitative RT-PCR and western blot analyses were conducted to understand whether the increase in cellular concentration of L444P GC observed in cells treated with lacidipine is due to upregulation of GC expression in addition to enhanced folding of L444P GC and lowered ERAD. L444P GC fibroblasts were treated with lacidipine (20 μM), diltiazem (20 μM), MG-132 (0.6 μM), celastrol (0.6 μM), or a combination thereof (Figure 4.2.13A). Lacidipine treatment was observed to enhance GC mRNA expression (3.1-fold) to an extent similar to MG-132 (3.1-fold) or celastrol (3.4-fold). Treatment with diltiazem resulted in a lower increase in GC expression (2.5-fold), most likely reflecting diltiazem's milder effect on UPR induction. Interestingly, addition of MG-132 resulted in an increase in both lacidipine- and diltiazem-mediated GC upregulation (4.5-

and 4.6-fold, respectively), whereas celastrol slightly lowered this expression (2.9- and 2.2-fold, respectively). These transcriptional changes were confirmed at the translational level by western blot analyses (Figure 4.2.13B). L444P GC fibroblasts were cultured with lacidipine (20 μM), MG-132 (0.6 μM), and celastrol (0.6 μM) for 48 hrs, and bands detected with a GC-specific antibody were quantified using NIH Java Image analysis software (Figure 4.2.13C). The L444P GC content of lacidipine-treated cells increased about 50% compared to that of untreated cells, similarly to what was observed in MG-132-treated cells. In addition, the combination of lacidipine and MG-132 caused a 2.3-fold increase in total L444P GC, which is higher than what was observed in cells treated with either one of these molecules, and is in agreement with the results obtained from quantitative RT-PCR. Celastrol treatment did not significantly affect GC protein accumulation. In summary, this data indicates that GC chromosomal expression is enhanced upon treatment with lacidipine and suggests that GC upregulation contributes to L444P GC folding rescue mediated by UPR induction.

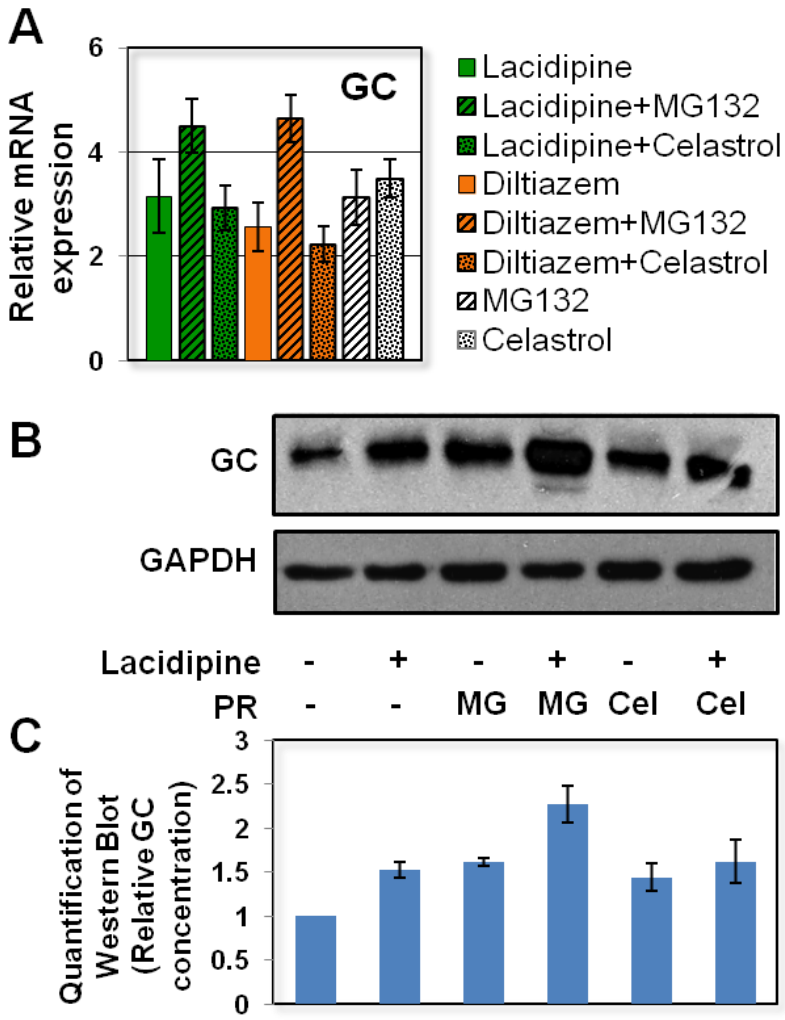

Figure 4.2.13. Upregulation of L444P GC expression in fibroblasts treated with lacidipine and diltiazem. A) Relative GC mRNA expression level was evaluated by quantitative RT-PCR in L444P GC fibroblasts treated with lacidipine (20 μM), diltiazem (10 μM), MG-132 (0.6 μM), and celastrol (0.6 μM) for 24 hrs ($p<0.01$). mRNA expression levels were calculated as described in Figure 4. The data is reported as mean ± SD. **B**) Representative Western blot analysis of cells treated with lacidipine (20 μM), MG-132 (0.6 μM), and celastrol (0.6 μM) for 48 hrs using GC specific antibody. **C**) Western blots band quantification. GC bands were quantified by NIH Java Image analysis software. GAPDH expression was used as a loading control. PR, proteostasis regulator; MG, MG-132; Cel, celastrol.

4.2.3. Discussion

Ubiquitously expressed voltage-gated LTCCs support inward current of Ca^{2+} ions. The function of Ca^{2+} ions as an intracellular second messenger has been reported in many cellular processes, ranging from gene expression to cardiac and smooth muscle contraction. Because Ca^{2+} mediates both physiological and pathological events, considerable effort has been devoted to the study of Ca^{2+} channel antagonists, a chemically and pharmacologically heterogeneous group of drugs widely used as therapeutic agents as well as research tools. The prototypical LTCC antagonists are diltiazem (a benzothiazepine), verapamil (a phelylalkylamine) and nifedipine (an 1,4-dihydropyridine) (Triggle, 2006). Diltiazem and verapamil are FDA-approved drugs for the treatment of hypertension and cardiac arrhythmias (Hockerman et al., 1997). They were reported to rescue folding, trafficking and activity of GC variants in fibroblasts derived from patients with GD (Mu et al., 2008a), but failed to rescue mutated GC activity in mice (Sun et al., 2009). In an effort to discover small molecules that efficiently rescue the folding of mutated GC variants by enhancing the cellular folding capacity but without inducing cytotoxicity, we tested a series of 1,4-dihydropyridines, a class of LTCC antagonists known to lower intracellular [Ca^{2+}] with higher selectivity than benzothiazepines and phelylalkylamine (Triggle, 2003).

Lacidipine was found to rescue the activity of GC variants carrying the two most common mutations, L444P and N370S, in fibroblasts derived from patients with GD. In particular, lacidipine mediates a substantially higher increase in L444P GC activity than what was observed using any other LTCC and RyRs blockers to date (Mu et al., 2008a; Ong et al., 2010; Wang et al., 2011a), and this increase is markedly enhanced by co-

treatment with proteostasis modulators MG-132 and celastrol. The nature of the chemical structure of LTCC blockers – with lacidipine highly hydrophobic, diltiazem and verapamil charged at physiologic pH (Triggle, 2003) – is likely to influence their cell permeability and explain why treatment of GD fibroblasts with lacidipine resulted in higher depletion of cytosolic [Ca^{2+}] and more effective remodeling of L444P GC proteostasis compared to diltiazem and verapamil.

L444P GC fibroblasts treated with lacidipine (and diltiazem for comparison) were used to conduct mechanistic studies and gain a better understanding of the molecular mechanisms involved in L444P GC proteostasis. We demonstrated that lacidipine induced rescue of mutated GC folding (Figures 4.2.1-4.2.6) and that this behavior correlates with its ability to i) lower cytoplasmic [Ca^{2+}], thereby counteracting the effect of GC substrate accumulation (Figure 4.2.7), ii) enhance the ER's folding capacity via substantial upregulation of BiP expression (Figures 4.2.8 and 4.2.9), confirming that BiP plays a key role in the folding of L444P GC, iii) induce the UPR (Figure 4.2.11) and upregulate GC expression (Figure 4.2.13), and iv) lower cytoxicity and limit UPR mediated apoptosis induction (Figure 4.2.12 and Table 4.2). An analogous mode of action was previously reported to explain the synergistic effect of two distinct small molecules, a proteostasis regulator (MG-132) and a RyRs blocker (ryanodine), on L444P GC folding rescue. Particularly, MG-132 was reported to induce BiP upregulation and UPR induction and ryanodine to lower intracellular [Ca^{2+}] and counteract UPR induced cytotoxicity (Chapter 4.1), suggesting that combining these different mechanisms of proteostasis regulation is an effective strategy to rescue mutated GC folding. In summary, this study sheds light on the cellular pathways involved in mutated GC folding and introduces a

novel strategy to rescue mutant GC folding via small molecule treatment that combines remodeling of two general cellular pathways involved in protein homeostasis: protein folding and Ca^{2+} homeostasis.

4.3. Inhibition of ER-associated degradation rescues native folding in frobroblasts derived from patients with lysosomal storage diseases

4.3.1. Introduction

In the previous chapters, we demonstrated that reporgramming the proteostasis network via modulation of intracellular Ca^{2+} homeostasis enables rescue of mutated, degradation-prone GC vairants (see Chapters 4.1 and 4.2; or papers Wang et al., 2011a and Wang et al., 2011b). Mechanistic studies conducted to investigate changes induced by Ca^{2+} blockers on the proteostasis network that directly influence rescue of mutated GC variants led to the observation that enhancing the pool of mutated GC folding intermediate in the ER amenable to folding rescue is critical to increase foding and trafficking of native GC. Specifically, increase in mutated GC activity correlates with i) upregulation of the main ER chaperone BiP, which is known to enhance ER retention and prevent ERAD of misfolding intermediates (Muresan and Arvan, 1998), and ii) upregulation of GBA transcription (Chapters 4.1 and 4.2). Both strategies, BiP and GC upregulation, increase the pool of GC folding intermediates that escapes ERAD and is amenable to folding rescue.

We hypothesized that native folding of mutated enzyme variants is limited by the rapid disposal of unstable folding intermediates via ERAD. Hence, we sought to investigate ERAD inhibition in LSD patient-derived cells and establish the role of this pathway in the development of loss-of-function phenotypes. We identified two small molecules ERAD inhibitors: Kifunensine (Kif), which inhibits ER mannosidase I

(Avezov et al., 2008; Fagioli and Sitia, 2001) and thus interferes with early substrate recognition, and Eeryastatin I (EerI), which inhibits p97 ATPase activity (Fiebiger et al., 2004; Wang et al., 2010), thereby limiting retrotranslocation of misfolded substrates (Appendix A; Figure 4.3.1). Treatment with ERAD inhibitors partially restores folding and activity of mutated GC variants in fibroblasts derived from GD patients. Rescue of mutated HexA was also observed in Tay-Sachs disease fibroblasts upon treatment with EerI, demonstrating the generality of this approach. Furthermore, we investigated the transcriptional changes that occur in GD fibroblasts in response to these two different mechanisms of ERAD inhibition, with particular attention to the expression of ER chaperones, the gene encoding GC, and UPR activation. Results from this study show that ERAD regulates the processing of unstable secretory proteins and that ERAD inhibition is a viable strategy to rescue native folding and activity of mutated lysosomal enzymes associated with the development of LSDs. EerI mediated inhibition of substrate retrotranslocation, although possibly more efficient in rescuing mutated GC folding, was observed to cause UPR induction and cytotoxicity. Kif-mediated inhibition of early substrate recognition, however, which is likely to prolong ER retention and substrate folding without causing accumulation of irremediably misfolded proteins, caused minimal activation of the UPR and did not result in induction of apoptosis.

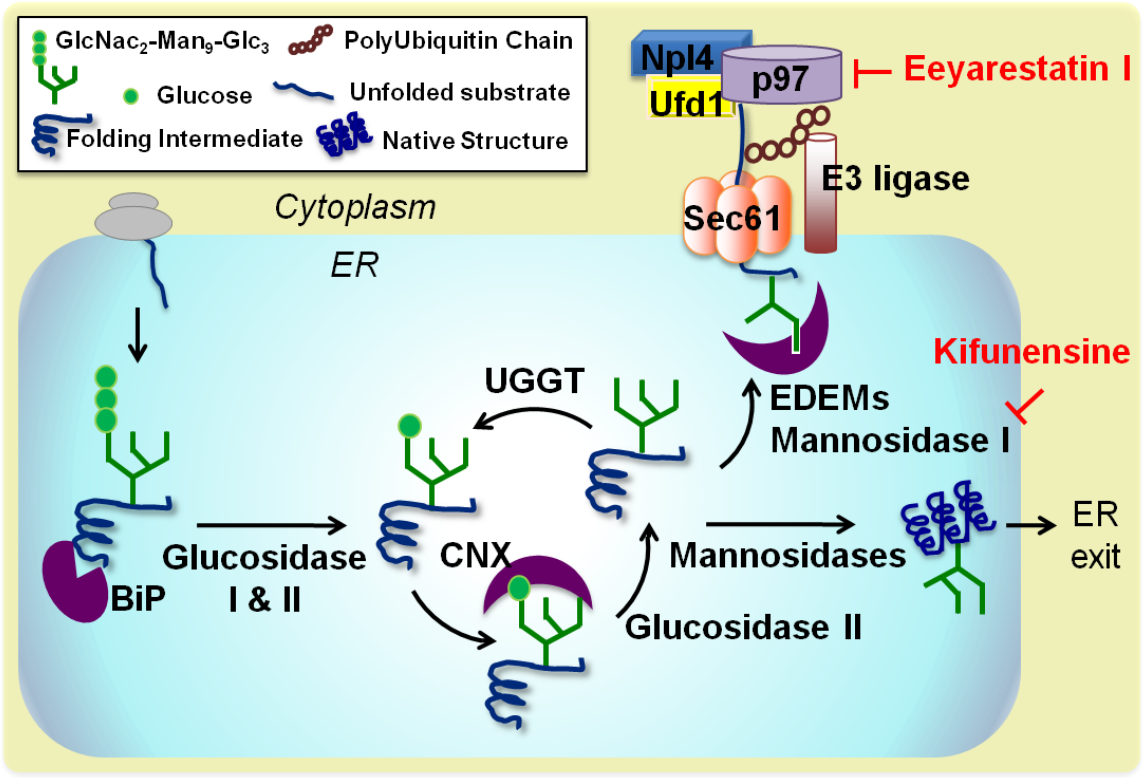

Figure 4.3.1. ERAD pathways and mechanisms of ERAD inhibition. As newly synthesized polypeptides are translocated into the ER, they are immediately recognized by BiP, which promotes substrate folding and solubility. They are then marked with an oligosaccharide precursor (GlcNAc2-Man9-Glc3), which is sequentially trimmed to allow substrate interaction with the lectin chaperones calnexin (CNX) and calreticulin (CRT). Specifically, interaction with the lectin chaperones occurs upon cleavage of the two terminal glucoses by glucosidase I and II and is terminated by removal of the last outermost glucose residue (GlcNAc2-Man9) by glucosidase II. At this point, natively folded proteins exit the ER while partially folded intermediates are reglucosylated by UDP-glucose:glycoprotein glucosyltransferase (UGGT) and re-enter the lectin folding cycle. In order to prevent excessive accumulation of folding intermediates, unstable misfolding-prone substrates are processed by ER mannosidase I, which cleaves three to four mannose residues from the oligosaccharidic group and promotes substrate binding with the ER degradation-enhancing α-mannosidase-like lectins (EDEM). ERAD substrates are then retrotranslocated to the cytoplasm via the Sec61 retrotranslocon, and polyubiquitinated. Substrate retrotranslocation is mediated by the p97 complex, which includes ubiquitin fusion degradation 1 (Ufd1) and nuclear protein localization 4 (Npl4). p97 ATPase provides the driving force for substrate extraction and shuffling to the proteasome. As shown in the schematic, Kifunensine and Eeyarestatin I, small molecules that function as ERAD inhibitors, block different steps of the ERAD pathway. Kifunensine inhibits ER mannosidase I and Eeyarestatin I inhibits p97 ATPase activity. (GlcNAc, N-acetylglucosamine; Man, mannose; Glc, glucose)

4.3.2. Results

ERAD inhibition enhances native folding, trafficking and activity of mutated GC in fibroblasts derived from patients with GD

In order to investigate the role of the ERAD pathway in the folding of mutated GC variants, L444P GC fibroblasts were cultured in the presence of ERAD inhibitors (Eeyarestatin I (EerI) and Kifunensin (Kif)) for 5 days, and GC activities were evaluated every 24 hours with the intact cell GC activity assay (Mu et al., 2008b). Culturing conditions resulting in maximal rescue of L444P GC activity are reported in Figure 4.3.2 (blue lines). L444P GC activity was observed to increase up to 2.0-fold in cells treated with EerI (8 μM final medium concentration, $p<0.001$) for 48 hrs compared to untreated cells, which corresponds to about 25% of the WT cellular activity (Figure 4.3.2A) and would be expected to ameliorate GD symptoms (Schueler et al., 2004).

We hypothesized that EerI-mediated ERAD inhibition prolongs ER retention of mutated GC, thereby enhancing the pool of GC folding intermediates amenable to folding rescue. Hence, we asked whether combining ERAD inhibition with enhancement of the cellular folding capacity could further increase the pool of natively folded GC that trafficks to the lysosomes. To investigate this question, EerI treated cells were cultured in the presence of MG-132 and celastrol, small molecules shown to function as proteostasis regulators and rescue GC folding through a mechanism distinct from ERAD modulation (Chapters 4.1 and 4.2). Experiments were designed to explore the addition of a constant concentration of proteostasis regulator (0.4, 0.6, or 0.8 μM) to a range of EerI concentrations. Co-administration of EerI (2 μM) and MG-132 (0.6 μM) for 48 hrs resulted in a dramatic 4.2-fold increase in L444P GC activity ($p<0.001$; Figure 4.3.2A)

compared to untreated cells, which corresponds to 52.5% of WT GC activity and is significantly higher than the activity of cells treated only with EerI (2.0-fold) or MG-132 (2.4-fold) under the same conditions. Co-treatment with EerI and celastrol was also observed to enhance L444P GC activity rescue (Figure 4.3.2B). Specifically, GD cells treated with EerI (5 μM) and celastrol (0.4 μM) for 48 hrs displayed a 3.1-fold increase in L444P GC activity ($p<0.001$), which is higher than what was observed in cells treated only with EerI (1.3-fold) or celastrol (1.4-fold) under the same conditions.

A similar set of experiments was conducted using Kif, the other ERAD inhibitor selected. Cell treatment with Kif (100 nM) modestly increased L444P GC activity (1.2-fold, 15% of WT activity; $p<0.01$), whereas co-administration of Kif (50 nM) and MG-132 (0.4 μM) led to a dramatic 3.8-fold increase in L444P GC activity (47.5% of WT activity; $p<0.01$) after 120 hours (Figure 4.3.2C). Co-treatment with Kif and celastrol was also explored (Figure 4.3.2D). Optimal culturing conditions (Kif 100 nM and celastrol 0.8 μM) resulted in 2.3-fold increase in L444P GC activity (28.8% of WT activity, $p<0.01$), again higher than what was found upon treatment with either molecule alone. Taken together, these results suggest that ERAD limits the folding and trafficking of L444P GC and that ERAD inhibition is a viable strategy to promote native folding and trafficking of this mutated, degradation-prone enzyme variant.

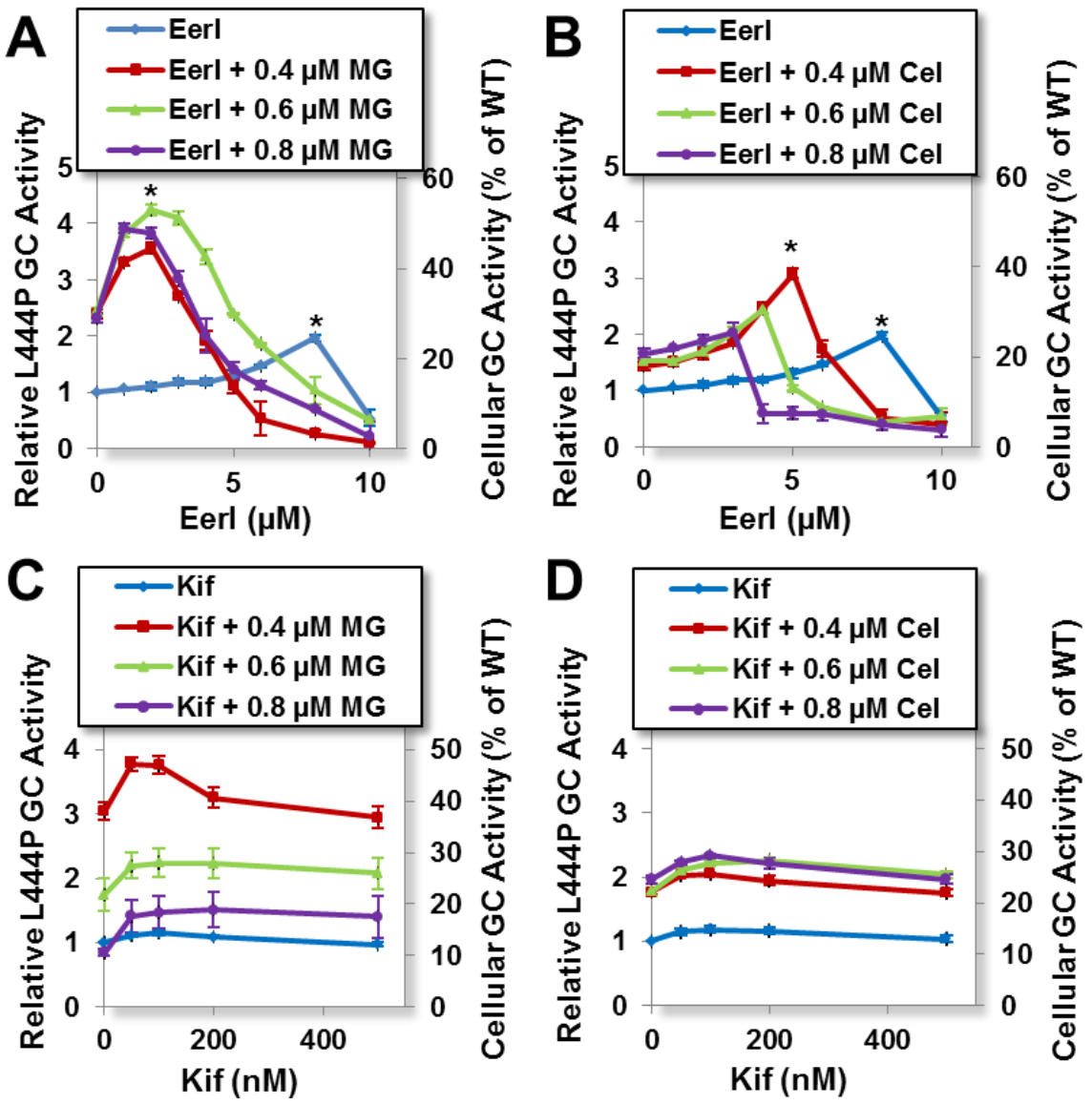

Figure 4.3.2. Cell treatment with ERAD inhibitors enhances L444P GC activity in GD patient-derived fibroblasts. Relative L444P GC activities were evaluated in cells treated with a range of concentrations of ERAD inhibitors (EerI or Kif) and constant doses of proteostasis regulators (MG-132 or celastrol: 0.4, 0.6, or 0.8 μM). Relative GC activities of L444P cells treated with **A)** EerI and MG-132 for 48 hrs, **B)** EerI and celastrol for 48 hrs, **C)** Kif and MG-132 for 120 hrs, and **D)** Kif and celastrol for 120 hrs. Relative GC activities were evaluated by normalizing GC activities measured in treated cells to the activity of untreated cells (left y axis), ($p<0.01$ if not specified; *$p<0.001$). The corresponding fraction of WT GC activity is also reported (right y axis). Experiments were repeated three times and data points are reported as mean ± SD. MG, MG-132; Cel, celastrol.

In order to confirm that the increase in GC activity measured in cells treated with EerI and Kif is caused by partial restoration of L444P GC folding and lysosomal trafficking, we investigated L444P GC glycosylation state, and its intracellular localization and trafficking.

L444P GC glycosylation state was investigated by endoglycosidase H (EndoH) treatment (see chapter 4.2; Wang et al. 2011b), using culture conditions that resulted in maximal GC activity rescue (EerI 6 μM, Kif 50 nM, MG-132 0.6 μM for 48 hrs). The total protein content was subjected to EndoH treatment. As described before (Chapter 4.2), GC detection by Western blot reveals a low MW band corresponding to partially glycosylated, ER-retained GC (EndoH-sensitive) and a high MW band corresponding to fully glycosylated, lysosomal GC (EndoH-resistant) (Maley et al., 1989). A representative Western blot (Figure 4.3.3A) and quantification of EndoH-resistant and EndoH-sensitive GC bands (Figure 4.3.3B) are reported. In untreated cells, nearly all L444P GC was detected as EndoH-sensitive, as expected (Chapter 4.2). A band corresponding to EndoH-resistant L444P GC was detected in cells treated with EerI, and its intensity was 1.6-fold higher than that detected in cells treated with MG-132 (results obtained using MG-132 were reported previously (Mu et al., 2008b) and are included here for comparison). Kif treatment caused a mild increase in GC EndoH-resistant pool, corresponding to about 13% of that of MG-132-treated cells. Co-treatment with MG-132 and EerI (2 μM) or Kif resulted in 2.6- and 1.4-fold increase, respectively, in the EndoH-resistant L444P GC, compared to treatment with MG-132 only, which is in agreement with results obtained from enzymatic assays (Figure 4.3.2A and 4.3.2C).

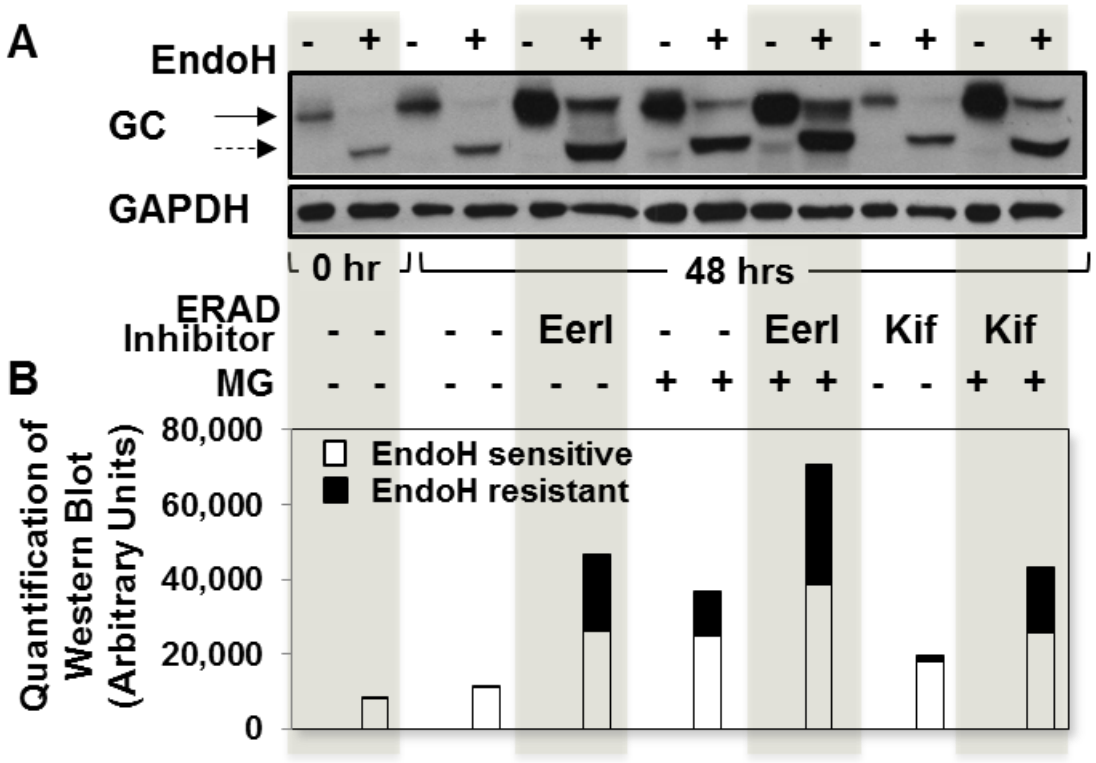

Figure 4.3.3. ERAD inhibitors promote L444P GC glycosylation in GD patient-derived fibroblasts. A) Western blot analyses of EndoH treated and untreated total protein content from L444P GC fibroblasts cultured with EerI (6 μM), Kif (50 nM), and MG-132 (0.6 μM) for 48 hrs and detected using GC-specific antibody. The solid and dashed arrows indicate EndoH resistant and EndoH sensitive bands respectively. **B**) Quantification of GC bands detected by western blot in EndoH treated samples. Quantification of lower MW, EndoH-sensitive bands corresponding to ER retained GC are reported in the white portion of the bars, and quantification of higher MW, EndoH-resistant bands corresponding to lysosomal GC are reported in the black top portions. Band analyses and quantifications were conducted using NIH ImageJ analysis software. Experiments were repeated three times and data points are reported as mean ± SD. MG, MG-132; Cel, celastrol.

L444P GC intracellular localization was evaluated using immunofluorescence microscopy and subcellular fractionation of L444P GC patient-derived fibroblasts treated with small molecules at concentrations corresponding to maximum activity rescue (EerI 6 μM, Kif 50 nM, and MG-132 0.6 μM) for 48 hrs. Immunofluorescence microscopy was conducted using antibodies specific for GC, for an ER marker (CNX), and for a

lysosomal marker (LAMP-1) to evaluate GC localization in the ER and in the lysosome, respectively. Co-localizations of GC and CNX (Figure 4.3.4A) and of GC and LAMP-1 (Figure 4.3.4B) are reported, respectively, in pink and purple (merged colors) and analyzed with ImageJ software to provide a co-localization heatmap. L444P GC was barely detectable in untreated cells due to extensive ERAD, as previously reported (Michelakakis et al., 1995). In agreement with the results obtained from GC enzymatic assays (Figure 4.3.2A), a significantly larger pool of GC was detected in the ER and in the lysosome upon EerI treatment. Furthermore, GC accumulation was observed to increase with increasing concentration of EerI, and to be further enhanced by co-treatment with EerI and MG-132 (Figure 4.3.4A-B). Kif treatment also enhanced GC localization in the ER and in the lysosomes compared to untreated cells, albeit to a lower extent than EerI treatment (Figure 4.3.4A-B). Co-treatment with Kif and MG-132 increased GC accumulation in the ER and in the lysosomes, again supporting the results obtained from GC enzymatic assays (Figure 4.3.2C).

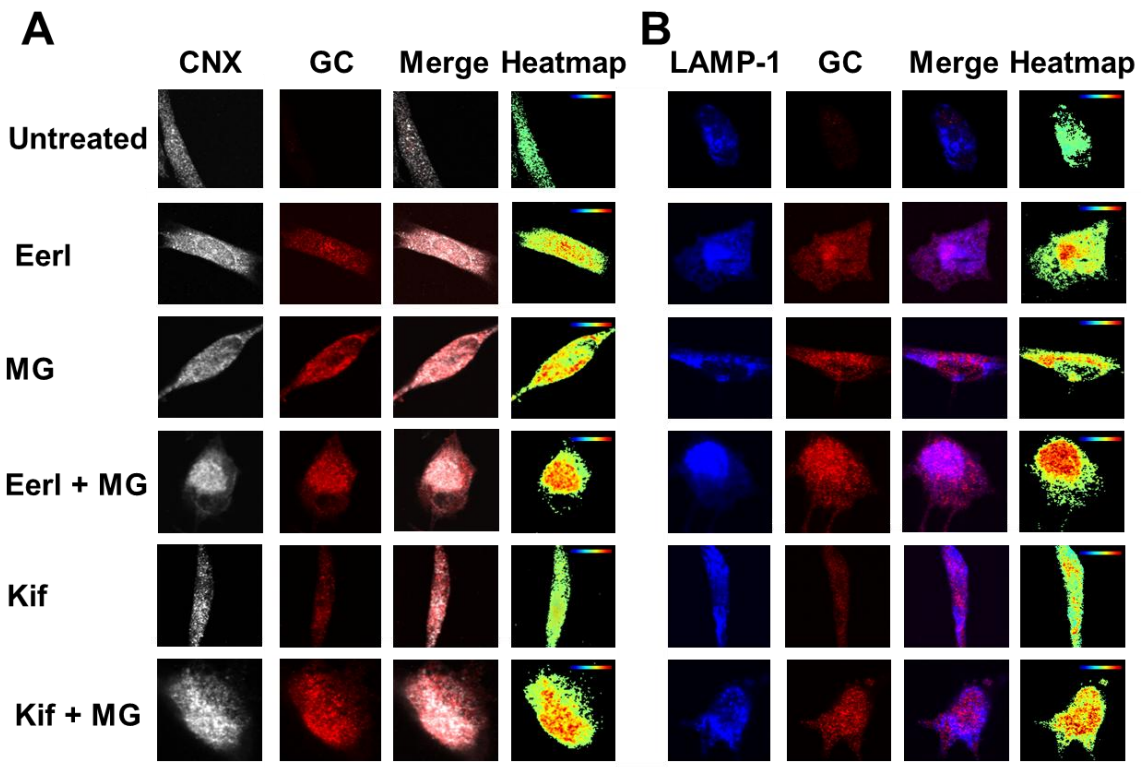

Figure 4.3.4. ERAD inhibitors promote L444P GC folding and lysosomal trafficking in GD patient-derived fibroblasts. Immunofluorescence microscopy of **A)** GC and CNX (an ER marker), and **B)** GC and LAMP-1 (a lysosomal marker) in L444P GC fibroblasts. Cells were treated with EerI (2 and 6 μM), Kif (50 nM) and MG-132 (0.6 μM) for 48 hrs. Colocalization of CNX (grey, column 1) and GC (red, column 2) is shown in pink (column 3). Colocalization of LAMP-1 (blue, column 1) and GC (red, column 2) is shown in purple (column 3). Heatmaps of co-localization images were obtained with NIH ImageJ analysis software (column 4). Hot colors represent positive correlation (co-localization), whereas cold colors represent negative correlation (exclusion).

Subcellular fractions of cell homogenates were collected upon Percoll density gradient centrifugation, and GC enzyme activity assay for each fraction was performed to evaluate L444P GC intracellular localization. Since hexosaminidase A (HexA) trafficking and activity are not altered in GD fibroblasts compared to WT fibroblasts, HexA activity was first evaluated in each fraction to distinguish fractions containing ER and lysosomes. HexA activity was detected in both low-density (#1-2) and high-density (#7-8) fractions

in untreated L444P GC cells (Figure 4.3.5, dashed line, right y-axis), which comprise the ER and the lysosomes, respectively, as previously reported (Ishii et al., 2007). In untreated cells, L444P GC activity (Figure 4.3.5, left y-axis) was barely detectable in low-density fractions (ER) and undetectable in high-density fractions (lysosomes). Treatment with MG-132 resulted in significant increase in L444P GC activity in both low- and high-density fractions, confirming that MG-132 promotes rescue of mutant GC folding and trafficking (Figure 4.3.5). A significant increase in GC activity was also detected in EerI treated cells, particularly in low-density ER fractions, confirming that EerI functions by inhibiting ERAD and prolonging ER retention. Kif treatment also enhanced GC activity both in the low- and high-density fractions compared to untreated cells, although to a lower extent than EerI treatment, in agreement with the results obtained from GC enzymatic assays (Figure 4.3.2A and 4.3.2C).

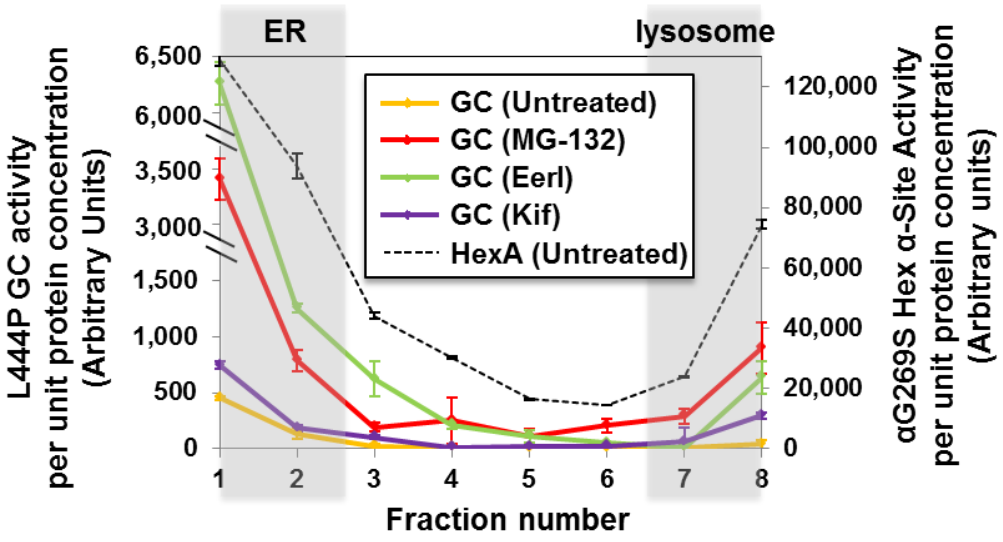

Figure 4.3.5. ERAD inhibitors enhance the activity of L444P GC in subcellular homogenate fractions in patient-derived fibroblasts. Relative GC activities of subcellular homogenate fractions were measured in untreated cells and cells cultured with EerI (6 μM), Kif (50 nM) and MG-132 (0.6 μM) for 48 hrs. Subcellular fractions were collected, numbered from low- to high-density (from 1 to 8) and subjected to GC activity assays. HexA activity was also measured in each fraction obtained from untreated cells to identify fraction containing the ER (#1-2) and lysosomes (#7-8). The total protein concentration of each fraction was determined by Nanodrop. GC enzyme activity (left y-axis) and HexA enzyme activity (right y-axis) of each fraction were normalized to the corresponding protein concentrations. Experiments were repeated three times and data points are reported as mean ± SD. MG, MG-132.

In order to investigate whether ERAD inhibition is a mutation-dependent strategy for the rescue of unstable GC variants, N370S GC fibroblasts were cultured in the presence of EerI and a proteostasis regulator, and GC activities were evaluated every 24 hrs for up to 3 days (Figure 4.3.6). EerI treatment (4 μM) for 72 hrs resulted in a 1.25-fold increase in GC activity (16% WT activity; $p<0.01$). Similar to what described for L444P GC cells, a lower concentration of EerI (2 μM) combined with MG-132 (0.2 μM) further enhanced N370S GC rescue, resulting in a 2.1-fold increase in activity compared to untreated cells (26% of WT activity, $p<0.001$), which is higher than what observed in the presence of either molecule alone (EerI 1.2-fold; MG-132 1.5-fold). When the same

experiment was conducted using celastrol as a proteostasis modulator, co-treatment with EerI (2 μM) and celastrol (0.2 μM) resulted in 1.4-fold increase in activity (18% of WT activity, $p<0.01$), which again is significantly higher than what observed using either molecule alone (EerI 1.2-fold; celastrol 1.2-fold).

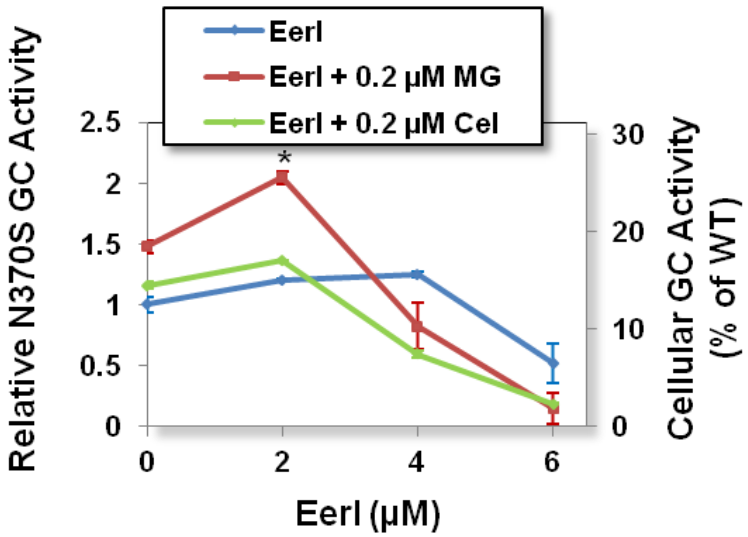

Figure 4.3.6. EerI enhances N370S GC activity in GD patient-derived fibroblasts. Relative N370S GC activities were measured in cells treated with proteostasis regulators (MG-132 0.2 μM; celastrol 0.2 μM) and a range of EerI concentrations for 72 hrs. Relative GC activities were evaluated as described in Figure 4.3.2 ($p<0.01$ if not specified; *$p<0.001$). Experiments were repeated three times and data points are reported as mean ± SD. MG, MG-132; Cel, celastrol.

To confirm that the observed increase in GC activity is due to rescue of the enzyme folding and trafficking, N370S GC cellular localization was evaluated by immunofluorescence microscopy in cells treated with EerI (2 μM), and MG-132 (0.2 μM). EerI treatment resulted in an increase in N370S GC accumulation in the ER and in the lysosomes compared to untreated cells. Co-administration of EerI and MG-132

further enhanced N370S GC concentration both in the ER and in the lysosomes (Figure 4.3.7A-B), confirming the results obtained from enzymatic assays.

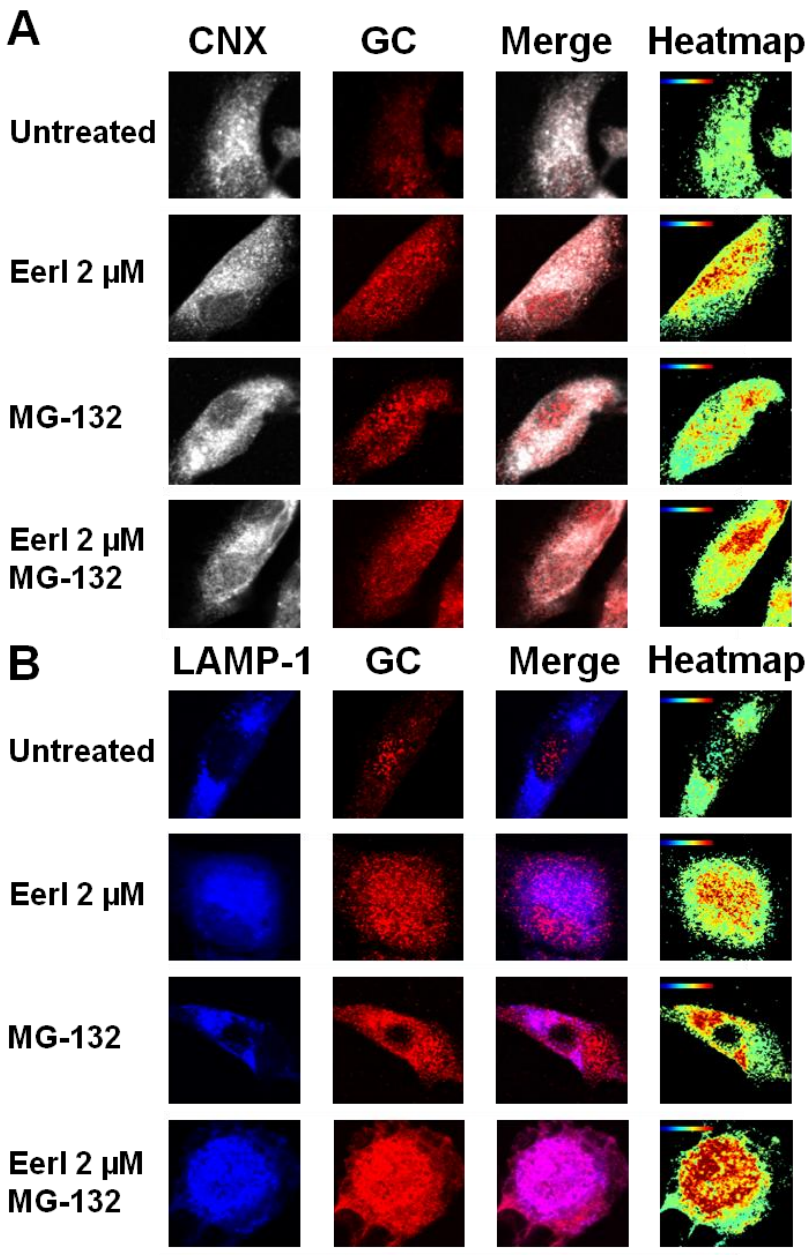

Figure 4.3.7. EerI facilitates N370S GC folding and lysosomal trafficking in GD patient-derived fibroblasts. Immunofluorescence microscopy images of **A)** GC and CNX (an ER marker), and **B)** GC and LAMP-1 (a lysosomal marker) in cells treated with EerI (2 µM) and MG-132 (0.2 µM) for 48 hrs. Colocalization images were analyzed as described in Figure 4.3.4.

In summary, these results demonstrate that ERAD prevents native folding of mutated, unstable GC and provide compelling evidence that ERAD inhibition is a viable strategy to rescue lysosomal activity of degradation-prone GC variants containing destabilizing, non-inactivating mutations. Interestingly, the activity rescue measured in N370S GC fibroblasts was consistently less pronounced than that observed in L444P GC fibroblasts. We suggest that this difference is due to the different destabilizing effects of the N370S and L444P substitutions. L444P GC is normally completely targeted to ERAD, whereas the N370S GC variant partially escapes degradation and can be detected throughout the secretory pathway (Sawkar et al., 2006b). Hence, ERAD is likely to have a more direct and rate-limiting role in L444P GC processing, and, not surprisingly, ERAD inhibition results in more efficient rescue of L444P GC than N370S GC folding.

ERAD inhibition enhances HexA activity in fibroblasts derived from patients with Tay-Sachs disease

A number of loss-of-function LSDs are caused by destabilizing mutations and degradation of secretory proteins. The demonstration that ERAD inhibition enhances folding of mutated GC variants motivated asking whether ERAD inhibition is a general strategy to rescue activity of mutated proteins containing misfolding, non-inactivating mutations associated with the development of LSDs. Thus, we investigated the folding of HexA, the protein activity deficient in Tay-Sachs disease. Specifically, we focused on one of the most prevalent mutations, the G269S substitution in the HexA α subunit, which destabilizes the protein native structure resulting in activity ~10% of WT (Tropak et al., 2004). Patient-derived fibroblasts harboring G269S HexA were cultured in the

presence of an ERAD inhibitor and a proteostasis modulator and HexA activity was measured as previously described (Mu et al., 2008b). Administration of EerI (6 μM) for 96 hrs led to 1.4-fold increase in G269S HexA α activity (14% of WT activity HexA activity; $p<0.01$. Figure 4.3.8). Addition of MG-132 (0.2 μM) to cells treated with EerI (2 μM) for 96 hrs caused a further increase in HexA activity (1.7-fold, ~17% of WT; $p<0.01$. Figure 4.3.8).

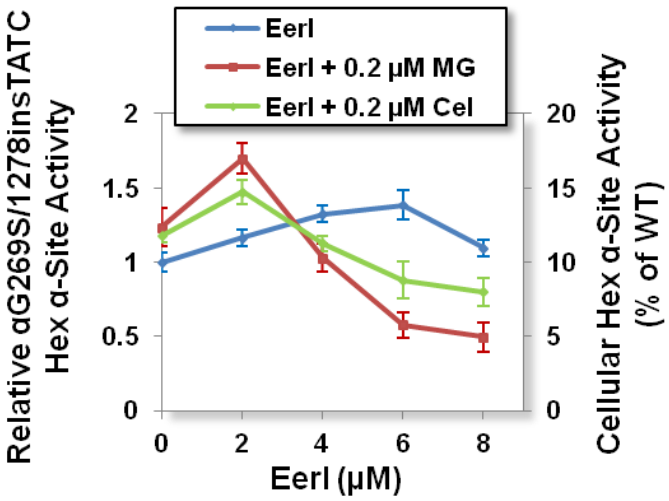

Figure 4.3.8. EerI enhances G269S HexA activities in Tay-Sachs patient-derived fibroblasts. Cells were cultured with proteostasis regulators (MG-132 0.2 μM; celastrol 0.2 μM) and a range of EerI concentrations for 96 hrs. Relative αG269S/1278insTATC HexA activities ($p<0.01$) were evaluated by normalizing HexA activity of treated cells to that of untreated cells (left y axis). The corresponding fraction of WT HexA activity is also reported (right y axis). Experiments were repeated three times and data points are reported as mean ± SD. MG, MG-132; Cel, celastrol.

These findings suggest that ERAD inhibition facilitates folding of destabilized enzyme variants prone to degradation. In summary, results from studies in Gaucher's and Tay-Sachs disease patient-derived cells indicate that the activity rescue observed upon treatment with ERAD inhibitors is inversely proportional to the loss of lysosomal activity normally associated with each enzyme variant.

ERAD inhibition via EerI treatment causes upregulation of BiP expression in fibroblasts derived from patients with Gaucher's disease carrying the L444P GC variant

We speculated that small molecule-mediated ERAD inhibition, by inducing accumulation of misfolded proteins in the ER, could lead to upregulation of ER chaperones. We previously reported that the ER luminal chaperone BiP plays a critical role in the rescue of L444P GC folding (Chapters 4.1 and 4.2). We asked whether the increase in mutant GC activity observed upon ERAD inhibition could be attributed to upregulation of BiP or other ER chaperones induced in response to the sudden load of misfolded proteins in the ER. Quantitative RT-PCR experiments were conducted to evaluate the expression levels of representative ER chaperones (BiP, CNX and CRT) in L444P GC fibroblasts treated with EerI (2 and 6 μM), Kif (50 nM), MG-132 (0.6 μM), or a combination thereof (Figure 4.3.9A-C).

BiP expression (Figure 4.3.9A) was mildly upregulated by EerI treatment at 2 μM (1.6-fold, $p<0.01$) but highly upregulated at 6 μM (9.2-fold) and upon co-treatment with EerI (2 μM) and MG-132 (15.7-fold). Hence, the highest upregulation of BiP expression was observed at conditions causing maximal rescue of GC activity, namely upon cell treatment with high concentration of EerI (6 μM) or co-treatment with MG-132 and low concentration of EerI (2 μM). These data demonstrate a correlation between BiP transcriptional regulation and GC activity rescue. The dramatic increase in BiP expression observed could be part of UPR induction, which was previously shown to facilitate GC folding rescue (See chapters 4.1 and 4.2; or papers Wang et al., 2011a and Wang et al., 2011b) and is analyzed below in more detail.

Interestingly, cell treatment with Kif under conditions observed to maximize L444P GC activity rescue only resulted in a moderate increase of BiP expression (2.0-fold, $p<0.01$), even when used in combination with MG-132 (2.2-fold, $p<0.01$). Hence, under the conditions tested, Kif-mediated ERAD inhibition does not lead to ER stress or chaperone upregulation. We suggest that the lower increase in BiP expression observed upon treatment with Kif compared to EerI is not an indication of the lower rescue of L444P GC activity, but rather of the two molecules' different mechanisms of action. In support of this hypothesis is evidence that even the addition of MG-132, which dramatically increases Kif mediated L444P GC rescue (Figure 4.3.9C), does not cause upregulation of BiP expression.

CNX was mildly upregulated by treatment with EerI or Kif, alone or in combination with MG-132 (Figure 4.3.9B). CRT expression was not substantially altered by EerI treatment, although it was upregulated (3.5-fold) by co-treatment with MG-132 and EerI (Figure 4.3.9C).

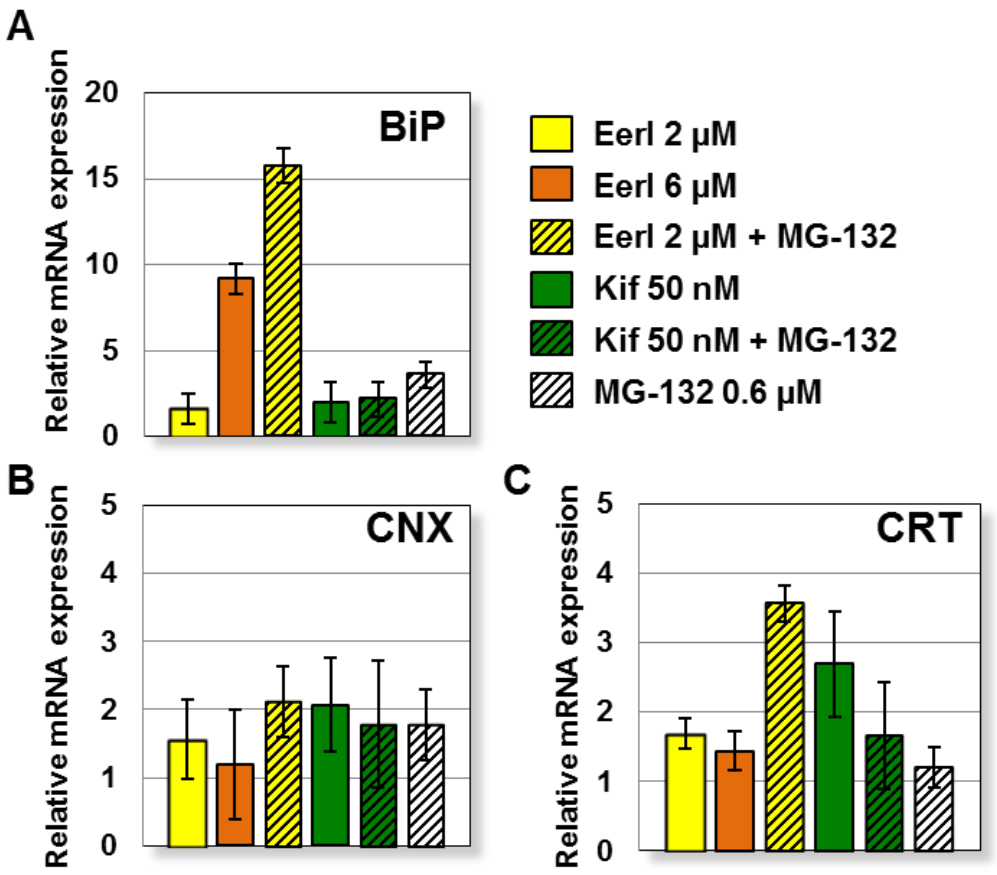

Figure 4.3.9. Upregulation of BiP transcriptional expression in L444P GC fibroblasts treated with ERAD inhibitors. Relative mRNA expression levels of **A)** BiP ($p<0.01$), **B)** CNX ($p<0.05$), and **C)** CRT ($p<0.05$) in L444P GC fibroblasts treated with EerI (2 and 6 µM), Kif (50 nM), and MG-132 (0.6 µM) for 24 hrs were obtained by quantitative RT-PCR, corrected by the expression of the housekeeping gene GAPDH, and normalized to those of untreated cells. The data is reported as mean ± SD.

Western blot analyses (Figure 4.3.10A) were conducted to confirm ER chaperone expression and bands were quantified with ImageJ software (Figure 4.3.10B). BiP protein accumulation was enhanced by treatment with EerI in a concentration-dependent fashion (EerI 2 µM caused 1.5-fold increase and EerI 6 µM resulted in 2.5-fold increase). Co-treatment with EerI and MG-132 further enhanced BiP accumulation (2.7-fold) compared to untreated cells. Kif treatment, however, caused very modest increase in BiP accumulation when used alone (1.2-fold) or in combination with MG-132 (1.6-fold).

CNX and CRT protein levels were minimally altered upon small molecule treatment. Overall, results from Western blot analyses are consistent with RT-PCR experiments, with the exception of CRT expression, for which transcriptional changes are not reflected at the translational level, suggesting that CRT upregulation by cell treatment with MG-132 and EerI does not translate into enhanced accumulation of CRT protein.

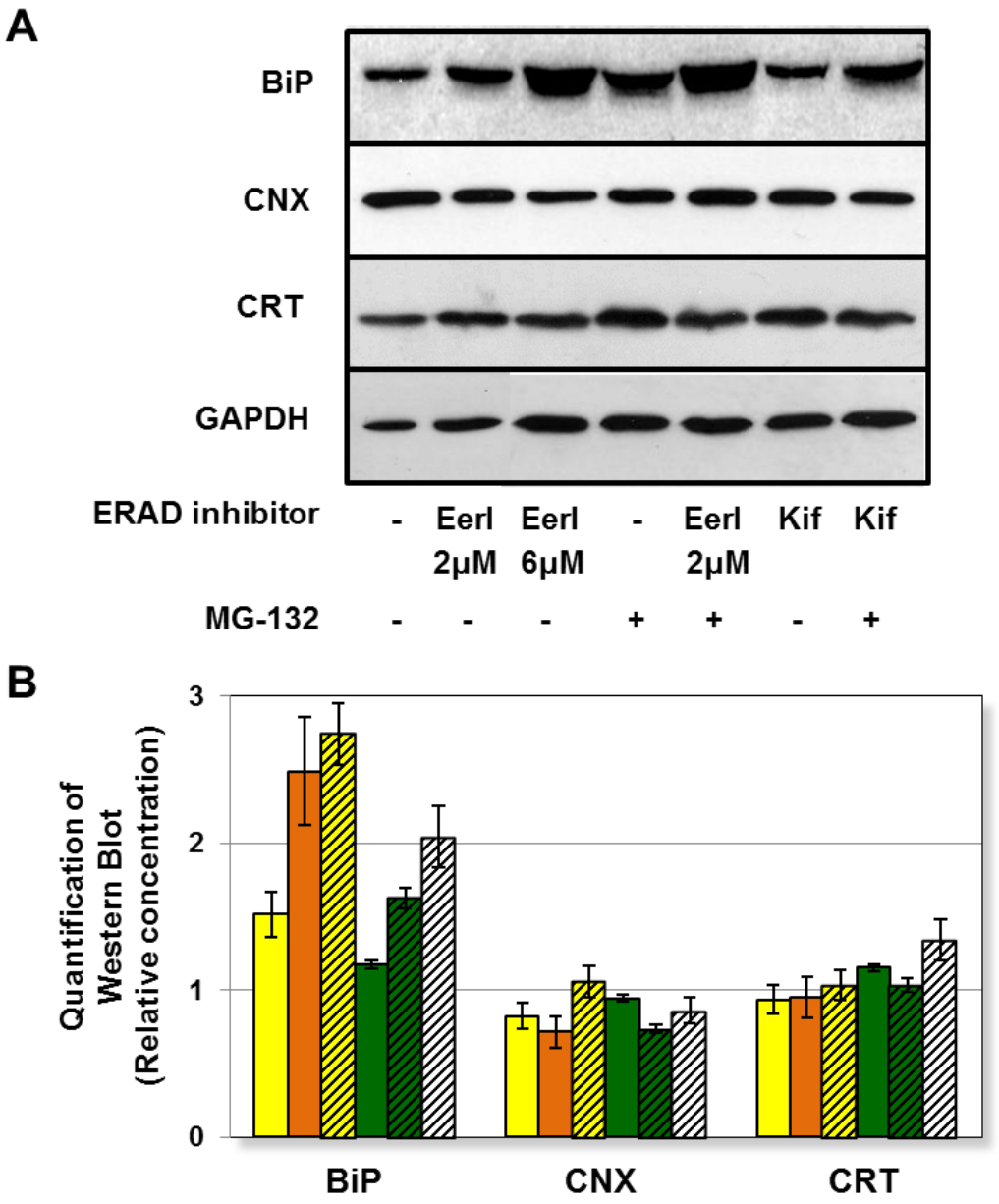

Figure 4.3.10. BiP protein accumulation in L444P GC fibroblasts treated with ERAD inhibitors. A) Western blot analyses of BiP, CNX, CRT, and GAPDH (used as loading control) in cells treated with EerI (2 and 6 μM), Kif (50 nM), and MG-132 (0.6 μM) for 48 hrs. **B)** Quantification of Western blot bands. ER chaperone band intensities were quantified with NIH ImageJ analysis software, corrected by GAPDH band intensities, and divided by the values obtained in untreated samples.

Induction of UPR depends on the mechanism of ERAD inhibition

Accumulation of misfolded proteins triggers ER stress, which in turn leads to UPR induction. In order to evaluate UPR induction in cells treated with ERAD inhibitors, we measured the expression of three representative proteins that are typically upregulated as part of the UPR: X-box binding protein-1 (Xbp-1), activating transcription factor 4 (ATF4), and C/EBP homologous protein (CHOP) (see Chapter 4.2 for a more detailed description of the UPR pathway; and Schroder and Kaufman, 2005). Quantitative RT-PCR was conducted to evaluate the expression of Xbp-1, ATF4, and CHOP in cells treated with EerI (2 and 6 μM), Kif (50 nM), MG-132 (0.6 μM), or a combination thereof.

Activation of the IRE1 signaling cascade involves splicing of Xbp-1 mRNA. Spliced Xbp-1 mediates induction of UPR genes, whereas the unspliced Xbp-1 precursor functions as a repressor (Ron and Walter, 2007). To evaluate activation of the IRE1 arm of the UPR, spliced and unspliced Xbp-1 mRNA were quantified by RT-PCR followed by gel electrophoresis (Figure 4.3.11A-B). MG-132 was previously shown to enhance Xbp-1 splicing (Mu et al., 2008b) and is reported here for comparison. Treatment with EerI resulted in Xbp-1 splicing in a concentration dependent fashion (EerI 2 μM, 1.3-fold increase in splicing; EerI 6 μM, 2.1-fold increase). Co-administration of EerI (2 μM) and MG-132 further increased Xbp-1 splicing (3.6-fold compared to MG-132 treatment). Kif treatment did not induce splicing of Xbp-1, and co-treatment with Kif and MG-132 resulted in increase in spliced Xbp-1 similar to that induced by treatment only with MG-132. In summary, Xbp-1 splicing was induced upon EerI but not by Kif treatment,

suggesting that activation of the IRE1 pathway depends on the specific mechanism of ERAD inhibition.

ATF4 expression was upregulated 4.4-fold by treatment with EerI and 6.0-fold by co-treatment with EerI and MG-132 ($p<0.05$), a clear indication of the PERK arm's activation in cells treated with EerI (Figure 4.3.11D). A considerably lower increase in ATF4 expression was observed in cells treated with Kif (2.5-fold, $p<0.01$). Moreover, co-treatment with Kif and MG-132 did not result in significant upregulation of ATF4 expression compared to treatment only with MG-132, again suggesting that UPR activation depends on the mechanism of ERAD inhibition.

CHOP was found to be highly upregulated upon EerI treatment (Figure 4.3.11C). Specifically, EerI 2 μM resulted in 4.2-fold increase in CHOP expression, EerI 6 μM in 19-fold increase, and co-administration of EerI (2 μM) and MG-132 in 24-fold increase ($p<0.01$), indicating that EerI mediated ERAD inhibition causes activation of the ATF6 pathway. Because CHOP plays a role in the induction of apoptotic pathways (Oyadomari and Mori, 2004), these results also suggest that EerI treatment might activate UPR-induced apoptosis, which is analyzed below. Treatment with Kif alone or in combination with MG-132 led to 2.2-fold and 6.5-fold CHOP upregulation, respectively, which are significantly lower than the values observed upon EerI treatment and do not exceed those observed upon treatment with MG-132 (Figure 4.3.11C).

In summary, we demonstrated that EerI, but not Kif, when used under conditions that promote rescue of L444P GC activity, is associated with dramatic activation of the UPR.

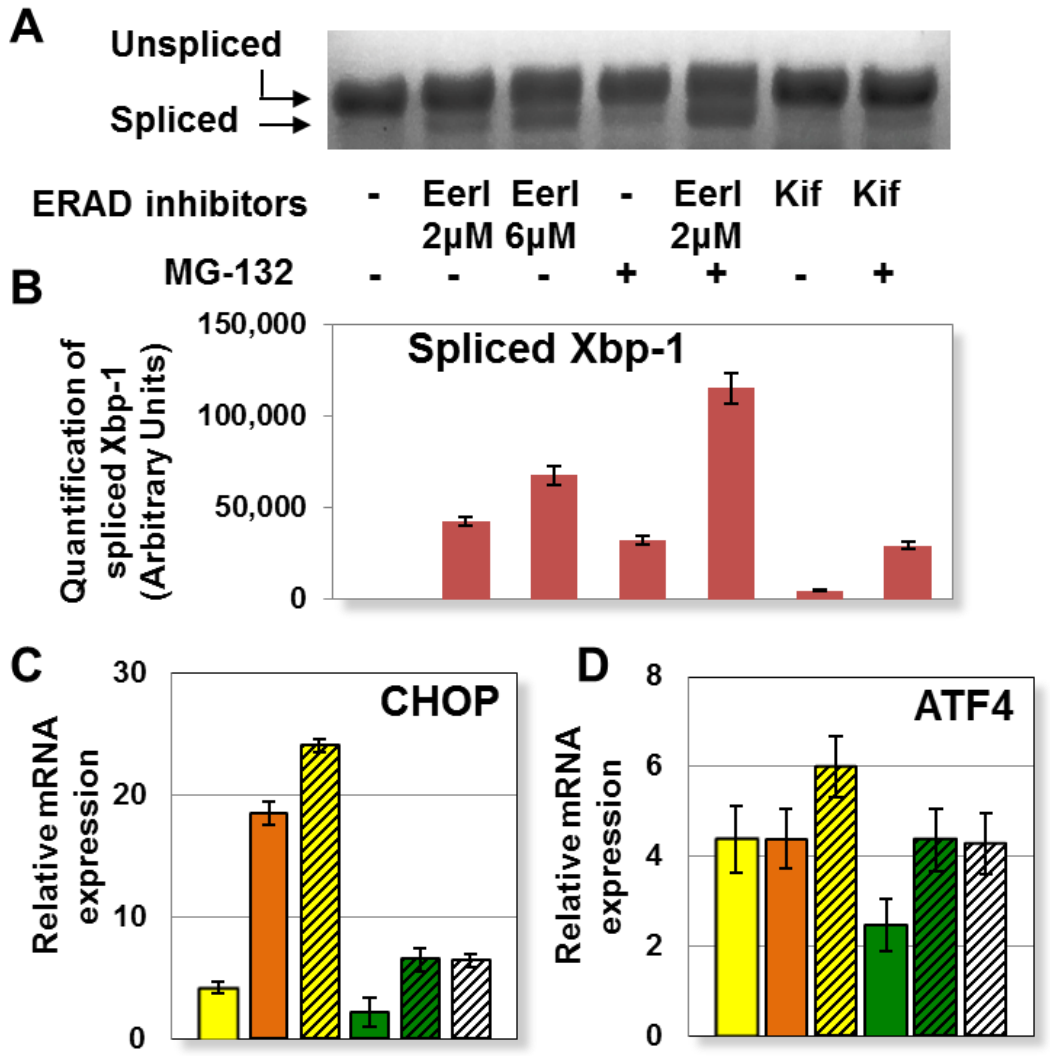

Figure 4.3.11. UPR activation in L444P GC fibroblasts treated with ERAD inhibitors. Cells were treated with EerI (2 and 6 μM), Kif (50 nM), and MG-132 (0.6 μM) for 24 hrs. **A)** Xbp-1 mRNA splicing was determined by RT-PCR followed by gel electrophoresis. **B)** Spliced Xbp-1 band intensities were quantified with the NIH ImageJ analysis software. Relative mRNA expression levels of **C)** CHOP ($p<0.01$), and **D)** ATF4 ($p<0.05$) were obtained by quantitative RT-PCR and calculated as described in Figure 4.3.9. The data is reported as mean ± SD.

Upregulation of the gene encoding GC (GBA) as well as of other genes encoding for lysosomal proteins associated with the development of LSDs was previously reported in cells treated with UPR inducing proteostasis regulators (Chapter 4.1). We asked whether ERAD inhibition, in addition to preventing GC degradation, it also increases GC

accumulation in the ER by upregulating its transcription. Quantitative RT-PCR was conducted to measure GC expression in L444P GC fibroblasts treated with EerI (2 and 6 μM), Kif (50 nM), and MG-132 (0.6 μM) (Figure 4.3.12A-C). EerI treatment was observed to enhance GC expression in a concentration-dependent fashion (EerI 2 μM, 2.3-fold; EerI 6 μM, 3.3-fold; $p<0.01$). Co-treatment with EerI (2 μM) and MG-132 (0.6 μM) resulted in 4.4-fold increase in GC expression ($p<0.05$), which is higher than what observed using EerI alone (2.3-fold), but comparable to treatment with MG-132 only (4.0-fold). A lower increase in GC expression was measured in cells treated with Kif (1.9-fold), as expected, considering the modest UPR induction caused by Kif treatment. Similar to what was observed for EerI, the increase in GC expression observed upon co-treatment with MG-132 (2.8-fold) was lower than that detected in cells treated only with MG-132 (4.0-fold).

GC expression was also investigated by Western blot analyses (Figure 4.3.12B-C). It is important to notice that changes in protein accumulation detected by Western blot are to be attributed to both GC transcriptional modulation caused by ERAD inhibition-induced UPR and GC post-translational processing caused by ERAD inhibition mediated protein rescue. L444P GC content was barely detectable in untreated cells, as expected, due to extensive ERAD (Sawkar et al., 2006b), whereas treatment with either ERAD inhibitor enhanced GC accumulation level. GC accumulation increased in EerI treated cells in a concentration-dependent fashion (cf. bands corresponding to EerI 2 μM and EerI 6 μM treatments). The addition of MG-132 further enhanced GC accumulation observed in EerI and Kif treated cells.

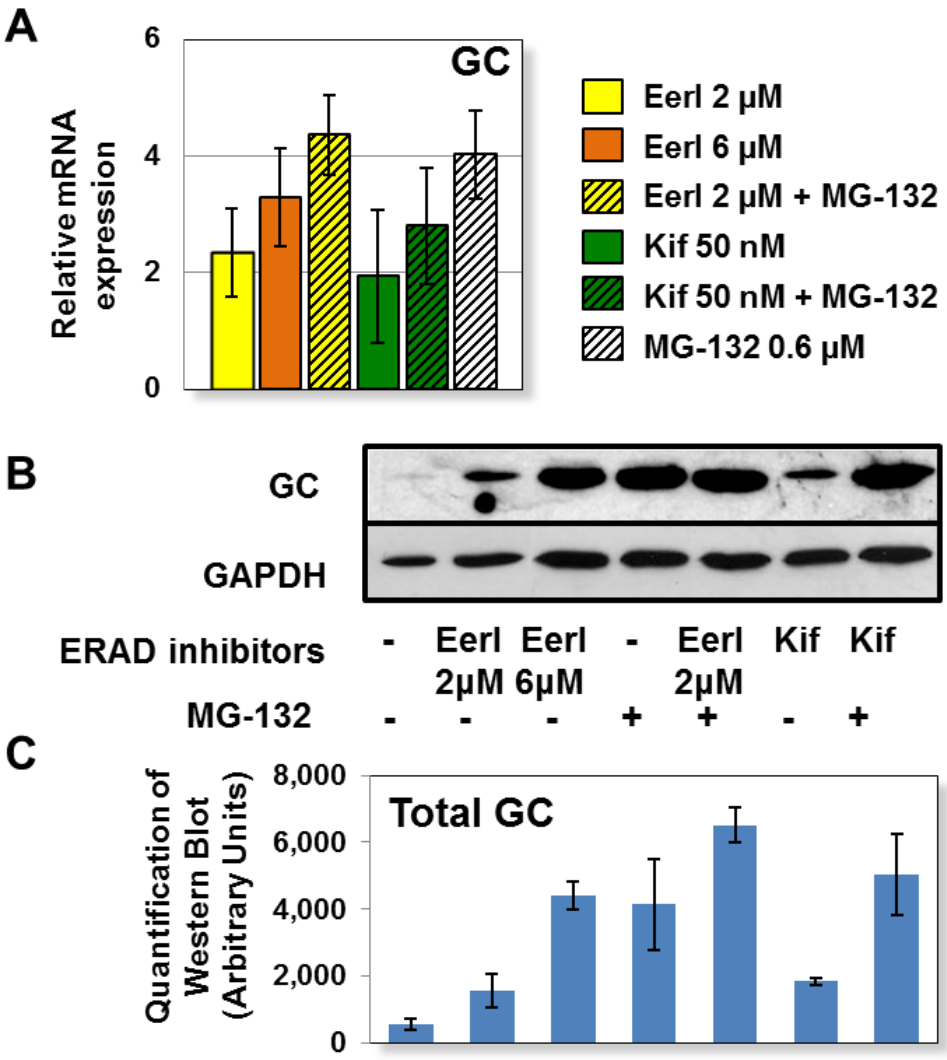

Figure 4.3.12. Upregulation of GC expression in L444P GC fibroblasts treated with ERAD inhibitors. Cells were treated with EerI (2 and 6 μM), Kif (50 nM), and MG-132 (0.6 μM). **A**) Relative mRNA expression levels of GC ($p<0.05$) were obtained by quantitative RT-PCR in cells treated with small molecules for 24 hrs and calculated as described in Figure 4.3.9. The data is reported as mean ± SD. **B)** Western blot analysis of cells treated with small molecules for 48 hrs using GC specific antibody. GAPDH expression was used as a loading control. **C)** Western blot band quantification. GC bands were quantified by NIH ImageJ analysis software and corrected by GAPDH band intensities.

In summary, ERAD inhibition resulted in both increase in GC transcription and cellular accumulation. GC upregulation was found to be proportional to the extent of UPR induction measured upon treatment with each specific ERAD inhibitor. However,

co-treatment with an ERAD inhibitor and a proteostasis modulator, MG-132, which was demonstrated to have a synergistic effect on the rescue of mutated GC activity (Figure 4.3.2A and 4.3.2C), did not cause a corresponding synergistic increase in GC transcription, suggesting that rescue of mutated GC cannot be solely attributed to the effect of ERAD inhibitors on GC expression.

If ER stress persists, prolonged UPR activation typically leads to induction of apoptosis (Schroder and Kaufman, 2005). We asked whether cell treatment with Eer and Kif influenced UPR-induced apoptosis. The CytoGLO^{TM} Annexin V-FITC Apoptosis Detection Kit was used to detect membrane rearrangement (Annexin V binding, a measurement of early apoptosis) and fragmentation (propidium iodide (PI) binding, a measurement of late apoptosis) in L444P GC fibroblasts treated with EerI (2 μM), Kif (50 nM), and MG-132 (0.6 μM) (Figure 4.3.13A-C). High Annexin V binding and consequently dramatic increase in cell fluorescence was observed upon cell treatment with EerI compared to untreated cells (Figure 4.3.13A). Addition of MG-132 to EerI treated cells resulted in even higher increase in Annexin V binding. However, we did not detect any increase in Annexin V binding in cells treated with Kif compared to untreated cells. Moreover, addition of Kif and MG-132 resulted in Annexin V binding indistinguishable from that observed in cells treated only with MG-132 (Figure 4.3.13B). Measurements of PI binding, which is taken as an estimate of the dead cell population, showed similar results. A 4.1% increase in dead cells was observed upon EerI treatment compared to untreated cells, whereas a negligible increase (0.4%) was observed upon Kif treatment (Figure 4.3.13C). These results demonstrate that while EerI treatment causes

dramatic increase in mutated GC activity at the cost of significant cell toxicity and apoptosis induction, treatment with Kif facilitates folding without induction of apoptosis.

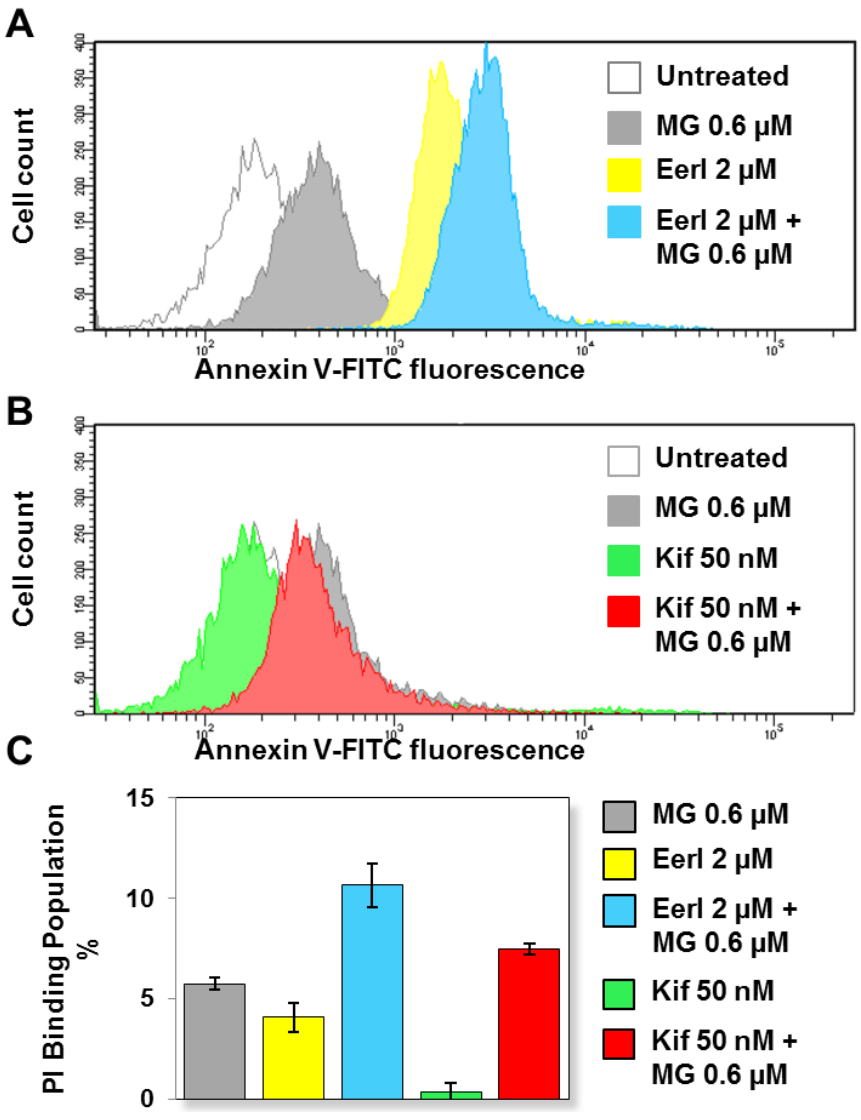

Figure 4.3.13. Apoptosis induction in L444P GC patient-derived fibroblasts treated with ERAD inhibitors. Flow cytometry histograms of Annexin V-FITC fluorescence intensities (x-axis, log scale) plotted against cell counts (y-axis, linear scale) obtained from the analysis of **A)** untreated cells and cells treated with MG-132 (0.6 μM), EerI (2 μM), and EerI (2 μM) and MG-132 (0.6 μM); **B)** untreated cells and cells treated with MG-132 (0.6 μM), Kif (50 nM), and Kif (50 nM) and MG-132 (0.6 μM) for 16 hrs. Three independent experiments were conducted and results of one representative experiment are reported. **C)** PI binding population change (%) of cells treated with EerI (2 and 6 μM), Kif (50 nM), and MG-132 (0.6 μM) for 16 hrs compared to untreated cells ($p<0.01$). Number of total counted cells: 10,000. The data is reported as mean ± SD.

4.3.3. Discussion

We demonstrated that inhibition of ERAD enhances folding, trafficking and lysosomal activity of mutated enzyme variants that cause two clinically distinct LSDs, Gaucher's and Tay-Sachs disease. Results from this work suggest that ERAD limits the folding of secretory proteins containing misfolding, destabilizing mutations and provide proof-of-principle of ERAD inhibition as a viable strategy to rescue loss-of-function phenotypes in fibroblasts derived from patients with LSDs.

ERAD inhibition was shown to promote folding of the two most common GC variants: L444P GC (Figures 4.3.2-4.3.5), which is typically completely targeted to ERAD (Grabowski, 1997), and N370S GC (Figures 4.3.6 and 4.3.7), a presumably less destabilized variant that is moderately resistant to ERAD and retains partial residual activity (Grace et al., 1994). ERAD inhibition was also observed to rescue folding of Tay-Sachs disease G269S HexA (Figure 4.3.8), which, similar to N370S GC, retains partial activity (Tropak et al., 2004). Interestingly, we consistently observed higher activity rescue in L444P GC cells, which normally display complete loss of activity, compared to N370S GC and G269S HexA cells. This observation suggests that the rescue in protein folding caused by treatment with ERAD inhibitors inversely correlates with the stability and residual activity of the mutated substrate.

Experimental evidence reported previously (Ron and Horowitz, 2005) and in this thesis suggests that the single-site mutations considered in this study cause destabilization of the protein native, lowest free energy conformation (Chapter 4.2). In order to quantify the stability of mutated variants, we conducted *in silico* analysis of folding free energy changes ($\Delta\Delta G$) between WT and mutant proteins using PoPMuSiC software (Gilis and

Rooman, 2000; Kwasigroch et al., 2002). ΔΔG values of 0.92 and 4.2 kcal/mol were obtained for N370S and L444P GC, respectively, indicating that both mutations have a destabilizing effect on native folding with the L444P substitution causing significantly higher loss of stability. A similar analysis conducted for the HexA protein revealed the ΔΔG caused by the G269S substitution to be 0.49 kcal/mol, which is comparable to the ΔΔG of N370S GC and considerably lower than that of L444P GC. These values correlate with the experimental results that indicate a relationship between protein stability and degradation.

ERAD inhibition and proteostasis modulation resulted in synergistic rescue of lysosomal activity in patient-derived cells (Figures 4.3.2, 4.3.6, and 4.3.8), indicating that a larger pool of unstable proteins that escapes ERAD and can engage the ER folding pathway is rescued by combining ERAD inhibition with upregulation of the cellular folding capacity. Interestingly, the activity window for EerI alone was consistently shifted toward lower concentrations when EerI was combined with a proteostasis regulator, implying that ER retention needs to be carefully modulated to meet the capacity of the cellular folding machinery. It remains to be determined whether EerI treatment results in higher activity rescue than Kif treatment due to higher efficiency of the molecular mechanism involved (p97 *vs* ER mannosidase inhibition).

Detailed investigations of the molecular mechanism of ERAD inhibition and consequent changes in the cellular folding capacity were conducted in L444P GC fibroblasts treated to block two different steps of the ERAD pathway and prevent early recognition of misfolding intermediates (Kif) or retrotranslocation of irremediably misfolded substrates (EerI) (Figure 4.3.1). ER stress and UPR normally observed upon

accumulation of misfolded proteins were investigated (Figures 4.3.9-4.3.12) and seemed to be highly dependent on the specific mechanism of ERAD inhibition. We speculate that by inhibiting retrotranslocation of irremediably misfolded proteins, EerI inevitably leads to significant accumulation of misfolded proteins and consequent induction of UPR and apoptosis. Kif, however, by preventing targeting of folding intermediates to the ERAD pathway, is expected to enhance retention of substrates that can still be assisted by ER chaperone pathway and reach native folding. As a result, Kif-mediated ERAD inhibition, despite promoting significant ER retention and folding of mutated GC, particularly when used in combination with a proteostasis modulator (Figures 4.3.2-4.3.5), does not cause ER stress, as demonstrated by investigating changes in ER chaperone expression (Figures 4.3.9-4.3.10), nor does it cause activation of UPR (Figure 4.3.11) or apoptosis (Figure 4.3.13).

Upregulation of the GC encoding gene, which was previously suggested to contribute to the rescue of GC activity mediated by UPR inducing proteostasis regulators (Chapters 4.1 and 4.2), was also observed in this study in association with UPR activation (Figure 4.3.12). Kif treatment, for instance, which did not cause significant UPR, was not associated with considerable increase in GC expression. Interestingly, co-treatment with Kif and MG-132, despite causing a dramatic increase in GC activity, did not result in UPR induction and GC upregulation. These results, taken together, suggest that the rescue of GC folding observed in cells treated with ERAD inhibitors, alone or in combination with proteostasis regulators, cannot be solely attributed to UPR activation.

Finally, ERAD inhibitors led to dramatically different levels of apoptosis induction (Figure 4.3.13). Specifically, Kif treatment did not cause cytotoxicity and did

not increase MG-132 associated induction of apoptosis. A next step would be detailed investigation to identify the steps of the ERAD pathway that can be modulated for the rescue of degradation-prone substrates without dramatically compromising protein homeostasis and disrupting the functioning of the folding quality control system.

4.4. Remodeling the proteostasis network to rescue native folding of glucocerebrosidase variants by inhibiting ER-associated degradation and enhancing ER folding

4.4.1. Introduction

In the previous chapters, we demonstrated that modulation of Ca^{2+} homeostasis in GD fibroblasts creates a folding environment more amenable to rescue of mutated GC folding (chapters 4.1 and 4.2) and that inhibiton of ERAD, by increasing ER retention of GC intermediates, results in increase in native folding and activity of mutated GC variants. Based these results, we speculated that restoring Ca^{2+} homeostasis in GD cells would create a folding environment particularly amenable to rescue of mutated GC folding via ERAD inhibition. Therefore, we attempted remodeling the proteostasis network to increase ER retention of unstable GC variants by inhibiting retrotranslocation and ERAD degradation and to enhance chaperone-mediated folding by restoring Ca^{2+} homeostasis (Figure 4.4.1). We report evidence suggesting that simultaneously inhibiting ERAD and enhancing the ER folding capacity by co-administering lacidipine and EerI to fibroblasts derived from patients with GD results in synergistic rescue of the folding and activity of the severely destabilized L444P GC variant. Moreover, we demonstrated that lacidipine treatment lowers EerI-mediated UPR induction and apoptosis. Upregulation of the anti-apoptotic gene Bcl-2 associated with lacidipine treatment was found to play a key role in preventing the induction of apoptosis in EerI-treated cells. Results from this work provide novel insights for the development of effective therapeutic strategies for the

treatment of GD based on remodeling the proteostasis network to rescue folding of unstable, degradation-prone GC variants.

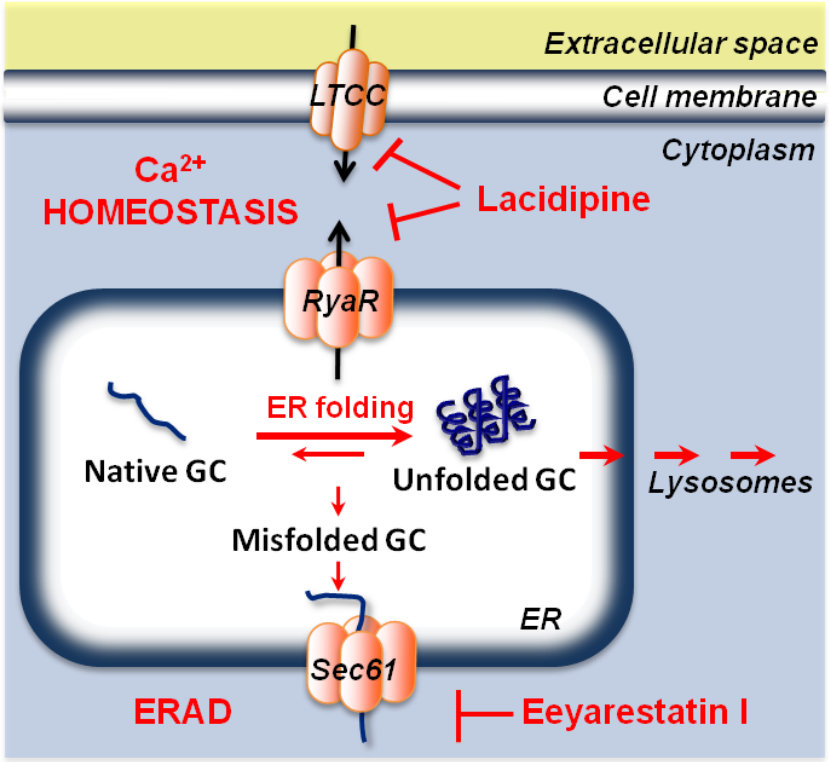

Figure 4.4.1. Inhibition of ERAD and modulation of Ca^{2+} homeostasis synergize to enhance the ER folding capacity in cells derived from patients with GD. Lacidipine enhances ER folding by restoring Ca^{2+} homeostasis in GD cells. Specifically, lacidipine inhibits extracellular Ca^{2+} influx through L-type voltage-gated Ca^{2+} channels (LTCC) on the plasma membrane and blocks ER Ca^{2+} efflux through ryanodine receptors (RyRs) on the ER membrane, thus restoring the intracellular gradient of [Ca^{2+}]. EerI treatment enhances retention of unstable proteins in the ER. Specifically, EerI inhibits p97 ATPase activity, which promotes retro-translocation of misfolded substrates from the ER to the cytoplasm for ER-associated degradation (ERAD). Lacidipine and EerI modulate distinct pathways of the proteostasis network involved in promoting native folding of GC.

4.4.2. Results

Inhibition of ERAD and modulation of Ca^{2+} homeostasis synergize to rescue L444P GC folding, trafficking and activity in fibroblasts derived from patients with Gaucher's disease

Experiments were conducted to simultaneously modulate Ca^{2+} homeostasis and ERAD inhibition in GD fibroblasts. Specifically, we used the LTCC blocker lacidipine, which restores Ca^{2+} homeostasis by inhibiting LTCC on the cell membrane and RyRs on the ER membrane (Chapters 4.1 and 4.2), and Eeyarestatin I (EerI), which blocks the ERAD pathway by inhibiting the p97 ATPase (Fiebiger et al., 2004; Wang et al., 2010), and investigated the activity and intracellular trafficking of mutated GC. Experiments were performed by administering a constant concentration of lacidipine (5, 10, or 20 μM) to fibroblasts derived from GD patients homozygous for the L444P GC allele that were cultured in medium supplemented with a range of EerI concentrations. GC enzymatic activity was evaluated every 24 hr for up to 72 hrs with the intact cell GC activity assay (Figure 4.4.2). Culturing conditions resulting in maximal rescue of L444P GC activity are reported in Figure 4.4.2. Co-treatment with EerI (6 μM) and lacidipine (20 μM) for 48 hr resulted in a 2.9-fold increase in L444P GC activity compared to untreated cells ($p<0.001$; Figure 4.4.2), which corresponds to 36% of WT activity and is compatible with effective treatment (Schueler et al., 2004). This increase in GC activity is significantly higher than that measured in cells treated only with EerI (1.6-fold) or lacidipine (1.8-fold) under the same conditions and was still observed after 72 hrs of incubation (EerI 6 μM and lacidipine 20 μM, 2.6-fold increase in GC activity, $p<0.01$).

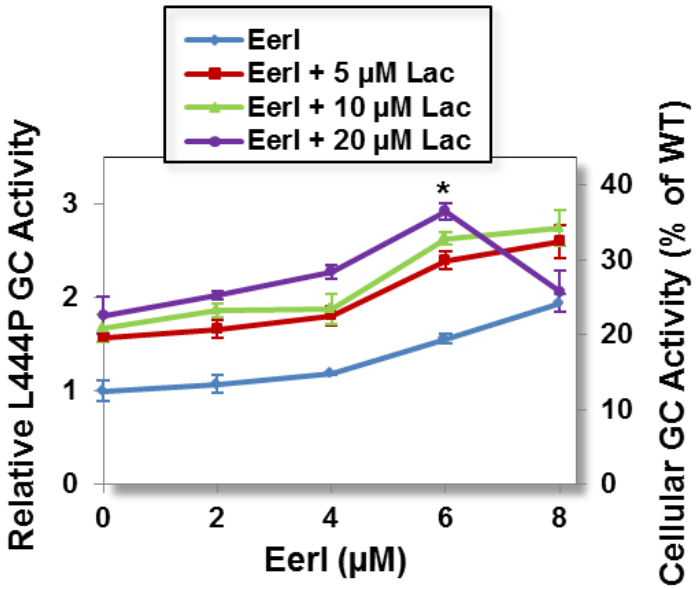

Figure 4.4.2. Co-treatment of GD patient-derived fibroblasts with EerI and lacidipine enhances the activity of L444P GC. L444P GC activities were evaluated in cells treated with a range of concentrations of EerI and constant doses of lacidipine (5, 10, or 20 μM) for 72 hrs. Relative GC activities were calculated by normalizing GC activities measured in treated cells to the activity in untreated cells (left y axis), ($p<0.01$ if not specified; *$p<0.001$). The corresponding fraction of WT GC activity is also reported (right y axis). Experiments were repeated three times and data points are reported as mean ± SD. Lac, lacidipine.

In order to verify that the increase in GC activity observed in cells treated with EerI and lacidipine is due to rescue of L444P GC folding and lysosomal trafficking, we investigated L444P GC intracellular localization. Cells were treated under culturing conditions that gave rise to maximal GC activity increase and analyzed by immunofluorescence microscopy. Specifically, L444P GC patient-derived fibroblasts were cultured with EerI (6 μM), lacidipine (10 μM) and a combination thereof for 48 hrs. GC localizations in the ER and in the lysosomes were detected with antibodies specific for GC, for an ER marker (CNX), and for a lysosomal marker (LAMP-1). Co-localization of GC and CNX (Figure 4.4.3A) and of GC and LAMP-1 (Figure 4.4.3B) is shown in pink and purple, respectively, in merged images. Heatmaps of co-localization images

were obtained with NIH ImageJ software. L444P GC was barely detectable in untreated cells due to extensive ERAD, as expected (Mu et al., 2008b). Treatment with lacidipine or EerI enhanced the pool of GC that accumulates both in the ER and in the lysosomes, as shown in Chapters 4.2 and 4.3. The addition of lacidipine to EerI treatment did not significantly increase GC accumulation in the ER compared to cells treated only with EerI, but resulted in a significantly larger pool of GC in the lysosomes compared to cells treated with either EerI or lacidipine. These results demonstrate that combining modulation of Ca^{2+} homeostasis and ERAD enhances rescue of GC folding intermediates that escape ERAD and promotes their trafficking through the secretory pathway, thereby leading to the increase in lysosomal GC activity observed with enzymatic assays (Figure 4.4.2).

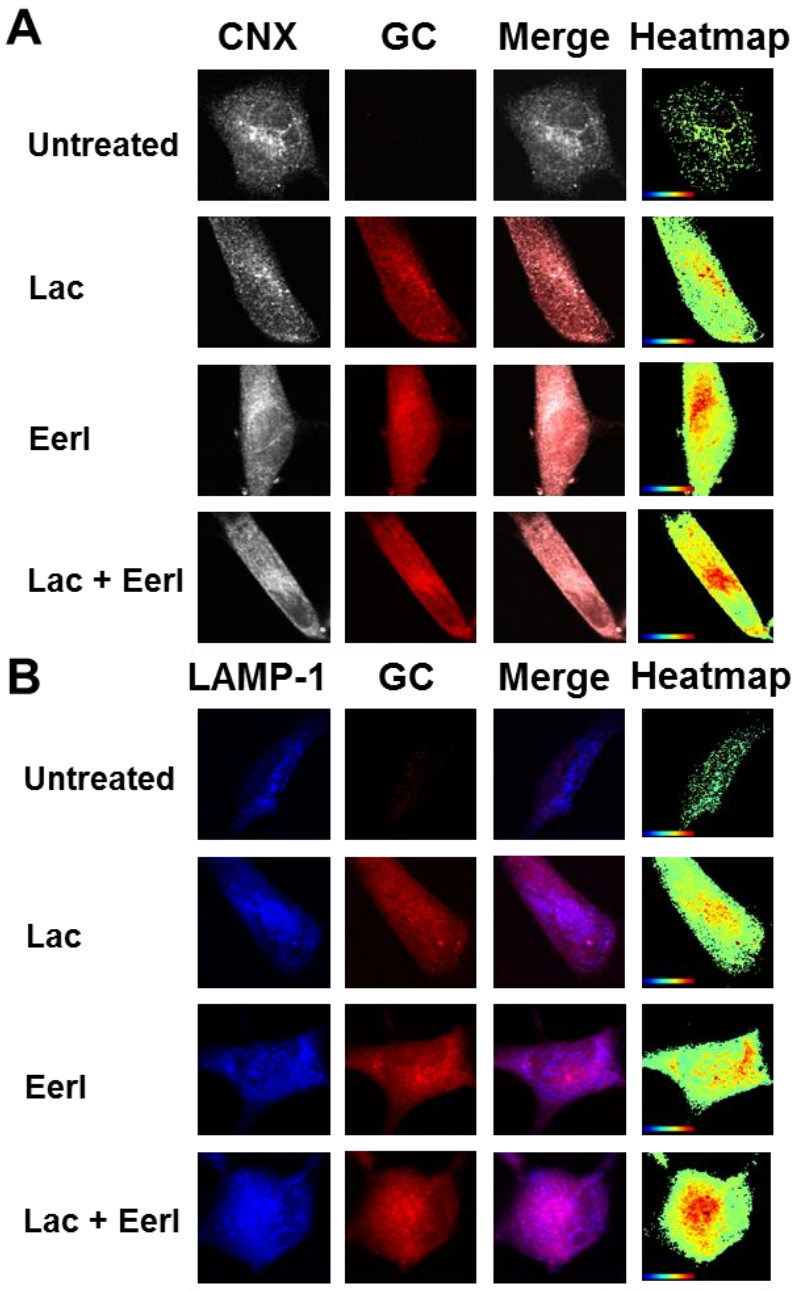

Figure 4.4.3. Co-treatment with EerI and lacidipine enhances the folding and lysosomal trafficking of L444P GC in patient-derived fibroblasts. Immunofluorescence microscopy of **A**) GC and CNX (an ER marker), and **B**) GC and LAMP-1 (a lysosomal marker) in L444P GC fibroblasts. Cells were treated with EerI (6 μM), and lacidipine (10 μM) for 48 hrs. Colocalization of CNX (grey, column 1) and GC (red, column 2) is shown in pink (column 3). Colocalization of LAMP-1 (blue, column 1) and GC (red, column 2) is shown in purple (column 3). Heatmaps of co-localization images were obtained with NIH ImageJ analysis software (column 4). Hot colors represent positive correlation (co-localization), whereas cold colors represent negative correlation (exclusion). Lac, lacidipine.

Lacidipine treatment attenuates the cytotoxic effect of EerI-mediated ERAD inhibition in fibroblasts derived from patients with Gaucher's disease

By inhibiting retrotranslocation of misfolded proteins, EerI treatment causes accumulation of misfolded intermediates in the ER and, consequently, ER stress and induction of the UPR (Chapter 4.3 or Wang et al., 2011c). UPR is activated to cope with the aberrant accumulation of misfolded proteins (Ron and Walter, 2007). Not surprisingly, moderate UPR induction was repeatedly reported to promote rescue of misfolding-prone GC variants (Mu et al., 2008b and Chapters 4.1-4.3). However, prolonged UPR induction observed upon sustained treatment with EerI was also observed to cause activation of apoptosis (Chapters 4.2 and 4.3). Cell treatment with lacidipine, on the other hand, was shown not to cause cytotoxicity under conditions observed to rescue folding of mutated GC variants (Chapters 4.2 and 4.3). Because lacidipine treatment also causes moderate UPR induction (Chapter 4.2), we hypothesized an anti-apoptotic effect associated with lacidipine treatment that protects cells from UPR-induced apoptosis (Rodriguez et al., 2010; Wang et al., 2011b). Therefore, we asked whether lacidipine treatment could counteract the cytotoxic effect of EerI and evaluated apoptosis in cells co-treated with lacidipine and EerI.

CytoGLO^{TM} Annexin V-FITC Apoptosis Detection Kit was used to monitor membrane rearrangement (Annexin V binding) and fragmentation (propidium iodide (PI) binding) that occur during early and late apoptosis, respectively. L444P GC fibroblasts were cultured with lacidipine (10 μM) and EerI (6 μM) for 16 hrs (Figure 4.4.4A-B). Similar to observations reported in chapters 4.1 and 4.2 (Wang et al., 2011b; Wang et al., 2011c), Annexin V binding affinity in cells treated with lacidipine was comparable to that

measured in untreated cells, whereas a dramatic increase in Annexin V binding was observed in cells treated with EerI, reflecting the onset of apoptosis. The addition of lacidipine to EerI-treated cells resulted in significant decrease in Annexin V binding compared to cells treated only with EerI, suggesting that lacidipine treatment partially alleviates EerI cytotoxic effect (Figure 4.4.4A). The dead cell population was evaluated by measuring PI binding affinity. A negligible increase (0.3%) in PI binding was observed upon lacidipine treatment, whereas EerI treatment caused a 10% increase ($p<0.01$; Figure 4.4.4B). The addition of lacidipine to EerI-treated cells reduced the PI binding population to 6.7% ($p<0.01$), confirming that lacidipine has an anti-apoptotic effect.

These results, taken together, prove that lacidipine treatment enhances EerI-mediated rescue of mutated GC native folding and activity but that it also counteracts its cytotoxic effect, therefore protecting the cells from UPR induced apoptosis, a particularly appealing property for development of therapeutic solutions based on the modulation of the proteostasis network.

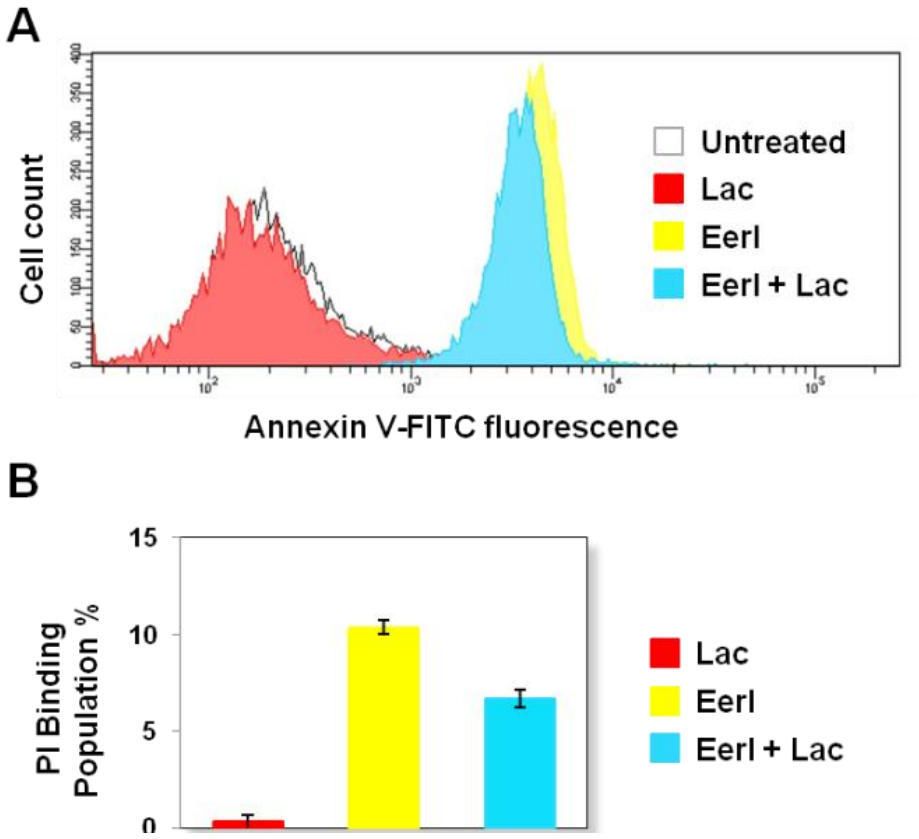

Figure 4.4.4. Lacidipine treatment attenuates EerI-mediated apoptosis induction in L444P GC patient-derived fibroblasts. A) Flow cytometry histograms of Annexin V-FITC fluorescence intensities (x-axis, log scale) plotted against cell counts (y-axis, linear scale) obtained from the analysis of untreated cells and cells treated with EerI (6 μM) and lacidipine (10 μM). Three independent experiments were conducted and results of one representative experiment are reported. **B**) PI binding population change (%) of cells treated with EerI (6 μM) for 16 hrs compared to untreated cells ($p<0.01$). Number of total cells counted: 10,000. The data is reported as mean ± SD.

Lacidipine treatment remodels EerI-mediated activation of the UPR pathway

Previous studies showed that EerI, when administered under conditions that result in maximal increase in L444P GC activity, is associated with significant UPR induction and cell apoptosis, whereas lacidipine treatment induces UPR but does not cause apoptosis (Chapter 4.2; Wang et al., 2011b). We reported above that lacidipine prevents apoptosis in cells treated with EerI (Figure 4.4.4). Therefore, we asked whether lacidipine affects UPR induction in EerI-treated cells. We measured the expression of three

representative UPR target proteins: X-box binding protein-1 (Xbp-1), activating transcription factor 4 (ATF4), and C/EBP homologous protein (CHOP) (Schroder and Kaufman, 2005). Quantitative RT-PCR was conducted to evaluate the expression levels of Xbp-1, ATF4, and CHOP in cells treated with lacidipine (10 μM) and EerI (6 μM).

The precursor mRNA of Xbp-1 is spliced upon activation of the IRE1 signaling cascade. Spliced Xbp-1 mRNA functions as an activator of the IRE1 branch of the UPR, while the unspliced precursor acts as a repressor (Ron and Walter, 2007). Spliced and unspliced forms of Xbp-1 mRNA were analyzed by RT-PCR followed by gel electrophoresis. Bands corresponding to spliced Xbp-1 mRNA were quantified with NIH ImageJ software to evaluate the activation level of the IRE1 arm of the UPR (Figure 4.4.5A-B). In agreement with results reported in Chapter 4.2, the amount of spliced Xbp-1 in lacidipine treated cells was similar to that of untreated cells (Wang et al., 2011b), whereas a considerable amount of spliced Xbp-1 was observed in cells treated with EerI (Wang et al., 2011c). In cells treated with both lacidipine and EerI, the amount of spliced Xbp-1 was found to further increase 1.7-fold compared to cells treated only with EerI, suggesting a synergistic effect of lacidipine and EerI on the induction of the IRE1 arm. Xbp-1 is an essential pro-survival UPR component and its activation is associated with attenuated apoptosis under ER stress conditions (Gupta et al., 2010). Hence, enhanced splicing of Xbp-1 in cells treated with lacidipine and EerI correlates with the decrease in apoptosis induction observed under same conditions.

The expression level of ATF4 was evaluated in order to monitor the activation of the PERK branch. ATF4 transcriptional expression was upregulated 1.8- and 4.4-fold in cells treated with lacidipine and EerI, respectively, compared to untreated cells,

indicating that these two proteostasis modulators have different effects on the induction of this arm of the UPR. Interestingly, the addition of lacidipine to EerI-treated cells was observed to reduce ATF4 expression to only 2.1-fold increase ($p<0.05$) compared to untreated cells, indicating that lacidipine suppresses EerI-mediated activation of the PERK arm (Figure 4.4.5C).

CHOP, a downstream effector of the ATF6 branch, was found to be highly upregulated by both lacidipine and EerI treatment (6.1- and 19-fold, respectively; Figure 4.4.5D). The addition of lacidipine to EerI-treated cells lowered CHOP upregulation to 15-fold ($p<0.05$). CHOP mediates UPR induced apoptosis activation (Oyadomari and Mori, 2004). These results confirm that lacidipine treatment suppresses UPR-induced apoptosis caused by EerI treatment as reported in Figure 4.4.4.

In summary, treatment with lacidipine was found to remodel the UPR pathway and lower UPR-induced apoptosis caused by treatment with EerI. Particularly, lacidipine inhibits the activation of PERK and ATF6 arms, which mediate induction of apoptosis, and enhances the activation of the pro-survival IRE1/Xbp-1 arm, thus counteracting the progression of the apoptotic cascade.

In Chapter 4.2, lacidipine treatment was shown to alter the expression of genes involved in the regulation of UPR-induced apoptosis, and, particularly, that it causes upregulation of the anti-apoptotic gene Bcl-2 (Wang et al., 2011b). We therefore asked whether the protective effect of lacidipine treatment observed in Eer-treated cells could be attributed to the upregulation of Bcl-2. The expression level of Bcl-2 was evaluated by performing quantitative RT-PCR in cells cultured with lacidipine (10 μM) and EerI (6 μM). Lacidipine treatment resulted in 3.0-fold increase in Bcl-2 expression compared to

untreated cells, whereas EerI treatment caused a 2.0-fold decrease. Co-treatment with lacidipine and EerI resulted in considerable upregulation of Bcl-2 expression (4.2-fold; $p<0.05$; Figure 4.4.5E). Interestingly, Bcl-2 was shown to prevent apoptosis induction mediated by CHOP (Szegezdi et al., 2006), for which expression is lowered in association with the upregulation of Bcl-2 in cells co-treated with lacidipine and EerI, again supporting the notion that lacidipine treatment lowers UPR-induced apoptosis.

Upregulation of the gene encoding GC (GBA) in cells treated with proteostasis modualtors was previously reported (Wang et al., 2011b; Wang et al., 2011c). We asked whether the synergistic effect of Ca^{2+} homeostasis modulation and ERAD inhibition could be attributed to GC transcriptional upregulation in addition to inhibition of GC degradation. Quantitative RT-PCR was conducted to measure the expression of GC in GD patient-derived fibroblasts treated with lacidipine (10 μM) and EerI (6 μM). Co-administration of lacidipine and EerI resulted in 5.2-fold upregulation of GC expression ($p<0.05$) compared to untreated cells, which is higher than what observed in cells treated only with lacidipine (2.5-fold) or EerI (3.3-fold) (Figure 4.4.5F).

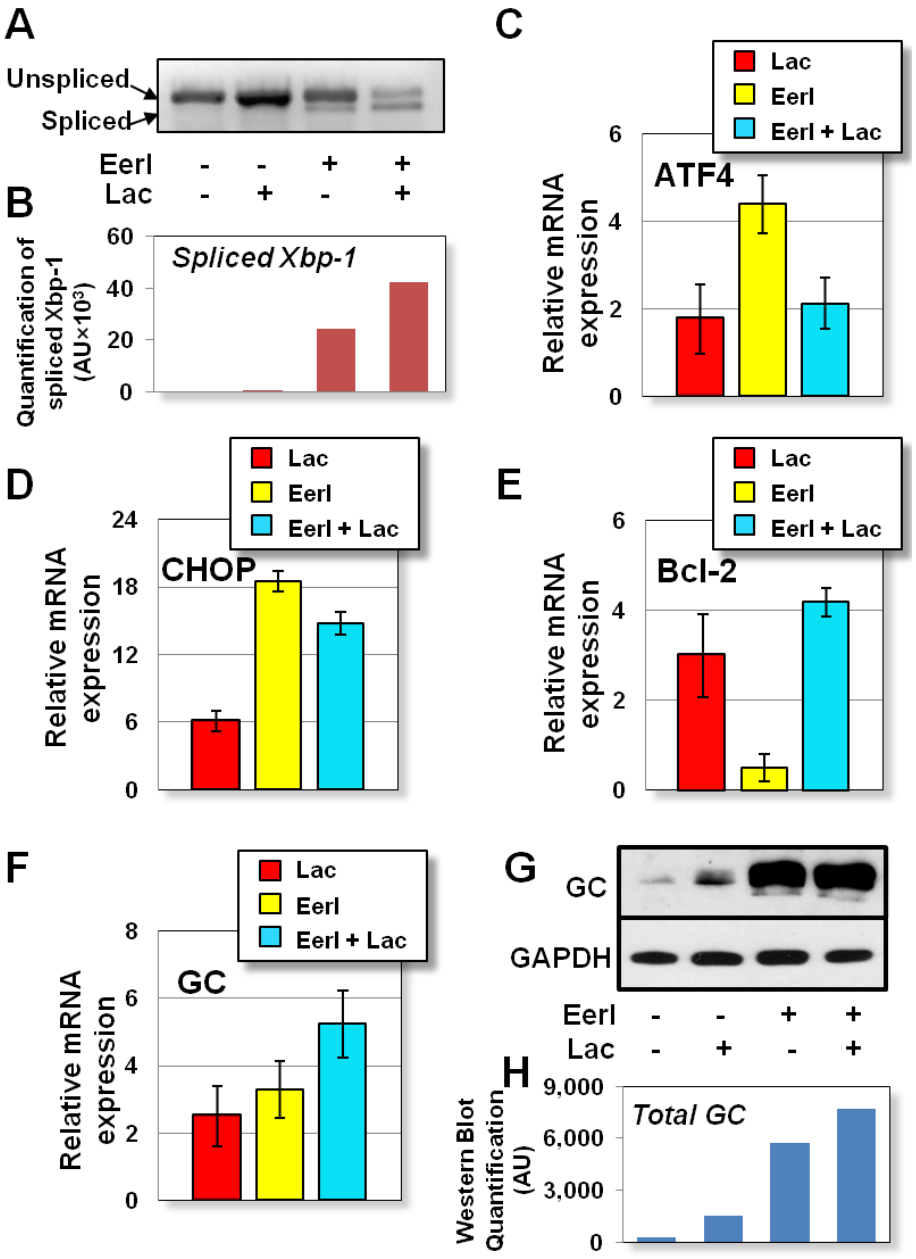

Figure 4.4.5. Lacidipine treatment remodels the UPR pathway in EerI-treated fibroblasts derived from GD patients. Cells were treated with EerI (6 µM) and lacidipine (10 µM) for 24 hrs. **A**) Xbp-1 mRNA splicing was determined by RT-PCR followed by gel electrophoresis. **B**) Spliced Xbp-1 band intensities were quantified with the NIH ImageJ analysis software. Relative mRNA expression levels of **C**) ATF4, **D**) CHOP, **E**) Bcl-2, and **F**) GC were obtained by quantitative RT-PCR, corrected by the expression of the housekeeping gene GAPDH, and normalized by that of untreated cells ($p<0.05$). The data is reported as mean ± SD. **G**) Western blot analysis of cells treated with EerI (6 µM) and lacidipine (10 µM) for 48 hrs using GC specific antibody. GAPDH expression was used as a loading control. **H**) Western blot band quantification. GC bands were quantified by NIH ImageJ analysis software and corrected by GAPDH band intensities.

GC expression was also evaluated by Western blot (Figure 4.4.5G-H). As shown in Figure 4H, L444P GC content was barely detectable in untreated cells, as expected, due to extensive ERAD (Sawkar et al., 2006b), whereas treatment with either lacidipine or EerI significantly enhanced GC protein accumulation. Co-treatment with lacidipine and EerI further enhanced GC accumulation (1.4-fold increase compared to EerI treatment alone) in agreement with the results obtained from quantitative RT-PCR.

In Chapters 4.1-4.3, we demonstrated that the increase in lysosomal GC activity observed upon chemically induced inhibition of ERAD or modulation of Ca^{2+} homeostasis in cells derived from patients with GD is partially due to the upregulation of BiP expression associated with UPR induction. Therefore, we analyzed BiP expression in fibroblasts derived from GD patients co-treated with lacidipine and EerI. BiP protein accumulation was evaluated by Western blot using a BiP-specific antibody (Figure 4.4.6A), and bands were quantified with NIH ImageJ software (Figure 4.4.6B). Co-administration of lacidipine and EerI resulted in 3.5-fold increase in BiP cellular accumulation, which is lower than that observed in cells treated only with EerI (4.4-fold). Similar to results reported in Chapters 4.2 and 4.3 describing cell treatment with lacidipine and EerI (Wang et al., 2011b; Wang et al., 2011c), CNX and CRT protein levels were not altered by lacidipine and EerI treatment. BiP is normally upregulated upon activation of the UPR (Schroder and Kaufman, 2005). Thus, the decrease in BiP expression observed in cells treated with EerI and lacidipine reflects lacidipine-mediated attenuation of UPR induction.

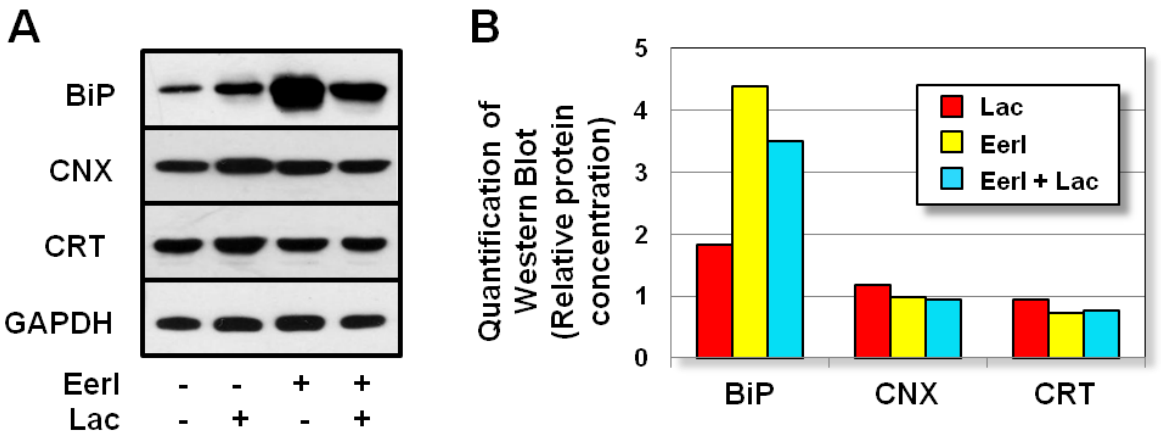

Figure 4.4.6. Lacidipine treatment attenuates BiP upregulation caused by EerI-mediated UPR activation. A) Western blot analyses of BiP, CNX, CRT, and GAPDH (used as loading control) in cells treated with EerI (6 μM) and lacidipine (10 μM) for 48 hrs. **B**) Quantification of Western blot bands. ER chaperone band intensities were quantified with NIH ImageJ analysis software, corrected by GAPDH band intensities, and divided by the values obtained in untreated samples.

Chemically induced upregulation of Bcl-2 enhances mutated GC activity rescue and cell viability

Bcl-2 is the prototype of an expanding family of proteins that regulate cell survival and apoptosis in multiple cell types (Chipuk et al., 2010). As discussed above, treatment with lacidipine prevents UPR induced apoptosis and cell death caused by EerI treatment. The addition of lacidipine to EerI treated cells results in upregulation of Bcl-2 expression to a considerably higher level than EerI treatment alone (Figure 4.4.5E). In order to investigate the role of Bcl-2 in cells treated for the rescue of mutated GC folding via UPR induction, we attempted to chemically induce Bcl-2 upregulation in cells derived from patients with GD. Fluvastatin was previously reported to prevent H_2O_2-induced apoptosis by upregulating Bcl-2 expression (Xu et al., 2008). We asked whether fluvastatin could counteract the apoptotic effect of prolonged UPR induction. Fluvastatin was administered to cells treated with UPR inducing proteostasis modulators known to

rescue native folding of mutated GC. MG-132 inhibits proteasomal degradation, which, in turn, causes induction of UPR and upregulation of chaperones in GD cells (Mu et al., 2008b). Co-treatment with EerI and MG-132 was found to dramatically enhance the activity of L444P GC (to 52% of WT activity), but at the cost of even higher induction of apoptosis (Chapter 4.3). We administered fluvastatin (100 nM) to cells treated with EerI (2 and 6 μM) and MG-132 (0.6 μM) and tested Bcl-2 expression, apoptosis and GC activity rescue. Fluvastatin treatment caused dramatic upregulation of Bcl-2 in GD cells (18.4-fold compared to untreated cells; $p<0.05$) and did not cause any cytotoxicity (Figure 4.4.7A-B). Upregulation of Bcl-2 and lowered apoptosis induction were also observed upon addition of fluvastatin in EerI-treated cells. Specifically, fluvastatin treatment caused a 4.6-fold increase in Bcl-2 expression in cells treated with EerI 2 μM and 5.2-fold in cells treated with EerI 6 μM compared to cells treated only with EerI ($p<0.05$; Figure 4.4.7A). Fluvastatin treatment also reduced apoptosis by 0.9% in cells treated with EerI 2 μM and by 3.7% in cells treated with EerI 6 μM ($p<0.01$; Figure 4.4.7B). Similar results were obtained upon addition of MG-132. Bcl-2 expression in cells treated with both EerI and MG-132 was downregulated (0.83-fold) compared to untreated cells. However, the addition of fluvastatin caused upregulation of Bcl-2 expression (2.8-fold; $p<0.05$) and decrease in dead cell population (4.0%; $p<0.01$). These results demonstrate that the upregulation of Bcl-2 expression enhances cellular tolerance to UPR-induced stress and cell survival, therefore preventing apoptosis in cells treated for the rescue of mutated GC folding.

To investigate whether chemically induced upregulation of Bcl-2 expression affects mutated GC activity rescue, patient-derived fibroblasts harboring L444P GC were

cultured with EerI (2 and 6 μM), MG-132 (0.6 μM), and fluvastatin (100 nM) for up to 72 hrs and GC activity was measured every 24 hrs (Figure 4.4.7C). Interestingly, chemically induced upregulation of Bcl-2 expression did not reduce the increase in L444P GC activity mediated by UPR induction. Compared to treatment with EerI (2 or 6 μM) alone, co-treatment with fluvastatin and EerI for 48 hrs did not affect L444P GC activity at low EerI concentration, but resulted in a modest increase at high EerI concentration (to 2.0-fold; $p<0.01$). Co-administration of EerI and MG-132 resulted in a 3.0-fold increase ($p<0.01$) in L444P GC activity as expected, which was further enhanced to 3.3-fold upon the administration of fluvastatin, indicating that upregulating Bcl-2 expression to maintain cell viability enhances EerI and MG-132 mediated L444P GC activity rescue.

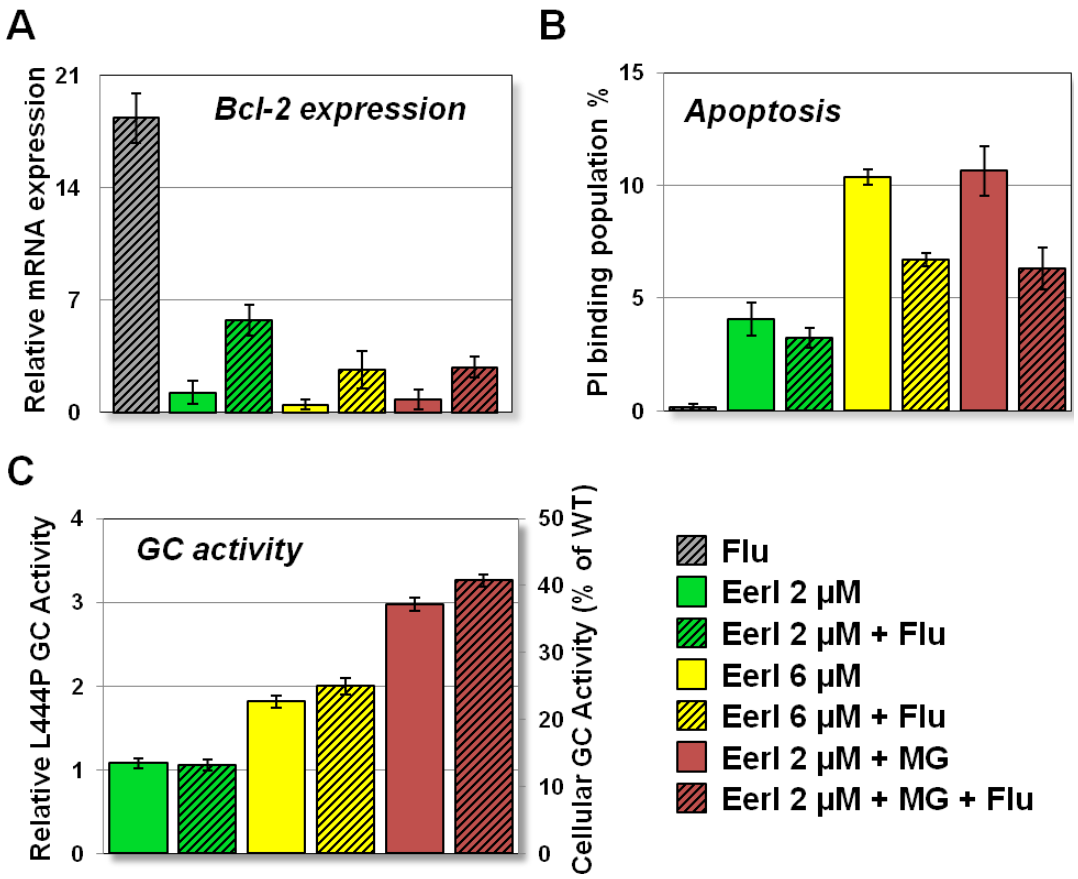

Figure 4.4.7. Upregulation of Bcl-2 protects GD cells from apoptosis caused by chemical modulation of the proteostasis network. A) Relative mRNA expression levels of Bcl-2 in cells treated with EerI (2 and 6 µM), MG-132 (0.6 µM), and fluvastatin (100 nM) for 24 hrs were obtained by quantitative RT-PCR and calculated as described in Figure 4.4.5 ($p<0.05$). **B**) PI binding population change (%) of cells treated with EerI (2 and 6 µM), MG-132 (0.6 µM), and fluvastatin (100 nM) for 16 hrs compared to untreated cells ($p<0.01$). The data is reported as mean ± SD. Number of total counted cells: 10,000. **C**) Relative L444P GC activities of GD fibroblasts treated with EerI (2 and 6 µM), MG-132 (0.6 µM), and fluvastatin (100 nM) for 48 hrs. Relative GC activities were evaluated as described in Figure 4.4.2 ($p<0.01$). Experiments were repeated three times and data points are reported as mean ± SD. MG, MG-132; Flu, fluvastatin.

4.4.3. Discussion

Inhibition of specific steps of the ERAD pathway results in rescue of L444P GC, a severely destabilized mutant commonly associated with neuronopathic GD. ERAD inhibition, however, while enhancing retention of unstable GC in the ER and ultimately resulting in increased lysosomal trafficking and activity, also leads to significant UPR induction and apoptosis (Chapter 4.3). In this study, we attempted to combine ERAD inhibition with modulation of Ca^{2+} homeostasis. Restoring Ca^{2+} homeostasis via lacidipine treatment proved to be an effective strategy to rescue L444P GC folding and activity by modulating the cell folding capacity, without, however, inducing apoptosis (Chapter 4.2). We found that restoring Ca^{2+} homeostasis in GD cells results in a folding environment more amenable to rescue native folding of mutated GC via ERAD inhibition. Combining these two distinct mechanisms of action (Figure 4.4.1) causes synergistic increase of lysosomal trafficking and activity of mutated GC (Figures 4.4.2 and 4.4.3). We found that cell treatment with lacidipine not only enhanced EerI-mediated rescue of mutated GC folding but also protected GD cells from UPR-induced apoptosis caused by ERAD inhibition (Figure 4.4.4).

Mechanistic studies revealed that lacidipine remodels the induction of UPR caused by ERAD inhibition. Signal transducers of the UPR can activate either cytoprotective or proapoptotic pathways (Lin et al., 2009). A pro-survival response is first initiated to reduce the load of misfolded proteins by boosting the ERAD pathway (Termine et al., 2009). This response is mediated by the induction of the IRE1 signaling cascade (Lin et al., 2007) via Xbp-1 splicing and activation (Gupta et al., 2010). If the proteotoxic stress persists, pro-apoptotic signals are elicited through the activation of

PERK and ATF6 signaling cascades via expression of ATF4 and its transcriptional target CHOP, which are upregulated simultaneously to attenuate IRE1 signaling (Kitamura, 2008; Lin et al., 2009). Analysis of the UPR in GD cells co-treated with EerI and lacidipine revealed that this combination enhances Xbp-1 splicing while lowering the activation of ATF4 and CHOP. These results imply that lacidipine remodels EerI-mediated UPR induction by enhancing the expression of the anti-apoptotic IRE1 arm and inhibiting the activations of the pro-apoptotic PERK and ATF6 arms (Figure 4.4.5).

The Bcl-2 protein family plays a key role in the activation of UPR-induced apoptosis (Youle and Strasser, 2008). It consists of anti-apoptotic proteins including Bcl-2, and pro-apoptotic proteins such as BAX and BAK (Youle and Strasser, 2008). Oligomerization and activation of BAX and BAK mediate induction of apoptosis (Youle and Strasser, 2008). CHOP upregulation causes downregulation of the anti-apoptotic Bcl-2 gene (McCullough et al., 2001; Zong et al., 2003), which, in turn, enables the activation of pro-apoptotic proteins (Szegezdi et al., 2006). Bcl-2 upregulation, on the other hand, blocks CHOP-induced apoptosis (McCullough et al., 2001). Moreover, Bcl-2 contributes to maintaining Ca^{2+} homeostasis by reducing $[Ca^{2+}]_{ER}$ efflux (Eckenrode et al., 2010; Rong et al., 2009). Bcl-2 was upregulated in L444P GC fibroblasts cultured with lacidipine (Wang et al., 2011b). Our results showed that lacidipine treatment enhances the expression of Bcl-2 in EerI-treated cells and protects cells from EerI-mediated apoptosis (Figure 4.4.4 and 4.4.5E). In addition, chemical induction of Bcl-2 expression enhances cell viability in GD cells treated with proteostasis modulators that induce the UPR (Figure 4.4.7).

In summary, this work demonstrates that combining modulation of Ca^{2+} homeostasis and ERAD inhibition synergistically enhances the ER folding capacity leading to dramatic increase in L444P GC folding, lysosomal trafficking and activity. The results reported herein provide insights for the development of strategies to modulate the proteostasis network without triggering activation of apoptosis.

Chapter 5

Materials and methods

5.1. Cell lines and cell culture

Patient-derived fibroblasts were obtained from Coriell Cell Repositories (Table 5.1).

Fibroblasts were grown in minimal essential medium with Earle's salts supplemented with 10% heat-inactivated fetal bovine serum and 1% glutamine Pen-Strep at 37℃ in 5% CO_2. Cell medium was replaced every 3 or 4 days. Monolayers were passaged upon reaching confluency.

Table 5.1. Cell lines

Cell line	Disease Diagnosed	Genotype	Protein Mutation
GM10915	Gaucher disease, type I	1448T>C	L444P homozygous
GM00852	Gaucher disease, type I	1226A>G	N370S, 84GG
GM13204	Tay-Sachs disease	805G>A, 1278insTATC	G269S, 1278insTATC
GM00498	Wild-type	-	-

5.2. Plasmids and primers

The human cDNA clones of BiP, Calnexin, Calreticulin, and GRP94 were obtained from Origene., The Tetracycline-Regulated Expression System (T-REx™) was from Invitrogen and is composed of the two plasmids pcDNA™4/TO and pcDNA™6/TR.

Table 5.2. Plasmids

Plasmid	Phenotype	Source
BiP	P11021; Human cDNA clone	Origene (SC108086)
Calnexin (CNX)	P27824; Human cDNA clone	Origene (SC108288)
Calreticulin (CRT)	P15253; Human cDNA clone	Origene (SC320287)
GRP94	P14625; Human cDNA clone	Origene (SC108810)
pcDNA™4/TO	T-REx™; Inducible vector	Invitrogen (V102020)
pcDNA™6/TR	T-REx™; Regulatory vector	Invitrogen (V102520)

Tables 5.3 and 5.4 include primers used in this study to construct plasmids and to perform quantitative RT-PCR, as described below.

Table 5.3. Cloning Primers

Gene	Primer	Sequence
BiP (HindIII/BamHI)	BiP.f	5'-GCGCGCGGTACCATGAAGCTCTCCCTGGTG-3'
	BiP1.r	5'-GATGAGTTTTTGTTCGGCGCCGG CCAACTCATCTTTTTCTGCTGTATCCTC -3'
	BiP2.r	5'-GCGCGCGTATTGGGATCCTCACAG ATCCTCTTCTGAGATGAGTTTTTGTTC-3'
CNX (KpnI/EcoRI)	Cnx.f	5'-GCGCGCGGTACCATGGAAGGGAAGTGG-3'
	Cnx1.r	5'-GAGTTTTTGTTCGGCGCCGGCCT CTCTTCGTGGCTTTCTGTTTCTTG -3'
	Cnx2.r	5'-GCGCGCGTATTGGAATTCTCACA GATCCTCTTCTGAGATGAGTTTTTGTTC-3'
CRT (HindIII/EcoRI)	Crt.f	5'-ATGCTACGAAAGCTTATGCTGCTA TCCGTGCCGCTGC -3'
	Crt1.r	5'-TAATCAGTTTCTGTTCACCACCACC CAGCTCGTCCTTGGC-3'
	Crt2.r	5'-GCGCCGCCCGAATTCTTACAGATCT TCTTCGCTAATCAGTTTCTGTTCAC-3'
GRP94 (EcoRI/XbaI)	Grp94.f	5'-TAGATACATGAATTCATGAGGGCCC TGTGGGTGCTGGG-3'
	Grp941.r	5'-CGCTAATCAGTTTCTGTTCACCACC ACCCAATTCATCTTTTTCAGCTGT-3'
	Grp942.r	5'-GCGCCGCCCTCTAGATTACAGATCT TCTTCGCTAATCAGTTTCTGTTCAC-3'

Table 5.4. RT-PCR Primers

Gene	GenBank Accession Code	Primer	Sequence
BiP	NM_005347	BiP.f	5'-GCC TGT ATT TCT AGA CCT GCC-3'
		BiP.r	5'-TTC ATC TTG CCA GCC AGT TG-3'
CNX	NM_001746	Cnx.f	5'-GCG TTG TGG GGC AGA TGA T-3'
		Cnx.r	5'-CCG GTT GAG GTG CAT CAG T-3'
CRT	NM_004343	Crt.f	5'-AAG TTC TAC GGT GAC GAG GAG-3'
		Crt.r	5'-GTC GAT GTT CTG CTC ATG TTT C-3'
Xbp-1	NM_005080	Xbp1.f	5'-TTA CGA GAG AAA ACT CAT GGC-3'
		Xbp1.r	5'-GGG TCC AAG TTG TCC AGA ATG C-3'
ATF4	NM_182810	ATF4.f	5’- GAC CAC GTT GGA TGA CAC TTG -3’
		ATF4.r	5’- GGG AAG AGG TTG TAA GAA GGT G-3’
ATF6	NM_007348	ATF6.f	5’-TGC TTC CAG CAG CAC CCA AGACT-3’
		ATF6.r	5’-CCC AGC AAC AGC AAG GAC TGG C-3’
CHOP	NM_004083	CHOP.f	5'-ACC AAG GGA GAA CCA GGA AAC G-3'
		CHOP.r	5'-TCA CCA TTC GGT CAA TCA GAG C-3'
BAK	NM_001188	BAK.f	5'-GTT TTC CGC AGC TAC GTT TTT-3'
		BAK.r	5'-GCA GAG GTA AGG TGA CCA TCT C-3'
BAX	NM_004324	BAX.f	5'-GGG TGG TTG GGT GAG ACT C-3'
		BAX.r	5'-AGA CAC GTA AGG AAA ACG CAT TA-3'
Bcl-2	NM_000633	Bcl-2.f	5'-GGG GAG GAT TGT GGC CTT C-3'
		Bcl-2.r	5'-CAG GGC GAT GTT GTC CAC C-3'
GC	NM_000157	GC.f	5'-CCA AGC CTT TGA GTA GGG TAA G-3'
		GC.r	5'-CCC GTG TGA TTA GCC TGG AT-3'
HEXA	NM_000520.2	HEXA.f	5'-CAA CCA ACA CAT TCT TCT CCA-3'
		HEXA.r	5'-CGC TAT CGT GAC CTG CTT TT-3'
TPP1	NM_000391.2	TPP1.f	5'-GAT CCC AGC TCT CCT CAA TAC G-3'
		TPP1.r	5'-GCC ATT TTT GCA CCG TGT G-3'
LAMP1	NM_005561.2	LAMP1.f	5'-ACG TTA CAG CGT CCA GCT CAT-3'

		LAMP1.r	5'-TCT TTG GAG CTC GCA TTG G-3'
ATP6V1H	NM_213619.1	ATP6V1H.f	5'-GGA AGT GTC AGA TGA TCC CCA-3'
		ATP6V1H.r	5'-CCG TTT GCC TCG TGG ATA AT-3'
PSAP	NM_002778.1	PSAP.f	5'-GCC AAC AGT GAA ATC CCT TCC-3'
		PSAP.r	5'-TCA GTG GCA TTG TCC TTC AGC-3'
TFEB	NM_007162.2	TFEB.f	5'-CCA GAA GCG AGA GCT CAC AGA T-3'
		TFEB.r	5'-TGT GAT TGT CTT TCT TCT GCC G-3'
M6PR	NM_002355.2	M6PR.f	5'-CTG GAG GAC TGG ACT GCT ACT-3'
		M6PR.r	5'-CTC CTA CCA AGT CGC AAG TTT T-3'
LIMP2	NM_005506.2	LIMP2.f	5'-GGC CGA TGC TGC TTC TAC A-3'
		LIMP2.r	5'-GGT CTC CCC TCT GAG GAT CTC-3'
GAPDH	NM_002046	GAPDH.f	5'-GTC GGA GTC AAC GGA TT-3'
		GAPDH.r	5'-AAG CTT CCC GTT CTC AG-3'

5.3. Chemicals and reagents

Celastrol and thapsigargin were purchased from Calbiochem. MG-132 and kifunensine were from Cayman Chemical. N-(n-Nonyl)-deoxynojirimycin (NN-DNJ), Conduritol B Epoxide (CBE), lacidipine and 4-Methylumbelliferyl 6-Sulfo-2-acetamido-2-deoxy-β-D-glucopyranoside (MUGS) were from Toronto Research Chemicals. Eeyarestatin I was from ChemBridge. 4-Methylumbelliferyl β-D-glucoside (MUG), tunicamycin, nicardipine and lercanidipine were from Sigma-Aldrich. DHBP Dibromide, ruthenium red, dantrolene, ryanodine, diltiazem and verapamil were from Tocris Bioscience. Fluvastatin was from Enzo Life Sciences. Fura-2, AM was from Anaspec. T-REx™ complete kit and lipofectamine 2000 were from Invitrogen. Bovine Serum Albumin was from Jackson ImmunoResearch Laboratories. TMB reagent, Propidium

Iodide solution, FITC Annexin V and its binding buffer were from BioLegend. Cell culture media were from Lonza.

5.4. Enzyme activity assays

The glucocerebrosidase (GC) activity assay was performed as previously described (Mu et al., 2008b). Briefly, 100 µl aliquots of 104 cells were plated in each well of a 96-well plate and incubated overnight to allow cell attachment. The medium was replaced with fresh medium containing small molecules on the next morning and the plates were incubated at 37 ℃ (small molecule concentrations and time of incubation are specified in each experiment). The medium was then aspirated and monolayers were washed with PBS three times. The assay reaction was started by the addition of 50 µl of 2.5 mM MUG in 0.2 M acetate buffer (pH 4.0) and stopped by the addition of 150 µl of 0.2 M glycine buffer (pH 10.8) to each well after 7 hrs of incubation at 37 ℃. Liberated 4-methylumbelliferone was measured (excitation 365 nm, emission 445 nm) with a SpectraMax Gemini plate reader (Molecular Device). Non-lysosomal GC activity was evaluated by measuring GC activities in the presence of Conduritol B Epoxide (CBE) at 1 mM final concentration. Relative GC activities were calculated by subtracting the background of non-lysosomal activity and normalizing the obtained values by the activity of untreated cells.

The hexosaminidase A (HexA) activity assay was performed as previously described (Mu et al., 2008b; Tropak et al., 2004). Cells were seeded and cultured as described for GC activity assay. HexA assay reaction was started by lysing the cells with

60 µl of 10 mM citrate/phosphate buffer (CP buffer, pH 4.2) containing 0.5% human serum albumin and 0.5% Triton X-100. The buffer was pipetted up and down three times to yield a well mixed cell lysate solution. Aliquots of 30 µl lysates were transferred to a new 96-well plate and mixed with 25 µl of 3.2 mM MUGS (dissolved in 10 mM CP buffer, pH 4.2) and incubated at 37 ℃ for 1 hr. The reaction was stopped by the addition of 200 µl aliquotes of 0.1 M 2-amino-2-methyl-1-propanol (pH 10.5). HexA activity was evaluated by measuring the fluorescence intensity of the solution at excitation 365 nm and emission 450 nm. Relative HexA activities were calculated by normalizing the obtained fluorescence values of treated cells to that of untreated cells.

5.5. Protein overexpression

The human cDNA encoding BiP (P11021), Calnexin (P27824), Calreticulin (P15253) and GRP94 (P14625) were cloned into pcDNA4/TO (Invitrogen). cDNA sequences were amplified by PCR using the primers reported in Table 5.3, adding the myc tag (N-EQKLISEEDL-C) at the 3' end of each sequence. PCR products were digested with the appropriate restriction enzymes (Table 5.3), and ligated into the inducible expression vector pcDNA4/TO digested likewise. Plasmid sequences were confirmed by automated sequencing.

Transfection procedures were performed as described: 10^4 cells were plated in each well of a 96-well plate and incubated overnight to allow cell attachment. Transfection reactions were performed when cells reached 70-80% confluency. The medium was replaced with fresh growth medium supplemented with serum but without

antibiotics. DNA concentrations of both the inducible pcDNA4/TO (containing genes encoding for ER chaperones) and the regulatory pcDNA6/TR plasmid (expressing the tetracycline repressor) were measured by Nanodrop 2000 and were diluted in optiMEM in 1:6 (w/w) ratio. For each well of a 96-well plate, 12.5 µl aliquots of diluted DNA were mixed with the same volume of optiMEM containing Lipofectamine 2000 reagent. After incubating the cells for 20 hrs, the transfection solution was replaced with complete culture medium to allow cell recovery for 24 hrs. Tetracycline was then added to the medium at concentrations ranging from 0 to 1.5 µg/ml every 24 hrs. Lysosomal GC activity was measured after 24, 48, and 72 hrs.

5.6. qRT-PCR and Xbp-1 splicing analysis

Quantitative RT-PCR was performed as following: 7×10^4 cells were plated in each well of a 24-well plate and incubated overnight before addition of small molecules to the culture medium. After 24 hrs of incubation with small molecules, cells were washed, collected in PBS and centrifuged at 200 *g* for 5 min. Following removal of the supernatant, cell pellet was resuspended in 5 µl Silver buffer provided in the RNAGEM™ reagent kit (ZyGEM). 1 µl of RNAGEM was added to each centrifuge tube and water was filled to a final volume of 50 µl. Total mRNA was extracted by incubating samples at 75 ℃ for 10 min. cDNA was synthesized by adding 4 µl qScript™ cDNA SuperMix reagent (Quanta Biosciences) to 16 µl of total RNA. The resulting solution was incubated first at 42 ℃ for 30 min and subsequently at 85 ℃ for 5 min in a thermal cycler. Total cDNA amount was measured by NanoDrop 2000 (Thermo Scientific) and diluted to 200 ng/µl.

Each quantitative RT-PCR reaction was prepared with 5 μl of total cDNA, 10 μl of PerfeCTa™ SYBR Green FastMix™ (Quanta Biosciences), 2 μl of 10 μM primer solution (Table 5.4), and 3 μl of deionized water. qRT-PCR was performed using the CFX96™ Real-Time PCR detection system (Bio-Rad). Samples were heated for 2 min at 95 ℃ and amplified in 45 cycles of 1 s at 95 ℃, 30 s at 60 ℃, and 30 s at 72 ℃. Analyses were conducted using CFX manager software (Bio-Rad) and the threshold cycle (C_T) was extracted from the PCR amplification plot. The ΔC_T value was calculated to describe the difference between the C_T of a target gene and the C_T of the housekeeping gene, GAPDH: $\Delta C_T = C_T$ (target gene) - C_T (GAPDH). The relative mRNA expression level of each target gene in treated cells was normalized to that measured in untreated cells: relative mRNA expression level = 2 exp [-(ΔC_T (treated cells) - ΔC_T (untreated cells))]. Each data point was evaluated in triplicate and measured three times.

RT-PCR analysis of Xbp-1 splicing was performed using total cDNA at 200 ng/μl concentration. Taq DNA polymerase and the Xbp-1 primers listed in Table 5.4 were used for the reverse transcription reactions. PCR products were separated on a 2.5% agarose gel. Spliced Xbp-1 bands were quantified using the NIH ImageJ analysis software.

5.7. Endoglycosidase H treatment

10^6 cells were plated in a 10 cm^2 cell culture dish and incubated overnight at 37 ℃. Following treatment with small molecules for 48 hrs, cells were collected and lysed with the complete lysis-M buffer supplemented with the protease inhibitor cocktail (Roche). Total protein concentrations were determined by Bradford assay, and each

sample was diluted to the same protein concentration. Endoglycosidase H (EndoH) treatment was performed by heating 9 µl of total protein content with 1 µl glycoprotein denaturing buffer (New England Biolabs) at 95 ℃ for 10 min, followed by incubation with 2 µl EndoH enzyme (New England Biolabs) at 37 ℃ for 1 hr. Aliquots of cell lysates were separated by 10% SDS-PAGE gel, and analyzed by Western blot.

5.8. Western blot analyses

Western blot analyses were performed using primary antibodies (rabbit anti-BiP, and mouse anti-CRT (Stressgen), mouse anti-CNX, and rabbit anti-Glucocerebrosidase (Sigma-Aldrich), or rabbit anti-GAPDH (Santa Cruz Biotechnology)) and appropriate secondary antibodies (HRP-conjugated goat anti-rabbit (Santa Cruz Biotechnology) or goat anti-mouse IgG (Stressgen)). Blots were visualized using SuperSignal West Femto Maximum (Pierce) and quantified by NIH ImageJ processing and analysis software.

5.9. Immunofluorescence microscopy

Glass coverslips were sterilized in 70% ethanol solution under UV radiation overnight. Coverslips were washed with PBS three times and placed in each well of a 6-well plate. In order to achieve better cell attachment, 500 µl aliquots of 100 µM poly-l-lysine solution were added on top of each coverslip and coverslips were incubated for 2 hrs at room temperature. After aspirating the poly-l-lysine solution, 10^5 cells in 2 ml

culture medium were seeded in each well and plates were incubated overnight. Cells were cultured in the presence of small molecules for 48 hrs, and fixed with 4% paraformaldehyde for 30 min. Following permeabilization with 0.1% Triton-X for 5 min, cells were incubated with 8% BSA/PBS for 1 hr. Primary antibodies diluted in 1% BSA/PBS were added to the cells and plates were incubated for 1 hr (rabbit anti-Glucocerebrosidase, and mouse anti-CNX (Sigma-Aldrich), or mouse anti-GM130 (BD Biosciences)). Upon washing three times with 0.1% Tween-20/PBS, cells were incubated with secondary antibodies for 1 hr (Dylight 488 goat anti-mouse IgG and Dylight 549 goat anti-rabbit IgG from KPL, and FITC anti-LAMP1 from Biolegend). After washing with 0.1% Tween-20/PBS for three times, coverslips were taken out from the plate and placed upside down on a new coverglass. Immunofluorescence images were obtained using an Olympus IX81 confocal microscope and analyzed using the Fluoview software. Co-localization heatmap images were analyzed using NIH ImageJ analysis software.

5.10. Subcellular fractionation

Subcellular fractionations were conducted as previously described (Ishii et al., 2007). Briefly, 10^6 cells were plated in a 10 cm^2 culture dish and incubated overnight for cell attachment. Cells were incubated with small molecules for 48 hrs, collected and centrifuged at 1,000 rpm for 5 min. Cell pellets were resuspended in sucrose buffer (0.25 M sucrose, 10 mM Hepes, and 1 mM EDTA, pH 7.4) on ice. Cells were homogenized with a Potter-Elvehjem Teflon-glass homogenizer and centrifuged at 1,000 *g* for 5 min. 1 ml of the supernatant was layered on top of a 40% Percoll solution in sucrose buffer

(9ml) and centrifuged at 25,000 *g* for 1 hr. Cell homogenates were collected into 8 fractions from the top of the centrifuge tube and used for GC enzymatic assay.

5.11. Immunocytochemistry studies

2×10^5 cells were seeded in each well of a 6-well plate and incubated overnight at 37 ℃. Cells were transfected with both the inducible pcDNA4/TO plasmid (containing genes encoding ER chaperones) and the regulatory pcDNA6/TR plasmid (constitutively expressing the tetracycline repressor) as described in Chapter 5.5. Chaperone expression was induced with 0.2 μg/ml tetracycline every 24 hrs for 48 hrs. Cells were collected and lysed with the complete lysis-M buffer containing a protease inhibitor cocktail (Roche). Total protein concentrations were determined by Bradford assay (Pierce), and each sample was diluted to the same protein concentration. Because a Myc tag was fused to the C-terminus of BiP, CNX, CRT and GRP94, ELISA experiments were conducted using an anti-Myc antibody to capture only recombinantly expressed proteins, and chaperone-specific antibodies were used for detection. 96-well ELISA plates were coated with 100 μl/well of 1 μg/ml capturing Myc tag antibody (Abcam) in 0.1 M sodium bicarbonate. Following overnight incubation at 4 ℃, plates were washed three times with 0.1% Tween-20/PBS, and incubated overnight with 200 μl/well of blocking buffer containing 0.01 g/ml BSA in PBS at 4 ℃. Plates were washed with 0.1% Tween-20/PBS again and 100 μl of PBS containing 1 mg/ml BSA was added to each well. 100 μl of antigen solution were added to first column of wells in a 96-well plate and serial dilutions were obtained by transferring 100 μl across the plate. Negative controls were included

and consisted of samples that did not contain antigen solution. Plates were incubated for 4 hrs at room temperature. Upon washing three times with 0.1% Tween-20/PBS, plates were incubated for 2 hours at room temperature with primary antibodies (rabbit anti-BiP, rabbit anti-CNX, and mouse anti-CRT (Stressgen), rabbit anti-GRP94 (Santa Cruz Biotechnology)), and subsequently with secondary antibodies (HRP conjugated goat anti-rabbit (Santa Cruz Biotechnology) or goat anti-mouse IgG (Stressgen)) for 1 hour. TMB substrate reagent was used to detect antibody binding according to the manufacturer's procedures.

5.12. Cytoplasmic [Ca^{2+}] measurement

Fura-2, AM was used to measure cytosolic [Ca^{2+}] according to the company's instructions (Anaspec). Briefly, 10^4 cells were plated in each well of a 96-well plate and incubated overnight to allow cell attachment. Ca^{2+} blockers were added to the culture medium of different samples and incubated for 5, 10, 20, 40 and 60 min respectively. Cells were washed twice with PBS and incubated with 30 µl of Ca^{2+} and Mg^{2+}-free PBS containing 5 µM Fura-2, AM and 0.05% (w/v) Pluronic F-127 (Invitrogen) at 37 ℃ for 30 min. Following additional washing steps, fluorescence was measured using excitation at 340 nm and 380 nm and emission at 510 nm with a TECAN Infinite M1000 fluorescence plate reader. Fluorescence ratio of excitation at 340 and 380 nm reflects relative intracellular Ca^{2+} level. Each data point was the average of at least 6 replicates.

5.13. mRNA chip analysis

7×10^4 cells were plated in each well of a 24-well plate and treated with small molecules for 24 hrs at 37 ℃ before total RNA was extracted. 200 ng of total RNA was amplified and purified using Illumina TotalPrep RNA Amplification Kit (Ambion) following kit instructions. Briefly, the first strand cDNA was synthesized by incubating RNA with T7 oligo (dT) primer and reverse transcriptase mix at 42 ℃ for 2 hours. RNase H and the DNA polymerase master mix were added into the reaction mix immediately following reverse transcription and reactions were incubated for 2 hours at 16 ℃ to synthesize the second strand of cDNA. RNA, primers, enzymes and salts that would inhibit *in vitro* transcription were removed through cDNA filter cartridges (provided with the amplification kit). Following *in vitro* transcription, biotinylated cRNA was synthesized by 14-hour amplification with dNTP mix containing biotin-dUTP and T7 RNA polymerase. Amplified cRNA was subsequently purified, and concentration was measured by NanoDrop ND-1000 Spectrophotometer (NanoDrop Technologies). An aliquot of 750 nanograms of amplified products was loaded onto Illumina Sentrix Beadchip Array Human-8 arrays, hybridized at 58 ℃ in an Illumina Hybridization Oven (Illumina) for 17 hours, washed and incubated with streptavidin-Cy3 to detect biotin-labeled cRNA on the arrays. Arrays were dried and scanned with BeadArray Reader (Illumina). The data was analyzed using BeadStudio software (Illumina). Clustering and pathway analysis were performed with GenomeStudio and Ingenuity Pathway Analysis (Ingenuity Systems, Inc.) software, respectively.

5.14. Cell toxicity assay

2×10^5 cells were seeded in each well of a 6-well plate and cultured with small molecules for 16 hrs at 37 ℃. Cells were collected and centrifuged at 200 *g* for 5 min. Cell pellets were resuspended in 100 μl binding buffer provided with CytoGLO™ Annexin V-FITC Apoptosis Detection Kit (IMGENEX). 5 μl aliquots of both Annexin V-FITC reagent and Propidium Iodide (PI) solution were added to each sample and incubated in the dark for 20 min. Cell toxicity were analyzed by flow cytometry (FACSCantoTM II, Beckon Dickingson) with a 488-nm Argon laser. Fluorescence intensities of both Annexin V-FITC and PI in each sample were evaluated and compared to the values obtained from untreated cells. A total number of 10,000 cells were counted, and the number of cells that bind to Annexin V-FITC or PI in treated cells was compared to that of untreated cells.

5.15. Statistical analysis

All data is presented as mean ± s.d., and statistical significance was calculated using a two-tailed *t*-test.

Chapter 6

Conclusions

In this work, we reported a number of cell and protein engineering strategies to restore the folding and activity of unstable, degradation-prone lysosomal enzymes associated with the development of lysosomal storage disorders (LSDs). The overarching goal was to modulate endogenous pathways underlying management of protein folding to enhance the innate cellular folding capacity. Specifically, we focused on reprogramming the ER folding quality control (QC) system to promote the native folding of mutated enzymes processed through the secretory pathway. The outcomes of this study include the design of chemical and genetic approaches to rescue the native folding of mutated, degradation-prone lysosomal enzymes. In addition, mechanistic studies were conducted to identify rate-limiting steps in the processing of these unstable protein variants that could be targeted for therapeutic applications.

Gaucher's disease (GD), the most common LSD, was used as a model system in this work. Currently, enzyme replacement therapy is available for most GD patients, but

this method fails to treat several affected areas, particularly the skeleton and the brain (Wraith, 2006). Bone marrow transplantation, although rarely performed, can reverse non-neurological aspects (Hoogerbrugge et al., 1995), but is not effective for the brain damage that occurs in the most severe cases of GD. Small molecule based oral treatments present a number of advantages over protein therapy, particularly for conditions requiring lifelong care management. Inhibitors of glucosylceramide synthesis are available for the treatment of GD patients with moderate clinical manifestations for which enzyme replacement therapy is not an option (Ficicioglu, 2008). Chemical chaperones, small molecules that rescue native folding of mutated GC enabling lysosomal trafficking and activity (Sawkar et al., 2006b), provide a promising alternative, but they are highly mutation-specific (Sawkar et al., 2005) and rarely proved effective to rescue glucocerebrosidase variants associated with neuronopathic manifestations of the disease (Khanna et al., 2010). Thus, therapeutic solutions for neuronopathic GD as well as other LSDs are still an urgent medical need. The L444P GC allele is a severely destabilized mutant always associated with neuronopathic symptoms in homozygous patients. We used fibroblasts derived from patients carrying L444P GC allele to develop strategies to restore the folding and activity of mutated GC variant.

Modulation of proteostasis modulation to enhance the cellular folding capacity was previously explored as a strategy to rescue the folding and lysosomal activity of destabilized GC variants in cells derived from patients with neuronopathic GD (Mu et al., 2008b). This strategy is based on the use of small molecules that modulate the composition of the proteostasis network and remodel cellular folding pathways. Owing to

their non-substrate-specific mechanisms, these regulators were shown to restore the activity of different enzymes associated with distinct LSDs (Mu et al., 2008b).

We first investigated strategies to modulate intracellular Ca^{2+} homeostasis. The accumulation of GC substrate glucosylceramide depletes Ca^{2+} storage in the ER through ryanodine receptors. Since $[Ca^{2+}]_{ER}$ affects ER chaperone expression and activity, we hypothesized that the depletion of $[Ca^{2+}]_{ER}$ hampers the folding of unstable GC variants. Thus, we used RyR blockers to restore Ca^{2+} homeostasis in GD patient-derived fibroblasts. We demonstrated that modulation of $[Ca^{2+}]_{ER}$ through RyRs inhibition in L444P GC fibroblasts re-establishes an ER folding environment more amenable to proteostasis regulation. Particularly, we found that the ER luminal chaperone BiP plays an important role in promoting the folding of mutated GC variants.

In order to identify small molecule Ca^{2+} channel blockers that restore intracellular Ca^{2+} homeostasis more efficiently than RyR blockers, we investigated cell treatment with LTCC blockers and identified their effect on mutated GC folding rescue. We used a number of LTCC blockers and found that treatment of fibroblasts derived from GD patients with lacidipine, an LTCC blocker that antagonizes Ca^{2+} mobilization through LTCC and RyRs (Gunther et al., 2008; Wishart et al., 2008), results in enhanced folding, trafficking and activity of mutated GC variants. Particularly, we demonstrated that lacidipine functions as a proteostasis regulator in patient-derived GD fibroblasts and rescues L444P GC folding with considerably higher efficiency than any other Ca^{2+} channel blocker reported before (Mu et al., 2008a; Ong et al., 2010; Wang et al., 2011a). We showed that lacidipine functions by i) lowering cytoplasmic $[Ca^{2+}]$, ii) remodeling the expression of ER chaperone and the unfolded protein response (UPR), and iii)

reducing cellular toxicity and apoptosis induction. Interestingly, the mechanism of action of lacidipine is significantly different from that activated by small molecules previously reported to function as proteostasis modulators (Mu et al., 2008b; Wang et al., 2011a).

Mechanistic studies conducted to investigate changes in the cellular folding network induced by treatment with proteostasis modulators also suggested that augmenting the pool of mutated GC in the ER via upregulation of the GC encoding gene is critical to promote its folding and trafficking (Wang et al., 2011a; Wang et al., 2011b). We hypothesized that enhancing ER retention and preventing ERAD of GC misfolding intermediates would lead to increasing the pool of GC folding intermediates that is amenable to folding rescue. To test this hypothesis, we treated fibroblasts derived from GD patients with small molecules that interfere with recognition or retrotranslocation of misfolded substrates. The generality of this approach was demonstrated by treating Tay-Sachs disease cells with an ERAD inhibitor to rescue the folding of mutated HexA. The different mechanisms of ERAD inhibition investigated were shown to enhance ER retention of mutated proteins, but were associated with dramatically different levels of ER stress, unfolded protein response (UPR) activation and UPR-induced apoptosis. Therefore, molecular targets of ERAD inhibition need to be carefully selected to prevent the disruption of functioning of the folding quality control system.

Furthermore, we proved that restoring Ca^{2+} homeostasis in GD cells creates a folding environment particularly amenable to mutated GC folding rescue via ERAD inhibition. Specifically, we remodeled the proteostasis network to simultaneously increase ER retention of unstable GC variants by inhibiting retrotranslocation and ERAD degradation and to enhance chaperone-mediated folding by restoring Ca^{2+} homeostasis.

We showed that this approach results in significantly higher rescue in the folding and activity of L444P GC than either approach applied individually. We also demonstrated that lacidipine treatment lowers EerI-mediated UPR induction and apoptosis through the upregulation of the anti-apoptotic gene Bcl-2, which plays a key role in preventing cytotoxicity that may result from modulation of the proteostasis network.

Chapter 7

Recommendations for further studies

In this work, we presented strategies to modulate the proteostasis network in fibroblasts derived from patients with LSD and restore the folding of mutated, degradation-prone lysoosomal enzyme variants. This study enabled the identification of endogenous proteins that influence the folding of unstable lysosomal enzymes and that could be targeted for therapeutic intervention in the development of treatments for multiple LSDs.

We identified a number of folding modulators that mediate significant increase in GC activity in fibroblasts derived from patients with GD. Some of these small molecules restore the folding and activity of GC mutants at the cost of cell apoptosis, whereas others enhance GC activity without causing cytotoxicity. Among the non-toxic proteostasis modulators, we reported the LTCC blocker lacidipine, which is an FDA approaved drug for the treatment of hypertension. Testing the function of lacidipine in mouse models of

GD will allow establishing its therapeutic potential and, particularly, its ability to ameliorate neuronopathic symptoms.

We also reported clear evidence that BiP upregulation is critically involved in the folding of GC mutants. Since GC folding and lysosomal trafficking is a multi-step process and is closely regulated by numerous enzymes of the proteostasis network, we expect that other endogenous proteins might affect the folding and activity of GC mutants. We recommend conducting a genetic screen for the isolation of genes that enhance folding of mutated GC variants. Optimization of the enzymatic assay currently available to measure GC activity, which is characterized by a narrow signal window, will be necessary to adapt it for high throughput applications.

References

Agmon, V., Cherbu, S., Dagan, A., Grace, M., Grabowski, G.A., and Gatt, S. (1993). Synthesis and use of novel fluorescent glycosphingolipids for estimating beta-glucosidase activity in vitro in the absence of detergents and subtyping Gaucher disease variants following administration into intact cells. Biochimica et Biophysica Acta *1170*, 72-79.

Alberts, B., Johnson, A., Lewis, J., Raff, M., Roberts, K., and Walters, P. (2002). The Shape and Structure of Proteins. Molecular Biology of the Cell; Fourth Edition *New York and London: Garland Science*.

Altarescu, G., Hill, S., Wiggs, E., Jeffries, N., Kreps, C., Parker, C.C., Brady, R.O., Barton, N.W., and Schiffmann, R. (2001). The efficacy of enzyme replacement therapy in patients with chronic neuronopathic Gaucher's disease. The Journal of Pediatrics *138*, 539-547.

Anfinsen, C.B. (1973). Principles that govern the folding of protein chains. Science *181*, 223-230.

Anfinsen, C.B., Haber, E., Sela, M., and White, F.H., Jr. (1961). The kinetics of formation of native ribonuclease during oxidation of the reduced polypeptide chain. Proceedings of the National Academy of Sciences of the United States of America *47*, 1309-1314.

Arvan, P., Zhao, X., Ramos-Castaneda, J., and Chang, A. (2002). Secretory pathway quality control operating in Golgi, plasmalemmal, and endosomal systems. Traffic *3*, 771-780.

Avezov, E., Frenkel, Z., Ehrlich, M., Herscovics, A., and Lederkremer, G.Z. (2008). Endoplasmic reticulum (ER) mannosidase I is compartmentalized and required for N-glycan trimming to Man5-6GlcNAc2 in glycoprotein ER-associated degradation. Molecular Biology of the Cell *19*, 216-225.

Awasthi, N., and Wagner, B.J. (2005). Upregulation of heat shock protein expression by proteasome inhibition: an antiapoptotic mechanism in the lens. Investigative Ophthalmology & Visual Science *46*, 2082-2091.

Balch, W.E., Morimoto, R.I., Dillin, A., and Kelly, J.W. (2008). Adapting proteostasis for disease intervention. Science *319*, 916-919.

Baumann, O., and Walz, B. (2001). Endoplasmic reticulum of animal cells and its organization into structural and functional domains. International Review of Cytology *205*, 149-214.

Bence, N.F., Sampat, R.M., and Kopito, R.R. (2001). Impairment of the ubiquitin-proteasome system by protein aggregation. Science *292*, 1552-1555.

Beutler, E. (2004). Enzyme replacement in Gaucher disease. PLoS Medicine *1*, e21.

Beutler, E., Kuhl, W., and Sorge, J. (1984). Cross-reacting material in Gaucher disease fibroblasts. Proceedings of the National Academy of Sciences of the United States of America *81*, 6506-6510.

Beutler, E., Nguyen, N.J., Henneberger, M.W., Smolec, J.M., McPherson, R.A., West, C., and Gelbart, T. (1993). Gaucher disease: gene frequencies in the Ashkenazi Jewish population. American Journal of Human Genetics *52*, 85-88.

Bodamer, O.A., and Hung, C. (2010). Laboratory and genetic evaluation of Gaucher disease. Wiener medizinische Wochenschrift *160*:600-4.

Brostrom, M.A., and Brostrom, C.O. (2003). Calcium dynamics and endoplasmic reticular function in the regulation of protein synthesis: implications for cell growth and adaptability. Cell Calcium *34*, 345-363.

Brown, C.R., Hong-Brown, L.Q., Biwersi, J., Verkman, A.S., and Welch, W.J. (1996). Chemical chaperones correct the mutant phenotype of the delta F508 cystic fibrosis transmembrane conductance regulator protein. Cell Stress Chaperones *1*, 117-125.

Brumshtein, B., Greenblatt, H.M., Butters, T.D., Shaaltiel, Y., Aviezer, D., Silman, I., Futerman, A.H., and Sussman, J.L. (2007). Crystal structures of complexes of N-butyl- and N-nonyl-deoxynojirimycin bound to acid beta-glucosidase: insights into the mechanism of chemical chaperone action in Gaucher disease. The Journal of Biological Chemistry *282*, 29052-29058.

Buccoliero, R., Bodennec, J., and Futerman, A.H. (2002). The role of sphingolipids in neuronal development: lessons from models of sphingolipid storage diseases. Neurochemical Research *27*, 565-574.

Buck, E., Zimanyi, I., Abramson, J.J., and Pessah, I.N. (1992). Ryanodine stabilizes multiple conformational states of the skeletal muscle calcium release channel. The Journal of Biological Chemistry *267*, 23560-23567.

Bukau, B., Weissman, J., and Horwich, A. (2006). Molecular chaperones and protein quality control. Cell *125*, 443-451.

Bush, K.T., Goldberg, A.L., and Nigam, S.K. (1997). Proteasome inhibition leads to a heat-shock response, induction of endoplasmic reticulum chaperones, and thermotolerance. The Journal of Biological Chemistry *272*, 9086-9092.

Chao, C.C., and Lin-Chao, S. (1992). A direct-repeat sequence of the human BiP gene is required for A23187-mediated inducibility and an inducible nuclear factor binding. Nucleic Acids Research *20*, 6481-6485.

Chen, L.H., Jiang, C.C., Kiejda, K.A., Wang, Y.F., Thorne, R.F., Zhang, X.D., and Hersey, P. (2007). Thapsigargin sensitizes human melanoma cells to TRAIL-induced apoptosis by up-regulation of TRAIL-R2 through the unfolded protein response. Carcinogenesis *28*, 2328-2336.

Chipuk, J.E., Moldoveanu, T., Llambi, F., Parsons, M.J., and Green, D.R. (2010). The BCL-2 family reunion. Molecular Cell *37*, 299-310.

Cox, T., Lachmann, R., Hollak, C., Aerts, J., van Weely, S., Hrebicek, M., Platt, F., Butters, T., Dwek, R., Moyses, C., *et al.* (2000). Novel oral treatment of Gaucher's disease with N-butyldeoxynojirimycin (OGT 918) to decrease substrate biosynthesis. Lancet *355*, 1481-1485.

Cox, T.M., Aerts, J.M., Andria, G., Beck, M., Belmatoug, N., Bembi, B., Chertkoff, R., Vom Dahl, S., Elstein, D., Erikson, A., *et al.* (2003). The role of the iminosugar N-butyldeoxynojirimycin (miglustat) in the management of type I (non-neuronopathic) Gaucher disease: a position statement. Journal of Inherited Metabolic Disease *26*, 513-526.

Daniel, C.J., Conti, B., Johnson, A.E., and Skach, W.R. (2008). Control of translocation through the Sec61 translocon by nascent polypeptide structure within the ribosome. The Journal of Biological Chemistry *283*, 20864-20873.

Desnick, R.J., and Schuchman, E.H. (2002). Enzyme replacement and enhancement therapies: lessons from lysosomal disorders. Nature Reviews Genetics *3*, 954-966.

Dobson, C.M. (1999). Protein misfolding, evolution and disease. Trends in Biochemical Sciences *24*, 329-332.

Dobson, C.M. (2003). Protein folding and misfolding. Nature *426*, 884-890.

Dorner, A.J., and Kaufman, R.J. (1994). The levels of endoplasmic reticulum proteins and ATP affect folding and secretion of selective proteins. Biologicals *22*, 103-112.

Dorner, A.J., Wasley, L.C., and Kaufman, R.J. (1992). Overexpression of GRP78 mitigates stress induction of glucose regulated proteins and blocks secretion of selective proteins in Chinese hamster ovary cells. The EMBO Journal *11*, 1563-1571.

Drummond, I.A., Lee, A.S., Resendez, E., Jr., and Steinhardt, R.A. (1987). Depletion of intracellular calcium stores by calcium ionophore A23187 induces the genes for glucose-regulated proteins in hamster fibroblasts. The Journal of Biological Chemistry *262*, 12801-12805.

Duksin, D., and Bornstein, P. (1977). Changes in surface properties of normal and transformed cells caused by tunicamycin, an inhibitor of protein glycosylation. Proceedings of the National Academy of Sciences of the United States of America *74*, 3433-3437.

Dvir, H., Harel, M., McCarthy, A.A., Toker, L., Silman, I., Futerman, A.H., and Sussman, J.L. (2003). X-ray structure of human acid-beta-glucosidase, the defective enzyme in Gaucher disease. EMBO Reports *4*, 704-709.

Eckenrode, E.F., Yang, J., Velmurugan, G.V., Foskett, J.K., and White, C. (2010). Apoptosis protection by Mcl-1 and Bcl-2 modulation of inositol 1,4,5-trisphosphate receptor-dependent Ca2+ signaling. The Journal of Biological Chemistry *285*, 13678-13684.

Ellgaard, L., Molinari, M., and Helenius, A. (1999). Setting the standards: quality control in the secretory pathway. Science *286*, 1882-1888.

Ellis, R.J., and Hartl, F.U. (1999). Principles of protein folding in the cellular environment. Current Opinions in Structural Biology *9*, 102-110.

Epstein, M. (1999). Role of a third generation calcium antagonist in the management of hypertension. Drugs *57 Suppl 1*, 1-10.

Epstein, S., Kirkpatrick, C.L., Castillon, G.A., Muniz, M., Riezman, I., David, F.P., Wollheim, C.B., and Riezman, H. (2012). Activation of the unfolded protein response pathway causes ceramide accumulation in yeast and INS-1E insulinoma cells. Journal of Lipid Research *53*, 412-420.

Fagioli, C., and Sitia, R. (2001). Glycoprotein quality control in the endoplasmic reticulum. Mannose trimming by endoplasmic reticulum mannosidase I times the proteasomal degradation of unassembled immunoglobulin subunits. The Journal of Biological Chemistry *276*, 12885-12892.

Fan, J.Q. (2003). A contradictory treatment for lysosomal storage disorders: inhibitors enhance mutant enzyme activity. Trends in Pharmacological Sciences *24*, 355-360.

Ficicioglu, C. (2008). Review of miglustat for clinical management in Gaucher disease type 1. Therapeutics and Clinical Risk Management *4*, 425-431.

Fiebiger, E., Hirsch, C., Vyas, J.M., Gordon, E., Ploegh, H.L., and Tortorella, D. (2004). Dissection of the dislocation pathway for type I membrane proteins with a new small molecule inhibitor, eeyarestatin. Molecular Biology of the Cell *15*, 1635-1646.

Fill, M., and Copello, J.A. (2002). Ryanodine receptor calcium release channels. Physiological Reviews *82*, 893-922.

Fink, A.L. (1999). Chaperone-mediated protein folding. Physiological Reviews *79*, 425-449.

Futami, T., Miyagishi, M., and Taira, K. (2005). Identification of a network involved in thapsigargin-induced apoptosis using a library of small interfering RNA expression vectors. The Journal of Biological Chemistry *280*, 826-831.

Futerman, A.H., and Pagano, R.E. (1991). Determination of the intracellular sites and topology of glucosylceramide synthesis in rat liver. The Biochemical Journal *280*, 295-302.

Futerman, A.H., Sussman, J.L., Horowitz, M., Silman, I., and Zimran, A. (2004). New directions in the treatment of Gaucher disease. Trends in Pharmacological Sciences *25*, 147-151.

Futerman, A.H., and van Meer, G. (2004). The cell biology of lysosomal storage disorders. Nature Reviews *5*, 554-565.

Gilis, D., and Rooman, M. (2000). PoPMuSiC, an algorithm for predicting protein mutant stability changes: application to prion proteins. Protein Engineering *13*, 849-856.

Ginzburg, L., and Futerman, A.H. (2005). Defective calcium homeostasis in the cerebellum in a mouse model of Niemann-Pick A disease. Journal of Neurochemistry *95*, 1619-1628.

Gorbatyuk, M.S., Knox, T., LaVail, M.M., Gorbatyuk, O.S., Noorwez, S.M., Hauswirth, W.W., Lin, J.H., Muzyczka, N., and Lewin, A.S. (2010). Restoration of visual function in P23H rhodopsin transgenic rats by gene delivery of BiP/Grp78. Proceedings of the National Academy of Sciences of the United States of America *107*, 5961-5966.

Grabowski, G.A. (1997). Gaucher disease: gene frequencies and genotype/phenotype correlations. Genetic Testing *1*, 5-12.

Grace, M.E., Newman, K.M., Scheinker, V., Berg-Fussman, A., and Grabowski, G.A. (1994). Analysis of human acid beta-glucosidase by site-directed mutagenesis and heterologous expression. The Journal of Biological Chemistry *269*, 2283-2291.

Griffiths, G., Hoflack, B., Simons, K., Mellman, I., and Kornfeld, S. (1988). The mannose 6-phosphate receptor and the biogenesis of lysosomes. Cell *52*, 329-341.

Griffiths, G., and Simons, K. (1986). The trans Golgi network: sorting at the exit site of the Golgi complex. Science *234*, 438-443.

Gunther, S., Kuhn, M., Dunkel, M., Campillos, M., Senger, C., Petsalaki, E., Ahmed, J., Urdiales, E.G., Gewiess, A., Jensen, L.J., *et al.* (2008). SuperTarget and Matador: resources for exploring drug-target relationships. Nucleic Acids Research *36*, 919-922.

Gupta, S., Deepti, A., Deegan, S., Lisbona, F., Hetz, C., and Samali, A. (2010). HSP72 protects cells from ER stress-induced apoptosis via enhancement of IRE1alpha-XBP1 signaling through a physical interaction. PLoS Biology *8*, e1000410.

Hammond, C., and Helenius, A. (1995). Quality control in the secretory pathway. Current Opinion in Cell Biology *7*, 523-529.

Hampton, R.Y. (2000). ER stress response: getting the UPR hand on misfolded proteins. Current Biology *10*, R518-521.

Hartl, F.U., Bracher, A., and Hayer-Hartl, M. (2011). Molecular chaperones in protein folding and proteostasis. Nature *475*, 324-332.

Helip-Wooley, A., and Thoene, J.G. (2004). Sucrose-induced vacuolation results in increased expression of cholesterol biosynthesis and lysosomal genes. Experimenal Cell Research *292*, 89-100.

Hochstrasser, M. (1996). Ubiquitin-dependent protein degradation. Annual Review of Genetics *30*, 405-439.

Hockerman, G.H., Peterson, B.Z., Johnson, B.D., and Catterall, W.A. (1997). Molecular determinants of drug binding and action on L-type calcium channels. Annual Review of Pharmacology and Toxicology *37*, 361-396.

Hoogerbrugge, P.M., Brouwer, O.F., Bordigoni, P., Ringden, O., Kapaun, P., Ortega, J.J., O'Meara, A., Cornu, G., Souillet, G., Frappaz, D., *et al.* (1995). Allogeneic bone marrow transplantation for lysosomal storage diseases. The European Group for Bone Marrow Transplantation. Lancet *345*, 1398-1402.

Hosokawa, N., Tremblay, L.O., You, Z., Herscovics, A., Wada, I., and Nagata, K. (2003). Enhancement of endoplasmic reticulum (ER) degradation of misfolded Null

Hong Kong alpha1-antitrypsin by human ER mannosidase I. The Journal of Biological Chemistry *278*, 26287-26294.

Hruska, K.S., LaMarca, M.E., Scott, C.R., and Sidransky, E. (2008). Gaucher disease: mutation and polymorphism spectrum in the glucocerebrosidase gene (GBA). Human Mutation *29*, 567-583.

Ishii, S., Chang, H.H., Kawasaki, K., Yasuda, K., Wu, H.L., Garman, S.C., and Fan, J.Q. (2007). Mutant alpha-galactosidase A enzymes identified in Fabry disease patients with residual enzyme activity: biochemical characterization and restoration of normal intracellular processing by 1-deoxygalactonojirimycin. The Biochemical Journal *406*, 285-295.

Jaenicke, R. (1991). Protein stability and molecular adaptation to extreme conditions. European Journal of Biochemistry *202*, 715-728.

Jeckel, D., Karrenbauer, A., Burger, K.N., van Meer, G., and Wieland, F. (1992). Glucosylceramide is synthesized at the cytosolic surface of various Golgi subfractions. The Journal of Cell Biology *117*, 259-267.

Jeyakumar, M., Butters, T.D., Dwek, R.A., and Platt, F.M. (2002). Glycosphingolipid lysosomal storage diseases: therapy and pathogenesis. Neuropathology and Applied Neurobiology *28*, 343-357.

Jin, T., Nakatani, H., Taguchi, T., Sonobe, H., Morimoto, N., Sugimoto, T., Akimori, T., Nakano, T., Namikawa, T., Okabayashi, T., Kobayashi, M. & Araki, K. (2006). Thapsigargin enhances cell death in the gastrointestinal stromal tumor cell line, GIST-T1, by treatment with Imatinib (Glivec). Journal of Health Science *52*, 110-117.

Jonsson, L.M., Murray, G.J., Sorrell, S.H., Strijland, A., Aerts, J.F., Ginns, E.I., Barranger, J.A., Tager, J.M., and Schram, A.W. (1987). Biosynthesis and maturation of glucocerebrosidase in Gaucher fibroblasts. European Journal of Biochemistry *164*, 171-179.

Kang, J.J., Hsu, K.S., and Lin-Shiau, S.Y. (1994). Effects of bipyridylium compounds on calcium release from triadic vesicles isolated from rabbit skeletal muscle. British Journal of Pharmacology *112*, 1216-1222.

Khanna, R., Benjamin, E.R., Pellegrino, L., Schilling, A., Rigat, B.A., Soska, R., Nafar, H., Ranes, B.E., Feng, J., Lun, Y., *et al.* (2010). The pharmacological chaperone isofagomine increases the activity of the Gaucher disease L444P mutant form of beta-glucosidase. FEBS Journal *277*, 1618-1638.

Kiefhaber, T., Rudolph, R., Kohler, H.H., and Buchner, J. (1991). Protein aggregation in vitro and in vivo: a quantitative model of the kinetic competition between folding and aggregation. Biotechnology *9*, 825-829.

Kitamura, M. (2008). Endoplasmic reticulum stress and unfolded protein response in renal pathophysiology: Janus faces. American Journal of Physiology-Renal Physiology *295*, 323-334.

Kleizen, B., and Braakman, I. (2004). Protein folding and quality control in the endoplasmic reticulum. Current Opinion in Cell Biology *16*, 343-349.

Kolter, T., Proia, R.L., and Sandhoff, K. (2002). Combinatorial ganglioside biosynthesis. The Journal of Biological Chemistry *277*, 25859-25862.

Korkotian, E., Schwarz, A., Pelled, D., Schwarzmann, G., Segal, M., and Futerman, A.H. (1999). Elevation of intracellular glucosylceramide levels results in an

increase in endoplasmic reticulum density and in functional calcium stores in cultured neurons. The Journal of Biological Chemistry *274*, 21673-21678.

Kornfeld, S., and Mellman, I. (1989). The biogenesis of lysosomes. Annual Review of Cell Biology *5*, 483-525.

Kwasigroch, J.M., Gilis, D., Dehouck, Y., and Rooman, M. (2002). PoPMuSiC, rationally designing point mutations in protein structures. Bioinformatics *18*, 1701-1702.

Lederkremer, G.Z., and Glickman, M.H. (2005). A window of opportunity: timing protein degradation by trimming of sugars and ubiquitins. Trends in Biochemical Sciences *30*, 297-303.

Lee, A.H., Iwakoshi, N.N., and Glimcher, L.H. (2003). XBP-1 regulates a subset of endoplasmic reticulum resident chaperone genes in the unfolded protein response. Molecular and Cellular Biology *23*, 7448-7459.

Lee, C.H., Poburko, D., Kuo, K.H., Seow, C.Y., and van Breemen, C. (2002). Ca(2+) oscillations, gradients, and homeostasis in vascular smooth muscle. American Journal of Physiology *282*, H1571-1583.

Lee, S., and Tsai, F.T. (2005). Molecular chaperones in protein quality control. Journal of Biochemistry and Molecular Biology *38*, 259-265.

Liao, W., Li, X., Mancini, M., and Chan, L. (2006). Proteasome inhibition induces differential heat shock protein response but not unfolded protein response in HepG2 cells. Journal of Cellular Biochemistry *99*, 1085-1095.

Lin, J.H., Li, H., Yasumura, D., Cohen, H.R., Zhang, C., Panning, B., Shokat, K.M., Lavail, M.M., and Walter, P. (2007). IRE1 signaling affects cell fate during the unfolded protein response. Science *318*, 944-949.

Lin, J.H., Li, H., Zhang, Y., Ron, D., and Walter, P. (2009). Divergent effects of PERK and IRE1 signaling on cell viability. PLoS ONE *4*, e4170.

Lindquist, S. (1986). The heat-shock response. Annual Review of Biochemistry *55*, 1151-1191.

Lloyd-Evans, E., Morgan, A.J., He, X., Smith, D.A., Elliot-Smith, E., Sillence, D.J., Churchill, G.C., Schuchman, E.H., Galione, A., and Platt, F.M. (2008). Niemann-Pick disease type C1 is a sphingosine storage disease that causes deregulation of lysosomal calcium. Nature Medicine *14*, 1247-1255.

Lloyd-Evans, E., Pelled, D., Riebeling, C., Bodennec, J., de-Morgan, A., Waller, H., Schiffmann, R., and Futerman, A.H. (2003). Glucosylceramide and glucosylsphingosine modulate calcium mobilization from brain microsomes via different mechanisms. The Journal of Biological Chemistry *278*, 23594-23599.

Lu, J., Chiang, J., Iyer, R.R., Thompson, E., Kaneski, C.R., Xu, D.S., Yang, C., Chen, M., Hodes, R.J., Lonser, R.R., *et al.* (2010). Decreased glucocerebrosidase activity in Gaucher disease parallels quantitative enzyme loss due to abnormal interaction with TCP1 and c-Cbl. Proceedings of the National Academy of Sciences of the United States of America *107*, 21665-21670.

Maegawa, G.H., Tropak, M., Buttner, J., Stockley, T., Kok, F., Clarke, J.T., and Mahuran, D.J. (2007). Pyrimethamine as a potential pharmacological chaperone for late-onset forms of GM2 gangliosidosis. The Journal of Biological Chemistry *282*, 9150-9161.

Maley, F., Trimble, R.B., Tarentino, A.L., and Plummer, T.H., Jr. (1989). Characterization of glycoproteins and their associated oligosaccharides through the use of endoglycosidases. Analytical Biochemistry *180*, 195-204.

Matovcik, L.M., Goodhouse, J., and Farquhar, M.G. (1990). The recycling itinerary of the 46 kDa mannose 6-phosphate receptor--Golgi to late endosomes--coincides with that of the 215 kDa M6PR. European Journal of Cell Biology *53*, 203-211.

McCullough, K.D., Martindale, J.L., Klotz, L.O., Aw, T.Y., and Holbrook, N.J. (2001). Gadd153 sensitizes cells to endoplasmic reticulum stress by down-regulating Bcl2 and perturbing the cellular redox state. Molecular and Cellular Biology *21*, 1249-1259.

Meivar-Levy, I., Horowitz, M., and Futerman, A.H. (1994). Analysis of glucocerebrosidase activity using N-(1-[14C]hexanoyl)-D-erythroglucosylsphingosine demonstrates a correlation between levels of residual enzyme activity and the type of Gaucher disease. The Biochemical Journal *303 (Pt 2)*, 377-382.

Meldolesi, J., and Pozzan, T. (1998). The endoplasmic reticulum Ca2+ store: a view from the lumen. Trends in Biochemical Sciences *23*, 10-14.

Michalak, M., Robert Parker, J.M., and Opas, M. (2002). Ca2+ signaling and calcium binding chaperones of the endoplasmic reticulum. Cell Calcium *32*, 269-278.

Michelakakis, H., Dimitriou, E., Van Weely, S., Boot, R.G., Mavridou, I., Verhoek, M., and Aerts, J.M. (1995). Characterization of glucocerebrosidase in Greek Gaucher disease patients: mutation analysis and biochemical studies. Journal of Inherited Metabolic Disease *18*, 609-615.

Morimoto, R.I., Kline, M.P., Bimston, D.N., and Cotto, J.J. (1997). The heat-shock response: regulation and function of heat-shock proteins and molecular chaperones. Essays Biochemistry *32*, 17-29.

Mu, T.W., Fowler, D.M., and Kelly, J.W. (2008a). Partial restoration of mutant enzyme homeostasis in three distinct lysosomal storage disease cell lines by altering calcium homeostasis. PLoS Biology *6*, e26.

Mu, T.W., Ong, D.S., Wang, Y.J., Balch, W.E., Yates, J.R., 3rd, Segatori, L., and Kelly, J.W. (2008b). Chemical and biological approaches synergize to ameliorate protein-folding diseases. Cell *134*, 769-781.

Muresan, Z., and Arvan, P. (1998). Enhanced binding to the molecular chaperone BiP slows thyroglobulin export from the endoplasmic reticulum. Molecular Endocrinology *12*, 458-467.

Nagasaki, K., and Fleischer, S. (1988). Ryanodine sensitivity of the calcium release channel of sarcoplasmic reticulum. Cell Calcium *9*, 1-7.

Nakatsukasa, K., and Brodsky, J.L. (2008). The recognition and retrotranslocation of misfolded proteins from the endoplasmic reticulum. Traffic *9*, 861-870.

Nishikawa, S., Brodsky, J.L., and Nakatsukasa, K. (2005). Roles of molecular chaperones in endoplasmic reticulum (ER) quality control and ER-associated degradation (ERAD). Journal of Biochemistry *137*, 551-555.

Nishikawa, S.I., Fewell, S.W., Kato, Y., Brodsky, J.L., and Endo, T. (2001). Molecular chaperones in the yeast endoplasmic reticulum maintain the solubility of proteins for retrotranslocation and degradation. The Journal of Cell Biology *153*, 1061-1070.

Offman, M.N., Krol, M., Silman, I., Sussman, J.L., and Futerman, A.H. (2010). Molecular Basis of Reduced Glucosylceramidase Activity in the Most Common Gaucher Disease Mutant, N370S. The Journal of Biological Chemistry *285*, 42105-42114.

Ong, D.S., Mu, T.W., Palmer, A.E., and Kelly, J.W. (2010). Endoplasmic reticulum Ca2+ increases enhance mutant glucocerebrosidase proteostasis. Nature Chemical Biology *6*, 424-432.

Oyadomari, S., and Mori, M. (2004). Roles of CHOP/GADD153 in endoplasmic reticulum stress. Cell Death and Differentiation *11*, 381-389.

Palmieri, M., Impey, S., Kang, H., di Ronza, A., Pelz, C., Sardiello, M., and Ballabio, A. (2011). Characterization of the CLEAR network reveals an integrated control of cellular clearance pathways. Human Molecular Genetics *20*, 3852-3866.

Pelled, D., Lloyd-Evans, E., Riebeling, C., Jeyakumar, M., Platt, F.M., and Futerman, A.H. (2003). Inhibition of calcium uptake via the sarco/endoplasmic reticulum Ca2+-ATPase in a mouse model of Sandhoff disease and prevention by treatment with N-butyldeoxynojirimycin. The Journal of Biological Chemistry *278*, 29496-29501.

Pelled, D., Trajkovic-Bodennec, S., Lloyd-Evans, E., Sidransky, E., Schiffmann, R., and Futerman, A.H. (2005). Enhanced calcium release in the acute neuronopathic form of Gaucher disease. Neurobiology of Disease *18*, 83-88.

Pepine, C. (1989). Nicardipine, a new calcium channel blocker: role for vascular selectivity. Clinical Cardiology *12*, 240-246.

Perkins, K.J., Byers, S., Yogalingam, G., Weber, B., and Hopwood, J.J. (1999). Expression and characterization of wild type and mutant recombinant human

sulfamidase. Implications for Sanfilippo (Mucopolysaccharidosis IIIA) syndrome. The Journal of Biological Chemistry *274*, 37193-37199.

Platt, F.M., Jeyakumar, M., Andersson, U., Priestman, D.A., Dwek, R.A., Butters, T.D., Cox, T.M., Lachmann, R.H., Hollak, C., Aerts, J.M., *et al.* (2001). Inhibition of substrate synthesis as a strategy for glycolipid lysosomal storage disease therapy. Journal of Inherited Metabolic Disease *24*, 275-290.

Powers, E.T., Morimoto, R.I., Dillin, A., Kelly, J.W., and Balch, W.E. (2009). Biological and chemical approaches to diseases of proteostasis deficiency. Annual Review of Biochemistry *78*, 959-991.

Putney, J.W., Jr., Broad, L.M., Braun, F.J., Lievremont, J.P., and Bird, G.S. (2001). Mechanisms of capacitative calcium entry. Journal of Cell Science *114*, 2223-2229.

Rapoport, T.A. (1992). Transport of proteins across the endoplasmic reticulum membrane. Science *258*, 931-936.

Ravid, T., and Hochstrasser, M. (2008). Diversity of degradation signals in the ubiquitin-proteasome system. Nature Reviews *9*, 679-690.

Reczek, D., Schwake, M., Schroder, J., Hughes, H., Blanz, J., Jin, X., Brondyk, W., Van Patten, S., Edmunds, T., and Saftig, P. (2007). LIMP-2 is a receptor for lysosomal mannose-6-phosphate-independent targeting of beta-glucocerebrosidase. Cell *131*, 770-783.

Rodriguez, D., Rojas-Rivera, D., and Hetz, C. (2010). Integrating stress signals at the endoplasmic reticulum: The BCL-2 protein family rheostat. Biochimica et Biophysica acta.

Ron, D., and Walter, P. (2007). Signal integration in the endoplasmic reticulum unfolded protein response. Nature Reviews *8*, 519-529.

Ron, I., and Horowitz, M. (2005). ER retention and degradation as the molecular basis underlying Gaucher disease heterogeneity. Human Molecular Genetics *14*, 2387-2398.

Rong, Y.P., Bultynck, G., Aromolaran, A.S., Zhong, F., Parys, J.B., De Smedt, H., Mignery, G.A., Roderick, H.L., Bootman, M.D., and Distelhorst, C.W. (2009). The BH4 domain of Bcl-2 inhibits ER calcium release and apoptosis by binding the regulatory and coupling domain of the IP3 receptor. Proceedings of the National Academy of Sciences of the United States of America *106*, 14397-14402.

Sardiello, M., Palmieri, M., di Ronza, A., Medina, D.L., Valenza, M., Gennarino, V.A., Di Malta, C., Donaudy, F., Embrione, V., Polishchuk, R.S., *et al.* (2009). A gene network regulating lysosomal biogenesis and function. Science *325*, 473-477.

Sawkar, A.R., Adamski-Werner, S.L., Cheng, W.C., Wong, C.H., Beutler, E., Zimmer, K.P., and Kelly, J.W. (2005). Gaucher disease-associated glucocerebrosidases show mutation-dependent chemical chaperoning profiles. Chemistry & Biology *12*, 1235-1244.

Sawkar, A.R., Cheng, W.C., Beutler, E., Wong, C.H., Balch, W.E., and Kelly, J.W. (2002). Chemical chaperones increase the cellular activity of N370S beta -glucosidase: a therapeutic strategy for Gaucher disease. Proceedings of the National Academy of Sciences of the United States of America *99*, 15428-15433.

Sawkar, A.R., D'Haeze, W., and Kelly, J.W. (2006a). Therapeutic strategies to ameliorate lysosomal storage disorders--a focus on Gaucher disease. Cellular and Molecular Life Sciences *63*, 1179-1192.

Sawkar, A.R., Schmitz, M., Zimmer, K.P., Reczek, D., Edmunds, T., Balch, W.E., and Kelly, J.W. (2006b). Chemical chaperones and permissive temperatures alter localization of Gaucher disease associated glucocerebrosidase variants. ACS Chemical Biology *1*, 235-251.

Schmitz, M., Alfalah, M., Aerts, J.M., Naim, H.Y., and Zimmer, K.P. (2005). Impaired trafficking of mutants of lysosomal glucocerebrosidase in Gaucher's disease. The International Journal of Biochemistry & Cell Biology *37*, 2310-2320.

Schroder, M., and Kaufman, R.J. (2005). The mammalian unfolded protein response. Annual Review of Biochemistry *74*, 739-789.

Schueler, U.H., Kolter, T., Kaneski, C.R., Zirzow, G.C., Sandhoff, K., and Brady, R.O. (2004). Correlation between enzyme activity and substrate storage in a cell culture model system for Gaucher disease. Journal of Inherited Metabolic Disease *27*, 649-658.

Scorrano, L., Oakes, S.A., Opferman, J.T., Cheng, E.H., Sorcinelli, M.D., Pozzan, T., and Korsmeyer, S.J. (2003). BAX and BAK regulation of endoplasmic reticulum Ca2+: a control point for apoptosis. Science *300*, 135-139.

Sun, Y., Liou, B., Quinn, B., Ran, H., Xu, Y.H., and Grabowski, G.A. (2009). In vivo and ex vivo evaluation of L-type calcium channel blockers on acid beta-glucosidase in Gaucher disease mouse models. PLoS ONE *4*, e7320.

Szegezdi, E., Logue, S.E., Gorman, A.M., and Samali, A. (2006). Mediators of endoplasmic reticulum stress-induced apoptosis. EMBO Reports *7*, 880-885.

Termine, D.J., Moremen, K.W., and Sifers, R.N. (2009). The mammalian UPR boosts glycoprotein ERAD by suppressing the proteolytic downregulation of ER mannosidase I. Journal of Cell Science *122*, 976-984.

Traub, L.M., and Kornfeld, S. (1997). The trans-Golgi network: a late secretory sorting station. Current Opinion in Cell Biology *9*, 527-533.

Travers, K.J., Patil, C.K., Wodicka, L., Lockhart, D.J., Weissman, J.S., and Walter, P. (2000). Functional and genomic analyses reveal an essential coordination between the unfolded protein response and ER-associated degradation. Cell *101*, 249-258.

Triggle, D.J. (2003). 1,4-dihydropyridine calcium channel ligands: Selectivity of action. The roles of pharmacokinetics, state-dependent interactions, channel isoforms, and other factors. Drug Development Research *58*, 5-17.

Triggle, D.J. (2006). L-type calcium channels. Current Pharmaceutical Design *12*, 443-457.

Trinchera, M., Fabbri, M., and Ghidoni, R. (1991). Topography of glycosyltransferases involved in the initial glycosylations of gangliosides. The Journal of Biological Chemistry *266*, 20907-20912.

Trombetta, E.S., and Parodi, A.J. (2003). Quality control and protein folding in the secretory pathway. Annual Review of Cell and Developmental Biology *19*, 649-676.

Tropak, M.B., Reid, S.P., Guiral, M., Withers, S.G., and Mahuran, D. (2004). Pharmacological enhancement of beta-hexosaminidase activity in fibroblasts from adult Tay-Sachs and Sandhoff Patients. The Journal of Biological Chemistry *279*, 13478-13487.

Ulloa-Aguirre, A., Janovick, J.A., Brothers, S.P., and Conn, P.M. (2004). Pharmacologic rescue of conformationally-defective proteins: implications for the treatment of human disease. Traffic *5*, 821-837.

Urano, F., Wang, X., Bertolotti, A., Zhang, Y., Chung, P., Harding, H.P., and Ron, D. (2000). Coupling of stress in the ER to activation of JNK protein kinases by transmembrane protein kinase IRE1. Science *287*, 664-666.

Vembar, S.S., and Brodsky, J.L. (2008). One step at a time: endoplasmic reticulum-associated degradation. Nature Reviews *9*, 944-957.

Vembar, S.S., Jonikas, M.C., Hendershot, L.M., Weissman, J.S., and Brodsky, J.L. (2010). J domain co-chaperone specificity defines the role of BIP during protein translocation. The Journal of Biological Chemistry *285*, 22484-94

Verkhratsky, A. (2005). Physiology and pathophysiology of the calcium store in the endoplasmic reticulum of neurons. Physiological Reviews *85*, 201-279.

Wang, F., Agnello, G., Sotolongo, N., and Segatori, L. (2011a). Ca2+ homeostasis modulation enhances the amenability of L444P glucosylcerebrosidase to proteostasis regulation in patient-derived fibroblasts. ACS Chemical Biology *6*, 158-168.

Wang, F., Chou, A., and Segatori, L. (2011b). Lacidipine remodels protein folding and Ca2+ homeostasis in Gaucher's disease fibroblasts: a mechanism to rescue mutant glucocerebrosidase. Chemistry & Biology *18*, 766-776.

Wang, F., Song, W., Brancati, G., and Segatori, L. (2011c). Inhibition of endoplasmic reticulum-associated degradation rescues native folding in loss of function protein misfolding diseases. The Journal of Biological Chemistry *286*, 43454-43464.

Wang, J., and Best, P.M. (1992). Inactivation of the sarcoplasmic reticulum calcium channel by protein kinase. Nature *359*, 739-741.

Wang, Q., Shinkre, B.A., Lee, J.G., Weniger, M.A., Liu, Y., Chen, W., Wiestner, A., Trenkle, W.C., and Ye, Y. (2010). The ERAD inhibitor Eeyarestatin I is a bifunctional compound with a membrane-binding domain and a p97/VCP inhibitory group. PLoS ONE *5*, e15479.

Ward, A., Chaffman, M.O., and Sorkin, E.M. (1986). Dantrolene. A review of its pharmacodynamic and pharmacokinetic properties and therapeutic use in malignant hyperthermia, the neuroleptic malignant syndrome and an update of its use in muscle spasticity. Drugs *32*, 130-168.

Welch, W.J., and Brown, C.R. (1996). Influence of molecular and chemical chaperones on protein folding. Cell Stress Chaperones *1*, 109-115.

Werner, E.D., Brodsky, J.L., and McCracken, A.A. (1996). Proteasome-dependent endoplasmic reticulum-associated protein degradation: an unconventional route to a familiar fate. Proceedings of the National Academy of Sciences of the United States of America *93*, 13797-13801.

Westerheide, S.D., Bosman, J.D., Mbadugha, B.N., Kawahara, T.L., Matsumoto, G., Kim, S., Gu, W., Devlin, J.P., Silverman, R.B., and Morimoto, R.I. (2004). Celastrols as inducers of the heat shock response and cytoprotection. The Journal of Biological Chemistry *279*, 56053-56060.

Wishart, D.S., Knox, C., Guo, A.C., Cheng, D., Shrivastava, S., Tzur, D., Gautam, B., and Hassanali, M. (2008). DrugBank: a knowledgebase for drugs, drug actions and drug targets. Nucleic Acids Research *36*, 901-906.

Wraith, J.E. (2006). Limitations of enzyme replacement therapy: current and future. Journal of Inherited Metabolic Disease *29*, 442-447.

Wu, C. (1995). Heat shock transcription factors: structure and regulation. Annual Review of Cell and Developmental Biology *11*, 441-469.

Wu, J.C., Liang, Z.Q., and Qin, Z.H. (2006). Quality control system of the endoplasmic reticulum and related diseases. Acta Biochimica et Biophysica Sinica *38*, 219-226.

Xu, P., and Robinson, A.S. (2009). Decreased secretion and unfolded protein response up-regulation are correlated with intracellular retention for single-chain antibody variants produced in yeast. Biotechnology and Bioengineering *104*, 20-29.

Xu, S.Z., Zhong, W., Watson, N.M., Dickerson, E., Wake, J.D., Lindow, S.W., Newton, C.J., and Atkin, S.L. (2008). Fluvastatin reduces oxidative damage in human vascular endothelial cells by upregulating Bcl-2. Journal of Thrombosis and Haemostasis *6*, 692-700.

Yoshida, I., Monji, A., Tashiro, K.-i., Nakamura, K.-i., Inoue, R., and Kanba, S. (2006). Depletion of intracellular Ca2+ store itself may be a major factor in thapsigargin-induced ER stress and apoptosis in PC12 cells. Neurochem International *48*, 696-702.

Youle, R.J., and Strasser, A. (2008). The BCL-2 protein family: opposing activities that mediate cell death. Nature Reviews *9*, 47-59.

Yu, Z., Sawkar, A.R., Whalen, L.J., Wong, C.H., and Kelly, J.W. (2007). Isofagomine- and 2,5-anhydro-2,5-imino-D-glucitol-based glucocerebrosidase pharmacological chaperones for Gaucher disease intervention. Journal of Medicinal Chemistry *50*, 94-100.

Zhao, H., and Grabowski, G.A. (2002). Gaucher disease: Perspectives on a prototype lysosomal disease. Cellular and Molecular Life Sciences *59*, 694-707.

Zong, W.X., Li, C., Hatzivassiliou, G., Lindsten, T., Yu, Q.C., Yuan, J.Y., and Thompson, C.B. (2003). Bax and Bak can localize to the endoplasmic reticulum to initiate apoptosis. Journal of Cell Biology *162*, 59-69.

Appendix A

Small molecules used in this study

Small Molecules	Chemical Structures	Functions
MG-132	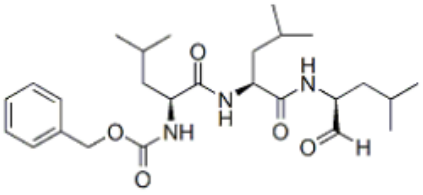	Proteostasis regulator (Mu et al., 2008b)
Celastrol	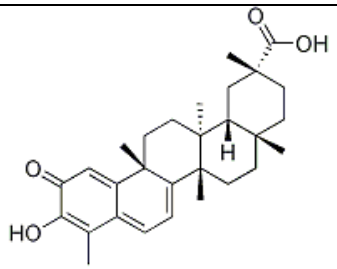	Proteostasis regulator (Mu et al., 2008b)
Ryanodine	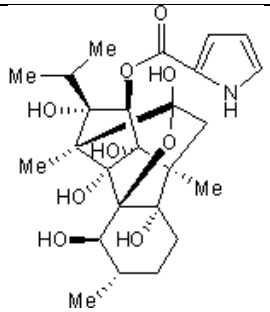	RyR blocker (Buck et al., 1992; Nagasaki and Fleischer, 1988)
Dantrolene	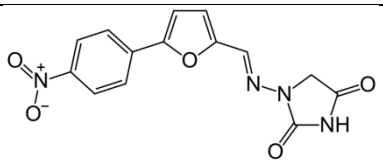	RyR blocker (Ward et al., 1986)

Lacidipine	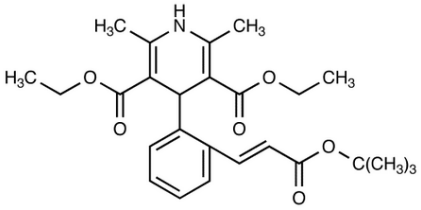	LTCC blocker; also inhibits RyRs (Gunther et al., 2008)
Lercanidipine	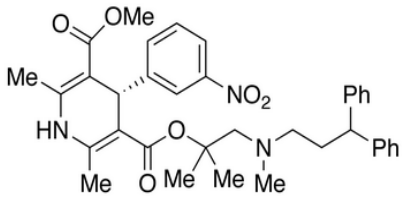	LTCC blocker, also prevents Ca^{2+} efflux from the ER (Wishart et al., 2008)
Nicardipine	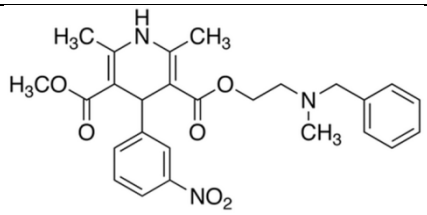	LTCC blocker, also prevents Ca^{2+} efflux from the ER (Wishart et al., 2008)
Nifedipine	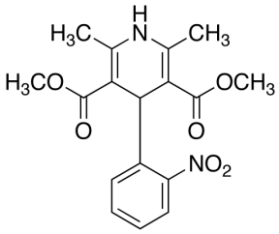	LTCC blocker (Gunther et al., 2008)
Nitrendipine	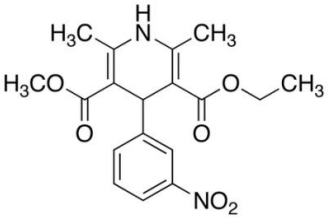	LTCC blocker (Gunther et al., 2008)
Diltiazem	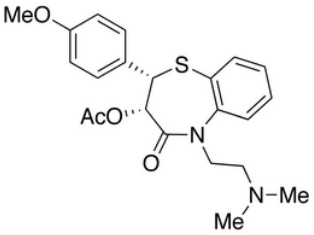	LTCC blocker; also inhibits RyRs (Gunther et al., 2008)

Verapamil	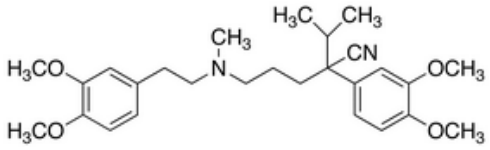	LTCC blocker; also inhibits RyRs (Gunther et al., 2008)
Eeyarestatin I **(EerI)**	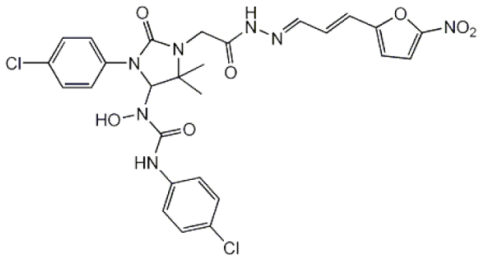	ERAD inhibitor; inhibits p97 ATPase activity (Fiebiger et al., 2004; Wang et al., 2010)
Kifunensine **(Kif)**	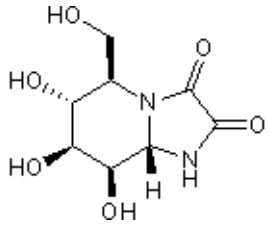	ERAD inhibitor; inhibits the activity of ER mannosidase I (Avezov et al., 2008; Fagioli and Sitia, 2001)
Thapsigargin	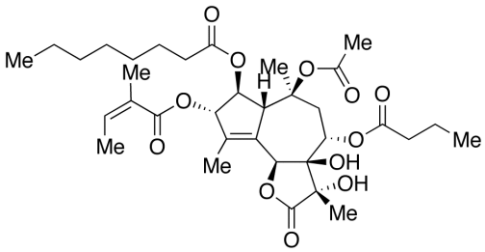	UPR inducer; inhibits the activity of SERCA pumps (Chen et al., 2007)
Tunicamycin	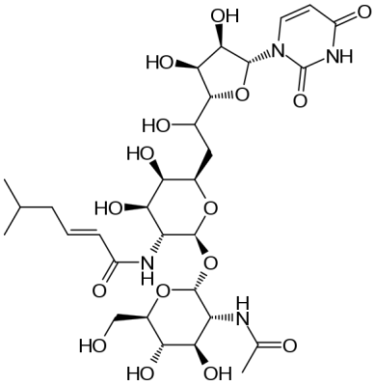	UPR inducer; inhibits protein glycosylation (Duksin and Bornstein, 1977)

A23187	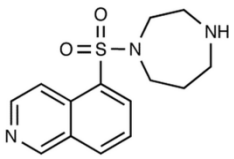	BiP promoter inducer (BiP 670); Ca^{2+} ionophore (Chao and Lin-Chao, 1992; Drummond et al., 1987)
NB-DNJ	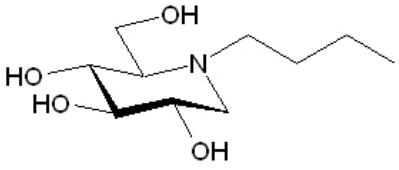	Glucosylceramide synthesis inhibitor; Glucosyltransferase inhibitor (Cox et al., 2000; Platt et al., 2001)

Appendix B

Global gene expression profile in fibroblasts derived from patients with GD treated with ryanodine and MG-132.

(M, MG-132; R, ryanodine; MR, MG-132 + Ryanodine)

	M	R	MR	
ER chaperones				
BiP/GRP78[a]	1.79	1.03	2.34	Heat shock 70kDa protein 5 (glucose-regulated protein, 78kDa)
ERdj1[a]	1.01	1.03	1.56	DnaJ (Hsp40) homolog, BiP co-chaperone
Sec63p/ERdj2[a]	1.18	1.16	1.29	SEC63 homolog (S. cerevisiae) (SEC63) localizes in ER pore complexes
ERdj3[a]	1.06	1.10	1.25	DnaJ (Hsp40) homolog, BiP co-chaperone
ERdj4[a]	2.85	1.11	3.49	DnaJ (Hsp40) homolog, BiP co-chaperone, stimulates BiP ATPase activity
ERdj5[a]	-1.12	1.10	-1.55	DnaJ (Hsp40) homolog, BiP co-chaperone, involved in folding and translocation of substrates across the ER membrane
BAP[a]	1.06	1.07	1.14	SIL1 homolog (S. cerevisiae), BiP nucleotide exchange factor
GRP94[a]	1.25	1.01	1.26	Heat shock protein 90kDa beta (Grp94) member 1 stabilizes misfolded proteins during cycles of calnexin binding
CNX[a]	1.34	1.06	1.46	Calnexin, lectin chaperone
CRT[a]	-1.06	1.06	-1.04	Calreticulin, lectin chaperone
EDEM1[a]	-1.09	-1.11	-1.29	ERAD enhancer, mannosidase alpha-like, catalyzes de-mannosylation and prevents aggregation of ERAD substrates
Derlin2[a]	-1.06	1.02	1.12	Der1-like domain family, member 2, promotes ERAD in conjunction with EDEM and p97
EDEM2[a]	1.11	-1.01	1.16	ERAD, mannosidase alpha-like 2. Stress-regulated mannosidase-like protein
EDEM3[a]	1.27	1.17	1.48	ERAD enhancer, mannosidase alpha-like 3, promotes trimming of mannose from ERAD susbtrates
UGGT	1.37	-1.30	1.00	UDP-glucose:glycoprotein glucosyltransferase 1 reglucosylates monoglucosylated proteins
a-glucosidase I	1.43	-1.05	1.28	Alpha-glucosidase I regulates trimming of the terminal alpha-1,2-glucose residue in the N-glycan-processing pathway
a-glucosidase II	1.52	1.12	1.28	Glucosidase, alpha, promotes CNX substrate release by regulating clevage of terminal glucose residues
a-mannosidase I	1.04	-1.13	-1.05	Mannosidase, alpha, promotes CNX substrate release by regulating cleavage of terminal mannose residues
Unfolded protein response				
ATF6 arm	**M**	**R**	**MR**	
ATF6	1.24	1.16	1.26	Activating transcription factor 6 (ATF6)
S1P	1.65	1.01	1.43	Membrane-bound TF peptidase, catalyzes the proteolytic activation of sterol regulatory element-binding proteins (SREBPs)
SREBP1	1.20	-1.29	-1.34	Sterol regulatory element binding TF 1 (SREBF1), transcriptional activator required for lipid homeostasis
SREBP2	1.74	-1.02	1.05	Sterol regulatory element binding TF 2 (SREBF2), transcriptional activator required for lipid homeostasis
HERP[a]	1.02	1.05	1.12	Homocysteine-inducible, ER stress-inducible, ubiquitin-like domain member 1 binds nonglycosylated BiP substrates and the proteasome
Luman	1.31	-1.06	1.40	cAMP responsive element binding protein 3 (CREB3) is activated upon intramembrane proteolysis, binds the cAMP response element
OASIS	-1.41	-1.48	-2.17	cAMP responsive element binding protein 3-like 1 (CREB3L1), membrane-bound TF activated by proteolytic cleavage
BBF2H7	-1.33	-1.07	-1.64	cAMP responsive element binding protein 3-like 2 (CREB3L2) hypothesized to contribute to the late phase of UPR signaling
PERK arm				
PERK	1.52	1.08	1.56	TIF 2-alpha kinase 2 (EIF2AK2) induced by autophosphorylation, phosphorylates the TiF EIF2S1, inhibiting translation
EIF2A	1.44	-1.07	1.39	TIF 2A, 65kDa (EIF2A) is phosphorylated to block the formation of ribosomal preinitiation complexes causing translation attenuation
EIF2B1	1.05	-1.16	1.17	TIF 2B, subunit 1 alpha, catalyzes the exchange of eukaryotic initiation factor 2-bound GDP for GTP
EIF2B2	-1.05	1.11	1.10	TIF 2B, subunit 2 beta, catalyzes the exchange of eukaryotic initiation factor 2-bound GDP for GTP
EIF2B4	-1.01	-1.04	1.06	TIF 2B, subunit 4 delta, catalyzes the exchange of eukaryotic initiation factor 2-bound GDP for GTP
EIF2B5	1.30	1.05	1.29	TIF 2B, subunit 5 epsilon, catalyzes the exchange of eukaryotic initiation factor 2-bound GDP for GTP
ATF4	1.31	1.00	1.45	Activating TF 4 (tax-responsive enhancer element B67), induced by phosphorylation of eIF2a
CCND1	-1.42	-1.17	-1.86	Cyclin D1 (CCND1) is essential for the control of the cell cycle at the G1/S (start) transition, degraded PERK during ER stress
GADD34	1.73	-1.09	1.87	Protein phosphatase 1, promotes dephosphorylation of eIF2SI by ser/thr-protein phosphatase PP1, reversing translation inhibition
GCN2	1.11	-1.02	1.09	TIF 2 alpha kinase 4 (EIF2AK4) phosphorylates the alpha subunit of EIF2 and mediates translational inhibition
EIF2AK1	1.69	1.06	1.55	TIF 2-alpha kinase 1 (EIF2AK1) mediates the phosphorylation of EIF2S1 and thus inhibition of translation initiation
IRE1 arm				
XBP1	-1.15	-1.08	-1.22	X-box binding protein 1 suppresses the activity of IRE1α, preventing formation of active, spliced XBP-1
IRE1	-1.81	1.02	-1.62	ER to nucleus signalling 1 (ERN1), ER sensor of unfolded proteins
HRD1[a]	1.92	-1.13	1.84	Synovial apoptosis inhibitor 1, synoviolin (SYVN1) acts as an E3 ubiquitin-protein ligase
HAC1	1.00	-1.48	1.02	Tripartite motif-containing 3 (TRIM3), downstream effector of IRE1, induces transctription of genes for attenuation of ER stress
SCAP	1.47	-1.09	1.32	SREBF chaperone escorts protein required for cholesterol and lipid homeostasis
INO1	-1.03	-1.09	1.15	Melanoma antigen family H, 1 (MAGEH1), key enzyme in phospholipid biosynthesis

	M	R	MR	
Sphingolipid metabolic pathway				
SPTLC1	1.49	1.03	1.53	Serine palmitoyltransferase, long chain base subunit 1 (SPTLC1), transcript variant 1
SPTLC1	1.14	1.00	1.23	Serine palmitoyltransferase, long chain base subunit 1 (SPTLC1), transcript variant 2
SPTLC2	1.46	-1.05	1.47	Serine palmitoyltransferase, long chain base subunit 2 (SPTLC2)
SGMS1	1.23	-1.10	-1.01	Sphingomyelin synthase 1 (SGMS1)
SGPP1	2.46	1.05	2.08	Sphingosine-1-phosphate phosphatase 1
LSD-associated genes				
	M	**R**	**MR**	
GBA	1.54	-1.09	1.41	Glucosidase, beta; acid (includes glucosylceramidase), Gaucher's disease
NPC1	3.43	1.12	3.89	Niemann-Pick disease, type C1 (NPC1)
HEXA	1.88	-1.06	1.99	Hexosaminidase A (alpha polypeptide) (HEXA), Tay-Sach's disease
GLA	5.97	1.18	7.35	Galactosidase, alpha (GLA), Fabry disease
GLB1	1.20	-1.18	1.21	Galactosidase, beta 1 (GLB1), GM1 gangliosidosis
MANBA	1.03	1.02	1.07	Mannosidase, beta A, lysosomal, a-mannosidosis disease
HEXB	1.04	1.02	1.12	Hexosaminidase B (beta polypeptide), GM2 gangliosidosis
AGA	-1.09	1.21	1.02	Aspartylglucosaminidase, Aspartylglucosaminuria disease
CTNS	1.90	-1.01	1.55	Cystinosis, nephropathic
LAMP2	1.43	1.03	1.70	Lysosomal-associated membrane protein 2 (LAMP2), Danon disease
ASAH1	-1.06	1.33	1.27	N-acylsphingosine amidohydrolase (acid ceramidase) 1, Farber disease
GALC	1.18	1.04	1.33	Galactosylceramidase, Krabbe disease
IDUA	1.19	-1.08	1.16	Iduronidase, alpha-L- (IDUA), Mucopolysaccharidosis I
IDS	1.73	1.24	1.95	Iduronate 2-sulfatase (Hunter syndrome) (IDS), Mucopolysaccharidosis II
IDS	1.37	1.08	1.54	Iduronate 2-sulfatase (Hunter syndrome) (IDS), Mucopolysaccharidosis II
NAGLU	1.00	-1.33	-1.28	N-acetylglucosaminidase, alpha- (Sanfilippo disease IIIB) (NAGLU), Mucopolysaccharidosis IIIB
SGSH	2.80	-1.13	2.45	N-sulfoglucosamine sulfohydrolase (sulfamidase) (SGSH), Mucopolysaccharidosis IIIA
GALNS	1.51	1.04	1.37	Galactosamine (N-acetyl)-6-sulfatase (Morquio syndrome, mucopolysaccharidosis type IVA) (GALNS), Mucopolysaccharidosis I
ARSB	1.03	-1.06	-1.07	Arylsulfatase B (ARSB), Mucopolysaccharidosis VI
GUSB	1.03	1.01	1.09	Glucuronidase, beta (GUSB), Mucopolysaccharidosis VII
SUMF1	-1.01	-1.03	1.03	Sulfatase modifying factor 1, Multiple sulfatase deficiency
CLN3	1.27	-1.11	1.41	Ceroid-lipofuscinosis, neuronal 3, Neuronal Ceroid Lipofuscinoses
CLN5	1.52	-1.04	1.84	Ceroid-lipofuscinosis, neuronal 5, Neuronal Ceroid Lipofuscinoses
CLN6	-1.93	-1.74	-3.20	Ceroid-lipofuscinosis, neuronal 6, late infantile, Neuronal Ceroid Lipofuscinoses
CLN8	3.18	-1.02	3.22	Ceroid-lipofuscinosis, neuronal 8 (epilepsy, progressive with mental retardation), Neuronal Ceroid Lipofuscinoses
GAA	1.45	-1.32	1.28	Glucosidase, alpha; acid (GAA), Pompe disease
NAGA	1.00	1.03	1.09	N-acetylgalactosaminidase, alpha-, Schindler disease

ER-associated degradation (ERAD)

Recognition	M	R	MR	
BIP/GRP78[a]	1.79	1.03	2.34	Heat shock 70kDa protein 5 (glucose-regulated protein, 78kDa)
HSP70	24.69	-1.09	32.99	Heat shock 70kDa protein 1A (HSPA1A)
HSP70	23.53	1.12	24.57	Heat shock 70kDa protein 1B (HSPA1B)
HSC70	2.91	1.02	2.98	Heat shock 70kDa protein 8 (HSPA8), transcript variant 2
HSC70	2.42	1.02	2.50	Heat shock 70kDa protein 8 (HSPA8), transcript variant 1
ERdj1[a]	1.01	1.03	1.56	DnaJ (Hsp40) homolog, BiP co-chaperone
ERdj2[a]	1.18	1.16	1.29	SEC63 homolog (S. cerevisiae) (SEC63) localizes in ER pore complexes
ERdj3[a]	1.06	1.10	1.25	DnaJ (Hsp40) homolog, BiP co-chaperone
ERdj4[a]	2.85	1.11	3.49	DnaJ (Hsp40) homolog, BiP co-chaperone, stimulates BiP ATPase activity
ERdj5[a]	-1.12	1.10	-1.11	DnaJ (Hsp40) homolog, BiP co-chaperone, involved in folding and translocation of substrates across the ER membrane
p58IPK	1.80	1.18	2.50	DnaJ (Hsp40) homolog, (DNAJC3) mediator of cotranslocational ER protein degradation
HDJ1	3.35	-1.01	4.60	DnaJ (Hsp40) homolog, subfamily B, member 1 (DNAJB1) interacts with HSP70 and stimulates its ATPase activity
HDJ2	2.25	1.06	2.61	Homo sapiens DnaJ (Hsp40) homolog, subfamily A, member 1 (DNAJA1). Hsc70 co-chaperone
HSJ1	1.75	-1.11	1.66	DnaJ (Hsp40) homolog, prevents substrate aggregation and de-ubiquitination, and sorts ERAD substrates to the proteasome
Cys string proteir	2.33	1.03	1.96	DnaJ (Hsp40) homolog, subfamily C, member 5 (DNAJC5), Hsp70 co-chaperone
BAP[a]	1.12	1.11	1.18	SIL1 homolog, ER chaperone (S. cerevisiae) (SIL1). BiP nucleotide exchange factor
GRP170	-1.07	-1.10	-1.07	Hypoxia up-regulated 1 (HYOU1) participates in protein folding and suppresses hypoxia-induced apoptotic cell death
HSPBP1	1.19	-1.18	1.37	Hsp70-interacting protein (HSPBP1). Hsp70 inhibitor
HSP110	4.52	1.19	4.84	Heat shock 105kDa/110kDa protein 1 (HSPH1) prevents the aggregation of denatured proteins in cells under severe stress
CRYAB	1.45	-1.11	1.59	Crystallin, alpha B (HSP20), prevents protein aggregation
Hsp26	-1.25	-1.25	-1.45	Heat shock protein, alpha-crystallin-related, B6
GRP94[a]	1.25	1.01	1.26	Heat shock protein 90kDa beta (HSP90B1) associates with OS-9, ERAD substrates and regulates OS-9-SEL1L-Hrd complex assembly
HSP90AA1	3.00	1.05	2.94	Heat shock protein 90kDa alpha (cytosolic), class A member 1 (HSP90AA1)
HSP90AB1	2.41	-1.08	2.57	Heat shock protein 90kDa alpha (cytosolic), class B member 1 (HSP90AB1)
CNX[a]	1.34	1.06	1.46	Calnexin, lectin chaperone
CRT[a]	-1.06	1.06	-1.04	Calreticulin, lectin chaperone
Targeting				
EDEM1[a]	-1.09	-1.11	-1.29	ERAD enhancer, mannosidase alpha-like 1, promotes de-mannosylation and prevents aggregation of ERAD substrates
EDEM2[a]	1.11	-1.01	1.16	ERAD, mannosidase alpha-like 2. Stress-regulated mannosidase-like protein
EDEM3[a]	1.27	1.17	1.48	ERAD enhancer, mannosidase alpha-like 3, promotes trimming of mannose from ERAD susbtrates
OS9	1.20	-1.03	1.27	Yos9 yeast homolog, selects ERAD substrates for retro-translocation
XTP3-B	1.34	1.07	1.49	XTP-3 forms an ER quality control scaffold with the HRD1-SEL1L complex and BiP
HERP[a]	1.02	1.05	1.12	Homocys-inducible, ER stress-inducible, ubiquitin-like domain member 1 binds to nonglycosylated BiP substrates and to the proteasome
SEC61A1	1.55	-1.09	1.28	Sec61 alpha 1 subunit (S. cerevisiae), composed of SEC61-a, SEC61-b, SEC61-g, part of complex SEC61-SEC62-SEC63
SEC61B	-1.34	-1.01	-1.10	Sec61 beta subunit (SEC61B)
SEC61G	1.09	1.50	1.23	Sec61 gamma subunit (SEC61G), transcript variant 2
SEC61G	-1.06	1.33	1.07	Sec61 gamma subunit (SEC61G), transcript variant 1
SEC62	1.18	-1.14	1.16	SEC62 homolog (S. cerevisiae) (SEC62)
Derlin1	1.32	1.01	1.65	Der1-like domain family, member 1 (DERL1) forms a channel for retrotranslocation of misfolded proteins to the cytosol
Derlin2[a]	-1.06	1.02	1.12	Der1-like domain family, member 2 (DERL2) forms the retrotranslocation channel, selective for lumenal glycoproteins
VIMP[a]	2.67	-1.28	2.18	Valosin-containing protein (VCP) targets the ubiquitinated nuclear factor kappaB inhibitor to the proteasome

ER-associated degradation (ERAD)

Ubiquitylation

UBE1	1.44	-1.03	1.20	Ubiquitin-activating enzyme E1 catalyzes the first step in ubiquitin conjugation
UBC6e	-1.01	1.21	1.11	Ubiquitin-conjugating enzyme E2, J1 (UBC6 homolog, yeast) catalyzes ER membrane protein ubiquitination
UBCH7/UBC7	1.83	-1.08	1.60	Ubiquitin-conjugating enzyme E2L 3 (UBE2L3) catalyzes ubiquitination and degradation of short-lived and misfolded proteins
UBCH5	1.12	1.31	1.13	Ubiquitin-conjugating enzyme E2D 2 (UBC4/5 homolog, yeast) functions in the E6/E6-AP-mediated ubiquitination of p53/TP53
SEL1L	1.77	-1.03	1.65	Sel-1 suppressor of lin-12-like (C. elegans) forms a ubiquitin-ligase complex with HRD1
HRD1(SYVN1)[a]	1.92	-1.13	1.84	Synovial apoptosis inhibitor 1, synoviolin (SYVN1) acts as an E3 ubiquitin-protein ligase
TEB4/MARCH 6	2.27	1.10	1.81	Membrane-associated ring finger (C3HC4) 6 (MARCH6) is a E3 ubiquitin-protein ligase
GP78	2.70	1.11	2.33	Autocrine motility factor receptor (AMFR) is a polytopic and integra lER membrane E3 ubiquitin-protein ligase
RMA1	-2.04	-1.26	-1.68	Ring finger protein 5 (RNF5) is a E3 ubiquitin-protein ligase
Chip	-1.39	1.00	-1.30	U-box containing protein, modulates the activity of chaperone complexes and exhibits E3 ligase activity
UFD2	1.34	1.00	1.45	Ubiquitination factor E4A (UFD2 homolog, yeast) (UBE4A)
UFD2	1.67	1.03	1.94	Ubiquitination factor E4B (UFD2 homolog, yeast) (UBE4B)

Proteasomal targeting and degradation

VCP(p97,VIMP)[a]	2.67	-1.28	2.18	Valosin-containing protein (VCP) targets ubiquitinated nuclear factor kappaB inhibitor to the proteasome
UFD1L	3.79	1.20	4.32	Ubiquitin fusion degradation 1 like (yeast) (UFD1L) essential component of the ubiquitin-dependent proteolytic pathway
NPLOC4	3.00	-1.17	2.79	Nuclear protein localization 4 homolog (S. cerevisiae) forms a retrotranslocation complex with UFD1L and VCP
RAD23A	-1.10	-1.07	-1.08	RAD23 homolog A (S. cerevisiae) (RAD23A) negatively regulates polyubiquitin/UBA interactions
RAD23B	-1.15	-1.09	-1.20	RAD23 homolog B (S. cerevisiae) (RAD23B)
Peptide N-glycan	2.03	1.21	2.41	N-glycanase 1 (NGLY1) deglycosylates N-linked glycoproteins in the cytoplasm and assists their degradation
Ataxin-3	-1.30	1.04	-1.14	Ataxin 3 (ATXN3) interacts with RAD23A and RAD23B, functions as transcriptional regulator, and as de-ubiquitinating enzyme
RPN10	1.78	1.05	1.88	Proteasome 26S subunit, non-ATPase, binds ubiquitin-conjugates, with selectivity for longer polyubiquitin chains
RPN13	2.43	1.00	2.40	Adhesion regulating molecule 1 (ADRM1) recruits the deubiquitinating enzyme UCHL5 at the 26S proteasome
RPT5	1.50	0.91	1.50	Proteasome 26S subunit, ATPase, involved in the ATP-dependent degradation of ubiquitinated proteins

Ryanodine receptor gating

	M	R	MR	
CAMK2D	1.57	1.35	1.64	Calcium/calmodulin-dependent protein kinase (CaM kinase) II delta (CAMK2D)
CAMK2D	1.48	-1.07	1.54	Calcium/calmodulin-dependent protein kinase (CaM kinase) II delta (CAMK2D)
CAMK2G	3.31	-1.11	3.86	Calcium/calmodulin-dependent protein kinase (CaM kinase) II gamma (CAMK2G)
CAMK2G	3.17	-1.29	3.63	Calcium/calmodulin-dependent protein kinase (CaM kinase) II gamma (CAMK2G)
CAMK2N1	-4.02	-1.24	-5.86	Calcium/calmodulin-dependent protein kinase II inhibitor 1 (CAMK2N1)
PPP1CA	-1.88	-1.40	-1.94	Protein phosphatase 1, catalytic subunit, alpha isoform (PPP1CA)
PPP1CB	-1.02	-1.03	-1.11	Protein phosphatase 1, catalytic subunit, beta isoform (PPP1CB)
PPP1CC	-1.35	1.02	-1.38	Protein phosphatase 1, catalytic subunit, gamma isoform (PPP1CC)

[a] Genes listed under multiple pathways because associated with different quality control functions.